Available online at www.sciencedirect.com
ScienceDirect
Coordination Chemistry Reviews 252 (2008) 2314–2345
COORDINATION CHEMISTRY REVIEWS
www.elsevier.com/locate/ccr

Review

NMR spectroscopy in coordination supramolecular chemistry: A unique and powerful methodology

Aurelia Pastor [a,*,1], Eloísa Martínez-Viviente [b,*]

[a] Departamento de Química Orgánica, Facultad de Química, Universidad de Murcia, Campus de Espinardo, Murcia 30100, Apdo. 4021, Spain
[b] Departamento de Química Inorgánica, Facultad de Química, Universidad de Murcia, Campus de Espinardo, Murcia 30100, Apdo. 4021, Spain

Received 22 November 2007; accepted 25 January 2008
Available online 2 February 2008

Contents

Abstract

Metal-mediated self-assembly is emerging as a very important strategy for the synthesis of supramolecular species. Still, a major challenge in coordination supramolecular chemistry continues to be the characterization of the self-assembled complexes and the investigation of their dynamic behaviour in solution. In this context, NMR spectroscopy appears as a unique and powerful methodology. This practical-oriented review describes the rich variety of NMR techniques which are applied to the investigation of different aspects of the structure and behaviour of supramolecular complexes. "Classic" 1D NMR spectra reflect characteristic chemical shifts due to metal–ligand interactions or encapsulation phenomena, as well as symmetry and chiral properties of host–guest assemblies. Mainstream ^{1}H, ^{13}C, ^{19}F and ^{31}P spectra are eventually complemented by

Abbreviations: bpy, 2,2′-bipyridyl; cod, 1,4-cyclooctadiene; dppdd, 1,12-bis(diphenylphosphino)dodecane; dppp, 1,3-bis(diphenylphosphino)propane; en, ethylenediamine; OTf, triflate (trifluoromethanesulfonate); qtpy, 2,2′:4,4″:4′,4‴-quaterpyridyl; tppb, 1,2,4,5-tetrakis-(diphenylphosphino)benzene; PTA, 1,3,5-triaza-7-phosphaadamantane.

* Corresponding authors. Fax: +34 968364143.
E-mail addresses: aureliap@um.es (A. Pastor), eloisamv@um.es (E. Martínez-Viviente).
[1] Fax: +34 968364149.

0010-8545/$ – see front matter © 2008 Elsevier B.V. All rights reserved.
doi:10.1016/j.ccr.2008.01.025

the use of NMR-active metal nuclides. Homo- and heteronuclear 2D correlation experiments are ubiquitous in the literature, providing through-bond and through-space connectivities. Increasingly, diffusion measurements are also gaining popularity in this field, being used to gain information about molecular size, intermolecular interactions and even association constants of supramolecular complexes. Knowledge about the thermodynamic properties and the dynamic behaviour of coordination supramolecular assemblies is essential for the development of their practical applications. The most frequently used NMR methodologies for the calculation of association constants (simple signal integration, NMR titration and diffusion measurements) and for the investigation of dynamic supramolecular equilibria (lineshape analysis, selective inversion recovery experiments and 2D EXSY spectra) are described, together with the use of variable-temperature investigations for the determination of the thermodynamic and activation parameters of self-assembly and encapsulation processes.

Keywords: Host–guest systems; Molecular recognition; NMR spectroscopy; Supramolecular chemistry; Self-assembly; Structure elucidation

1. Introduction

Supramolecular chemistry has evolved during the last three decades into an extraordinarily dynamic and truly interdisciplinary field of research, fuelling major developments at the interfaces of chemistry with areas such as biology, physics, materials science and engineering [1–3]. Applications include molecular recognition, ion-exchange, selective binding and encapsulation, development of receptors and sensors, catalysis, drug delivery strategies, biomimetics and nanoscale electronic and mechanical devices [4,5]. The term *supramolecular*, coined by Lehn [1], refers to ordered molecular aggregates held together by noncovalent intermolecular forces, such as hydrogen bonds, π–π-stacking interactions, electrostatic and van der Waals forces, hydrophobic effects or even metal–ligand bonds. Such a broad definition has made supramolecular chemistry an extremely wide and diverse domain [6].

Supramolecular species are usually generated by *spontaneous self-assembly* of predesigned building blocks, equipped with complementary recognition sites [7,8]. When compared with "traditional" covalent synthesis, self-assembly reveals itself as a highly convergent synthetic protocol, fast, facile and self-corrected by thermodynamically controlled equilibria [3,9–11], features which have long been exploited by Nature [8,12]. Complex, large and ordered discrete structures can be predictably obtained from relatively simple synthons, usually organic hydrogen-bond donors and acceptors [13] or metal and ligand components [9,10,14–19]. In particular, *metal-directed self-assembling* is emerging as one of the most widely used strategies for the synthesis of supramolecular species [20], due to the combination of defined, directed interactions and high binding constants [10,16,19]. The variety of oxidation states, coordination numbers, geometries and stabilities of transition metal complexes allows a precise control over the structure and dynamics of the resulting assemblies [10,15]. Moreover, metallosupramolecular structures may find novel applications owing to their electronic, redox or magnetic properties [17,18,21] as well as by the reactivity of the metal centres, most notably as catalysts [22,23]. Indeed, the development of fully functional metallosupramolecular devices is one of the present major challenges in chemistry [10,18,24].

A particularly active field within coordination supramolecular chemistry is the design of *3D nanocages* [9,10,16,25] to be used as containers for a variety of guests. High selectivity in guest encapsulation, reversible guest uptake and release, stabilization of reactive species [26,27] and effective control of host–guest dynamics [9,10,16,28] are commonly found features, pointing to potential applications of these coordination cages as molecular receptors, memory storage devices, drug releasers or reaction vessels for cavity-directed stoichiometric [29–32] and catalytic [23,32–35] reactions.

In spite of all this progress, a major challenge in supramolecular chemistry continues to be the characterization of the self-assembled complexes [10,36]. Slight modifications in the nature of metal and ligands, a change of solvent, or the presence of an appropriate guest may have great impact on the characteristics of the resulting assemblies [37–40]. Single-crystal X-ray diffraction analysis provides the most reliable structural information in the solid-state but, unfortunately, suitable crystals of supramolecular assemblies are often not available. Moreover, packing-forces may result in solid-state structures different from those existing in solution, where, additionally, equilibria between different stoichiometries may occur [41]. Analysis of the inclusion geometry of the guest is also important, as molecules in a specific environment may show unique properties and reactivity [42]. Another relevant field in many applications is the investigation of the kinetic and thermodynamic properties of the assembly and encapsulation processes [28,43].

In this context, NMR spectroscopy appears as a *unique and powerful methodology* for the investigation of supramolecular systems. With the help of practical examples taken from the recent literature we will try to show in this review the rich variety of NMR techniques which are applied to the investigation of different aspects of the structure and behaviour of supramolecular complexes. We start with the "classic" 1D spectra and the information they provide about complexation-induced chemical shifts, the symmetry of the complexes and eventual diastereomeric excesses resulting from enantioselective recognition. We also mention the use of NMR-active metal nuclides as a useful complement to mainstream ^{1}H, ^{13}C, ^{19}F and ^{31}P spectra. We describe many examples of the application of 2D NMR techniques to detect homo- (COSY, TOCSY) and heteronuclear (HMQC, HMBC) through-bond correlations. These methods are very efficient for establishing connectivities and consequently they are an invaluable tool for structural assignment. Other 2D experiments are designed to detect homo- (NOESY, ROESY) and heteronuclear (HOESY) through-space interactions based on the nuclear Overhauser effect. NOE interactions can be intra- and intermolecular and, thus, they provide information about the spatial structure of the molecules and their relative positions, an

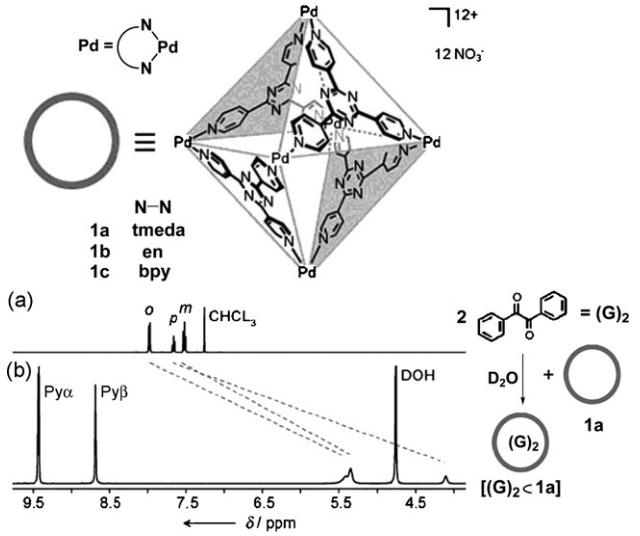

Fig. 1. Up: Structure of the self-assembled $[Pd_6L_4]^{12+}$ cages **1a–c**. Down: ^{1}H NMR (500 MHz) of (a) diphenylethanedione in $CDCl_3$ and (b) the inclusion complex within host **1a**, in D_2O. The shift to lower frequency of the ^{1}H resonances of the guest can be clearly observed. Pyα and Pyβ represent the pyridine α and β protons of **1a**. Reproduced with permission from Ref. [30]. Copyright Wiley-VCH Verlag GmbH & Co. KGaA.

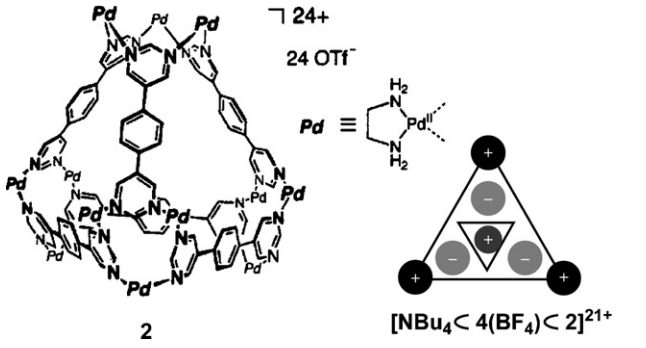

Fig. 2. Structure of the self-assembled $[Pd_{12}L_6]^{24+}$ cage **2** and schematic representation of the onion-like triple-layered structure of the inclusion complex $[NBu_4 \subset \mathbf{4}(BF_4) \subset \mathbf{2}]^{21+}$. Structure reprinted with permission from Ref. [45]. Copyright (2003) American Chemical Society.

especially interesting aspect in the case of host–guest assemblies or ionic species. A separate section is dedicated to diffusion measurements based on the pulsed-field gradient spin-echo (PGSE) methodology. This technique is becoming increasingly popular due to its potential for the investigation of aggregation, encapsulation and other intermolecular and interionic interactions which lie at the heart of supramolecular chemistry. Finally, we describe the most frequently used NMR methodologies for the calculation of association constants (simple signal integration, NMR titration and diffusion measurements) and for the investigation of the dynamic supramolecular equilibria (lineshape analysis, selective inversion recovery experiments and 2D EXSY spectra). We also show examples of variable-temperature investigations allowing the determination of the thermodynamic and activation parameters of self-assembly and encapsulation processes.

2. Structural characterization

2.1. 1D NMR spectroscopy

Changes in the 1D NMR spectra of the molecules involved in a self-assembly process are usually the first information source about the resulting structure. For *inclusion phenomena*, chemical shift changes or the appearance of separate NMR peaks are indicative of the formation of a host–guest complex. Thus, the resonances of an included guest are usually shifted to lower frequencies with respect to the free molecule, due to the anisotropic effect of the aromatic walls of the host [44]. Reports of such low-frequency ^{1}H shifts of guest molecules are ubiquitous in the literature. A very recent example has been provided by Fujita and co-workers [30], for the encapsulation of diphenylethanedione within the $[Pd_6L_4]^{12+}$ cage **1a** (Fig. 1). The guest ^{1}H resonances are shifted by 2.1–3.5 ppm to lower frequency with respect to the free ligand. In this host–guest complex, the photocleavage of the α-diketone is suppressed, and kinetically unfavoured cyclization products may be obtained [30]. The same research group [45] has reported the formation of an unusual cation–cation host–guest assembly between the $[Pd_{12}L_6]^{24+}$ cage **2** and a NBu_4^+ guest (Fig. 2). The single-crystal X-ray analysis shows a layer of four BF_4^- anions located between the cationic host and guest, forming a triple-layered onion-like structure, with other four BF_4^- anions placed outside the host. This observation is in agreement with the ^{19}F NMR solution spectrum, which shows two BF_4^- resonances in a 1:1 ratio ($\delta = -152.5$ and -150.1 ppm), assigned to the internal and external anions, respectively. Dalcanale and co-workers [46] have also used ^{19}F NMR to detect the inclusion of one of the eight triflate anions inside the tetranuclear Pd^{II} assembly **3** (Scheme 1). Two ^{19}F resonances in a 1:7 ratio ($\delta = -81.5$ and -78.2 ppm) were observed. In another interesting application, Raymond and co-workers [47] have reported the encapsulation of alkali ion–crown ether complexes into the

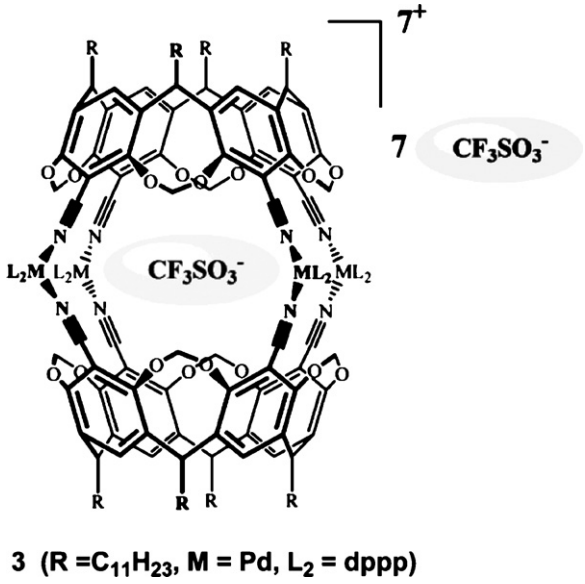

Scheme 1. The tetranuclear Pd^{II} cage **3**, with an encapsulated triflate anion. Reprinted with permission from Ref. [46]. Copyright (2005) American Chemical Society.

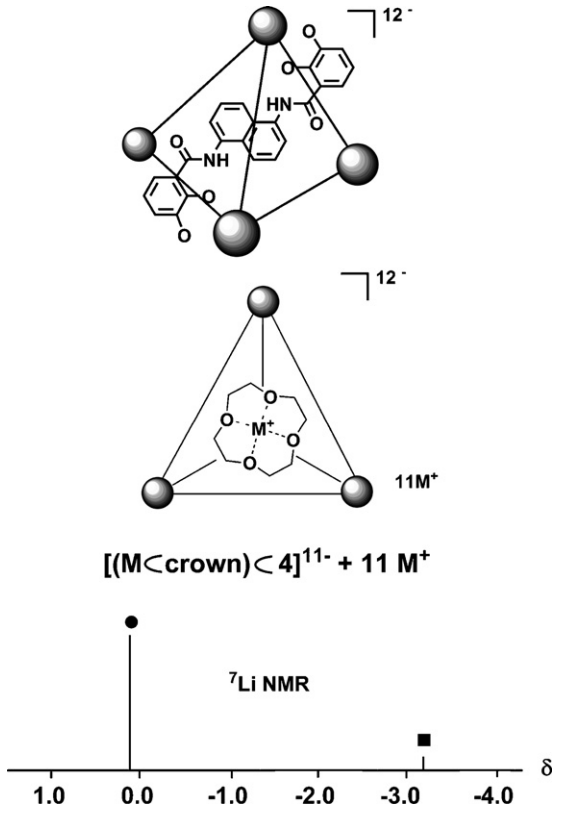

Fig. 3. Up: Schematic drawing of the tetrahedral $[Ga_4L_6]^{12-}$ host **4** (the rods represent the ligands and the spheres the metal ions). Center: Schematic drawing of the encapsulation within **4** of a crown ether and an alkali metal cation ($M = Li^+$, Na^+ or K^+). Down: Schematic representation of the ^{7}Li NMR spectrum (D_2O) of $Li_{11}[Li^+ \subset [12]crown\text{-}4) \subset \mathbf{4}]$. The filled circle represents fully solvated Li^+ ions located outside the cluster and the filled square represent Li^+ ions complexed to the crown ether and encapsulated inside the cluster.

$[Ga_4L_6]^{12-}$ assembly **4** (a "host within a host"). As shown in Fig. 3, the complexation of a Li^+ ion by the encapsulated [12]crown-4 ether results in the appearance of a new ^{7}Li resonance at lower frequency than the solvated Li^+ ions.

When suitable ^{1}H of ^{19}F resonances are not available, ^{13}C-enriched guests may be used to facilitate NMR investigations. Shinkai and co-workers [48] have proven the inclusion of [60]fullerene into the calixarene-based trinuclear Pd^{II} capsule **5a** by the observation of a separate resonance for the encapsulated ^{13}C-enriched fullerene ($\delta = 141$ ppm), while the free fullerene appears at 143 ppm (Fig. 4). The encapsulation of fullerenes in organorhodium porphyrins has been similarly detected [49,50].

Specific shifts to lower frequency of the NMR resonances of the guest can be used to analyze the inclusion geometry of the host–guest complex. Fujita and co-workers have reported several applications of this principle. In one example [51], the two methyl groups of a 4,4′-dimethylbiphenyl guest trapped inside the hexanuclear dodecapyridine Pd^{II} host **6** (Scheme 2) resonate at very different frequencies, $\delta(^1H) = 1.83$ and -0.25 ppm. Clearly, the strongly shielded methyl group is located closer to the pyridine rings of the host, and the flipping of the guest along its long axis is not taking place. In another application [52], the inclusion of 1- or 2-adamantol inside the $[Pd_6L_4]^{12+}$ cage **1b** (drawn in Fig. 1) results in significant low-frequency shifts

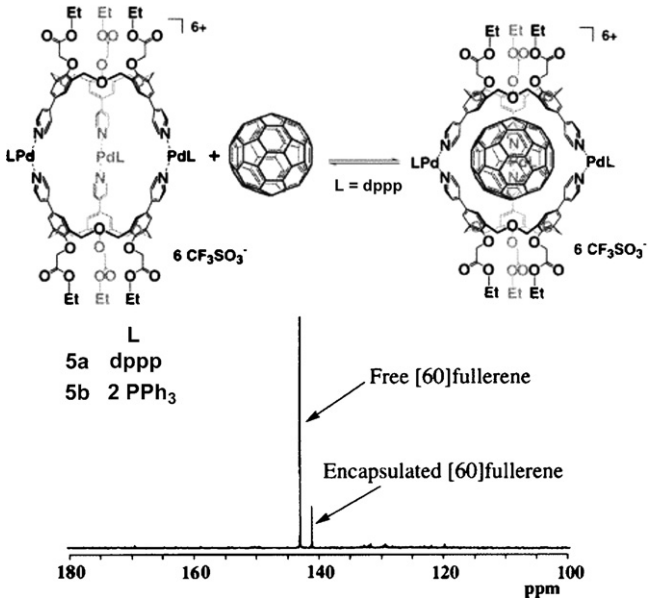

Fig. 4. Up: Encapsulation of [60]fullerene inside the trinuclear Pd^{II} homooxacalix[3]arene-based capsule **5a**. Down: Partial ^{13}C NMR (150 MHz, $Cl_2CDCDCl_2$) spectrum of ^{13}C-enriched [60]fullerene in the presence of **5a**. Reprinted with permission from Ref. [48]. Copyright (1999) American Chemical Society.

only for the hydrophobic moiety of the guest, suggesting that the interior of the host is highly hydrophobic, causing the hydroxyl group of the guest to be pointed outwards. Not only can the chemical shifts of the guest be informative, specific *high- and low-frequency shifts* [53] of the protons of the host may also provide information about the location of an aromatic guest inside the cavity [54].

Changes in the 1D NMR spectra of the organic ligands upon coordination-driven self-assembling are also frequently diagnostic of the formation and even the structure of the resulting metallocage. Thus, the loss of electron-density upon coordination to a metal usually results in shifts to higher frequency of the adjacent ligand protons. In the tetranuclear Pd^{II} complex **7** (Scheme 3), closely related to **3**, complexation of the pyridyl groups of the tetrakis (4-pyridylethynyl) cavitand resulted in shifts to higher frequency of the pyridyl α protons [38]. Curiously, for **7** no encapsulation of TfO^- was observed (there is

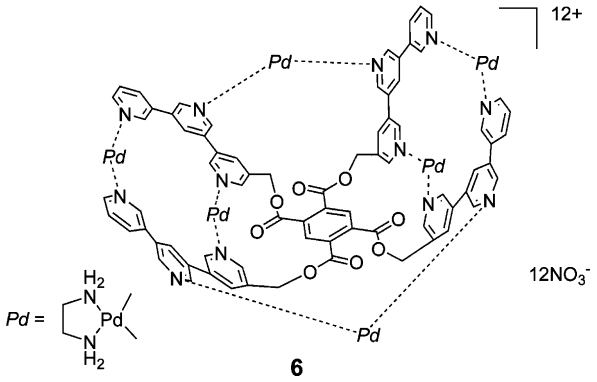

Scheme 2. Hexanuclear dodecapyridine host **6**.

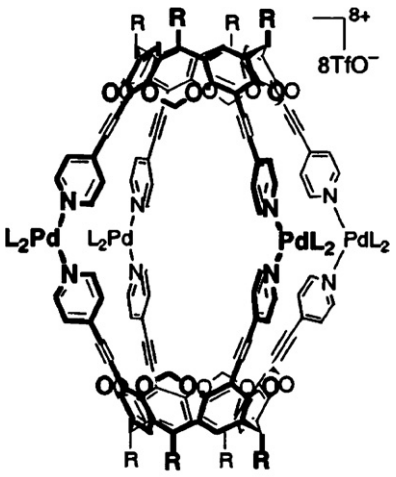

7 (R = $(CH_2)_6CH_3$, L_2 = dppp)

Scheme 3. The tetranuclear Pd^{II} homo-cavitand cage **7**. Reprinted with permission from Ref. [38]. Copyright (2004) American Chemical Society.

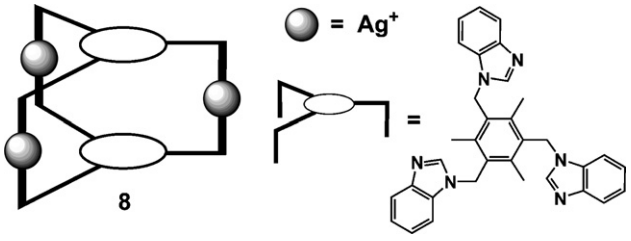

Scheme 4. Schematic drawing of the $[Ag_3L_2]^{3+}$ trigonal cage **8**.

a single ^{19}F resonance at −80 ppm), as opposed to **3**. Similar shifts to higher frequency have been observed for other pyridyl-containing cavitands [55]. For the trigonal cage $[Ag_3L_2]^{3+}$ **8** (Scheme 4) very different shifts to higher frequency of the ligand protons are observed, as a result of the combined effect of metal coordination and ring currents within the cage [56].

The symmetry of the *host* may also provide information about the situation of the guest inside the cavity. A very nice example is provided by the $[Pd_6L_4]^{12+}$ nanocage **1c** (drawn in Fig. 1) [42]. As shown by the ^1H NMR spectrum (Fig. 5a), the empty cage has a *T* symmetry, being all twelve pyridine rings equivalent. Upon strong 1:2 complexation of 4,4′-dimethoxydibenzoyl (**9**) the pyridine protons of the host are split into six pairs (Fig. 5b), due to desymmetrization of the host into S_4 symmetry, resulting from the orthogonal twisted disposition of the two guest molecules. Thus, *the host displays the symmetry of the guest*. In another example [57], the *T* symmetry of the $[Ga_4L_6]^{12-}$ cluster **4** (drawn in Fig. 3) is reduced to C_3 upon encapsulation of $[CpRu\{\eta^6\text{-}C_6H_5(CH_2)_nSO_3\}]$ ($n = 4, 6, 8, 10$), an indication that the alkyl sulfonate arm of the guest protrudes through a triangular face of the tetrahedron.

The control of the stereochemistry in the synthesis of supramolecular complexes, as well as the enantioselective recognition of a chiral guest by a chiral host, have been long-pursued goals. Stang and Olenyuk were the first to report chiral self-assembly of a chiral metallamacrocycle [58] and a unique polyhedra with rare *T* symmetry [59]. Shortly after that, Rebek and co-workers described organic self-assembled chiral capsules [60,61]. In some cases, diastereomeric excesses (de's) of up to 60% were observed upon encapsulation of chiral guests by a chiral host [60]. These investigations show that transfer of chirality between guest and capsule is possible, in spite of the weak intermolecular forces involved in molecular recognition. The de's are easily determined by integration of the resolved resonances for the diastereomeric host–guest complexes in the ^1H NMR spectra [60]. Reports of chiral molecular recognition by self-assembled coordination molecular capsules are less abundant [62]. Some examples have been provided by the groups of Fujita and Hiraoka [63] and Raymond and co-workers [31,32,64,65]. The latter has reported several applications of ^1H, ^{19}F and ^{31}P NMR for the determination of de's when the chiral $[Ga_4L_6]^{12-}$ capsule **4** binds chiral phosphonium guests [64], chiral organometallic complexes (Fig. 6) [65], or even hosts partially diastereoselective C–H activation reactions [31,32]. Shinkai and co-workers [66] have reported the use of a chiral-shift reagent (Pirkle's reagent) for the estimation of a 40% de upon inclusion of the chiral ammonium guest ***S*-10** inside the trinuclear Pd^{II} helical structure **5b** (drawn in Fig. 4), existing as a pair of *M* and *P* enantiomers (Fig. 7). Without addition of the shift reagent, the ^1H NMR resonances of the two diastereomeric

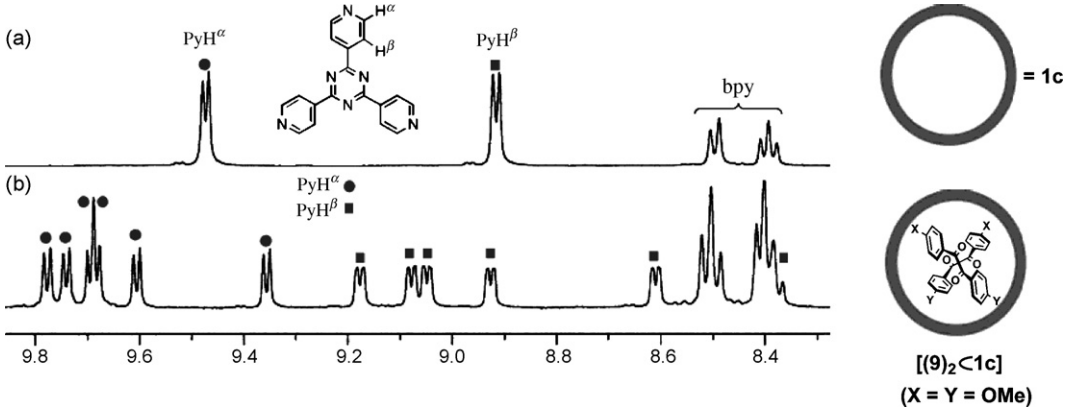

Fig. 5. ^1H NMR (500 MHz, D_2O) observation of the enclathration of two molecules of 4,4′-dimethoxydibenzoyl (**9**) inside the $[Pd_6L_4]^{12+}$ nanocage **1c** (drawn in Fig. 1). (a) Empty **1c**, showing a single set of pyridine resonances. (b) [(**9**)$_2$ ⊂ **1c**]. Six PyH^{α} protons are observed at $\delta = 9.35$–9.8 ppm and six PyH^{β} protons at $\delta = 8.35$–9.2 ppm. Spectra reproduced with permission from Ref. [42]. Copyright Wiley-VCH Verlag GmbH & Co. KGaA.

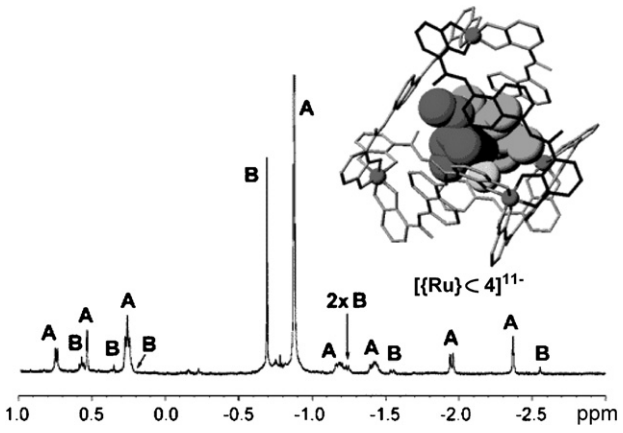

Fig. 6. Partial ^{1}H NMR spectrum (500 MHz, D_2O) of the host-guest complex $[\{Cp^{*}(Ru(2\text{-ethylbutadiene})(H_2O)\} \subset \mathbf{4}]^{11-}$, reflecting the large diastereomeric excess (70%, A = major diastereomer, B = minor diastereomer). A model of the Λ,Λ,Λ-(*S*) diastereomer is shown. Reprinted with permission from Ref. [65]. Copyright (2004) American Chemical Society.

host–guest assemblies $[(\mathbf{\mathit{S}\text{-}10})_2 \subset \mathbf{5b}]^{8+}$ do not resolve, probably due to the absence of an aromatic ring in the guest [66].

In addition to the most commonly used NMR-active isotopes (^{1}H, ^{13}C, ^{19}F and ^{31}P), coordination complexes may contain a useful NMR probe in the metal itself. Isotopes such as ^{7}Li ($I = 3/2$, 92.6% abundance), ^{103}Rh ($I = 1/2$, 100%), ^{107}Ag ($I = 1/2$, 51.8%), ^{109}Ag ($I = 1/2$, 48.2%), ^{195}Pt (I = 1/2, 33.8%), ^{199}Hg ($I = 1/2$, 16.9%) and ^{207}Pb ($I = 1/2$, 22.6%) are sometimes an adequate tool for the investigation of metallosupramolecular assemblies. The chemical shifts of these nuclides expand over very wide ranges and are usually extremely sensitive to their immediate environment. Additionally, structural information can be read-out from the coupling patterns induced by these isotopes in the spectra of other, more common, nuclei, such as ^{1}H or ^{31}P.

We have already mentioned ^{7}Li NMR spectroscopy (Fig. 3). Another nice application of this isotope is the investigation of a solvent-dependent monomer–dimer equilibrium involving the lithium-controlled assembly of dinuclear Ti^{IV} catecholate complexes (Fig. 8) [39]. In d^6-DMSO, a solvent with a great tendency to coordinate the Li^+ ions, the dimer $Li[(\mu\text{-}Li)_3\{L_3Ti\}_2]$ (**11**) is destabilized and only the resonance of the solvated Li^+ cations of the monomer $Li_2[L_3Ti]$ (**12**) is observed, at $\delta(^{7}Li) = -0.53$ ppm. In d^8-THF, on the contrary, a monomer–dimer equilibrium

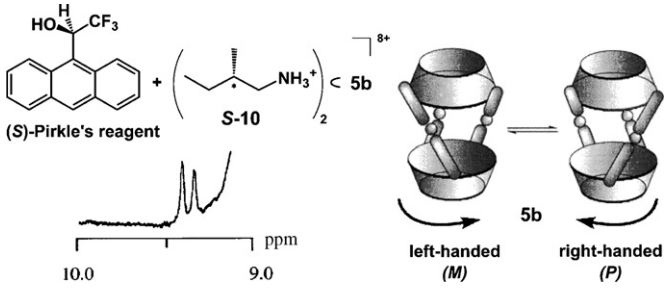

Fig. 7. A section of the ^{1}H NMR spectrum (600 MHz, $Cl_2CDCDCl_2$), of $[(\mathbf{\mathit{S}\text{-}10})_2 \subset \mathbf{5b}]^{8+}$ in the presence of (*S*)-Pirkle's reagent. Reprinted with permission from Ref. [66]. Copyright (2001) American Chemical Society.

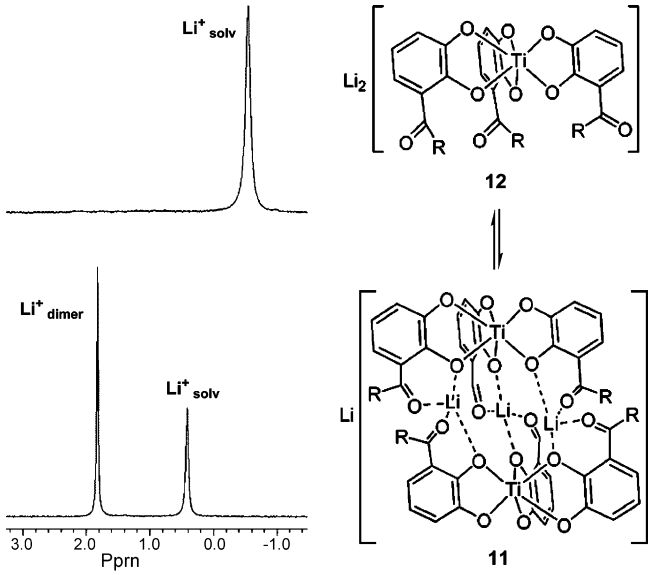

Fig. 8. ^{7}Li NMR (194.3 MHz) investigation of the equilibrium involving the lithium-controlled assembly of dinuclear catecholate complexes. Top: ^{7}Li NMR spectrum of "$Li_2[L_3Ti]$" (R = H) in d^6-DMSO, showing the resonance of solvated Li^+ in the monomer **12**. Bottom: same spectrum in d^8-THF, showing an additional signal for Li^+ bound in the dimer **11**. Reprinted with permission from Ref. [39]. Copyright (2005) American Chemical Society.

exists, and two ^{7}Li resonances are detected at $\delta = 0.41$ ppm and $\delta = 1.82$ ppm, for solvated and complexed Li^+, respectively.

^{195}Pt, together with ^{31}P NMR, has been used to elucidate the structure of the self-assembled water-soluble triplatinacyclophanes **13a–c** (Scheme 5) [67]. The $^{195}Pt\{^{1}H\}$ NMR spectra display a triplet at $\delta \approx -3940$ ppm, with $^{1}J_{PtP} \approx 2450$ Hz, which unequivocally points to a *trans*-P–Pt–P arrangement in the macrocycles. On the contrary, the non-water-soluble triplatinacyclophanes **14a–c** display a *cis*-P–Pt–P arrangement, showing a triplet in the ^{195}Pt NMR spectra at $\delta \approx -4420$ ppm with $^{1}J_{PtP}$ in the range 3600–3668 Hz [68]. The molecular rectangle **15** (Scheme 6) [69] has also been characterized by ^{195}Pt NMR. A single resonance is observed at −4517 ppm, appearing as a doublet of doublets due to the coupling with the two inequivalent ^{31}P nuclei ($^{1}J_{PtP} = 3629$ and 1535 Hz).

Lehn and co-workers have extensively used ^{109}Ag NMR spectroscopy to characterize Ag^{I} grid-type metalloarchitectures [70–72]. For the [3 × 3] grid **16**, self-assembled from nine Ag^+

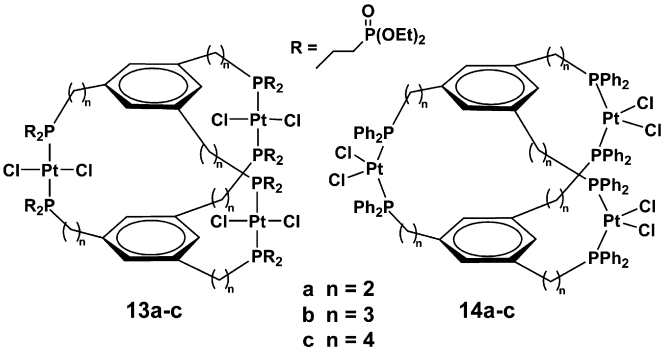

Scheme 5. Cage-structured triplatinacyclophanes **13a–c** and **14a–c**.

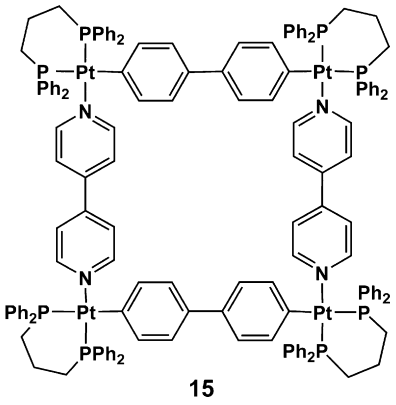

Scheme 6. Molecular rectangle **15**.

ions and six tritopic N-donor ligands (Fig. 9) [70], the ^{109}Ag NMR spectrum shows the expected 4:4:1 resonances (576.1, 507.6 and 406.1 ppm), for the silver ions located at the corners, the midpoints of the edges and the center of the grid, respectively. The self-assembly of multinuclear Ag^+ coordination species containing chiral bipyridine ligands of the CHIRAGEN family has also been investigated by ^{109}Ag NMR [73]. At low temperature and high pressure, an equilibrium between hexa- and tetranuclear circular helicates was detected. The same research group [74] has used ^{207}Pb NMR data to characterize the linear coordination array **17**, formed by binding of five Pb^{2+} ions to an helical polyheterocyclic strand, which undergoes complete uncoiling upon complexation (Scheme 7). The ^{207}Pb NMR spectrum of **17** displays three signals in a 1:2:2 ratio (δ = 1653, 1143 and 1139 ppm), corresponding to Pb^{II} nuclei in three different chemical environments. The "uncoiling" of the ligand is promoted by a change from a *transoid*,*transoid* conformation, leading to helical winding, to an induced *cisoid*,*cisoid* conformation, resulting from tridentate coordination to the Pb^{II} ion. This system represents thus a motional dynamic device. A related application has been recently reported [75].

Hawthorne and co-workers have investigated the host–guest chemistry of macrocyclic multidentate mercuracarborands [76–78]. The sequential reaction of [12]mercuracarborand-4 (**18**) (δ_{Hg}^{199} = −1212 ppm) with $^{n}Bu_4NI$ to generate **18**·I^- (δ_{Hg}^{199} = −810 ppm) and **18**·I_2^{2-} (δ_{Hg}^{199} = −714 ppm) was followed by ^{199}Hg NMR spectroscopy (Fig. 10) [77].

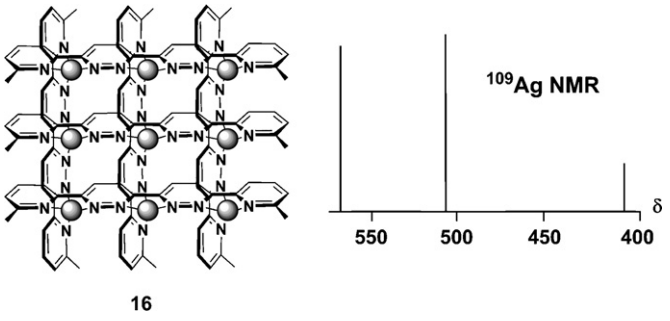

Fig. 9. Left: Self-assembled [3x3] grid complex $[Ag_9L_6]^{9+}$ (**16**) (L = 6,6′-bis[2-(6-methylpyridyl)]-3,3′-bipyridazine). The spheres represent Ag^+ ions. Right: Schematic representation of the ^{109}Ag NMR spectrum (CD_3NO_2) of **16**.

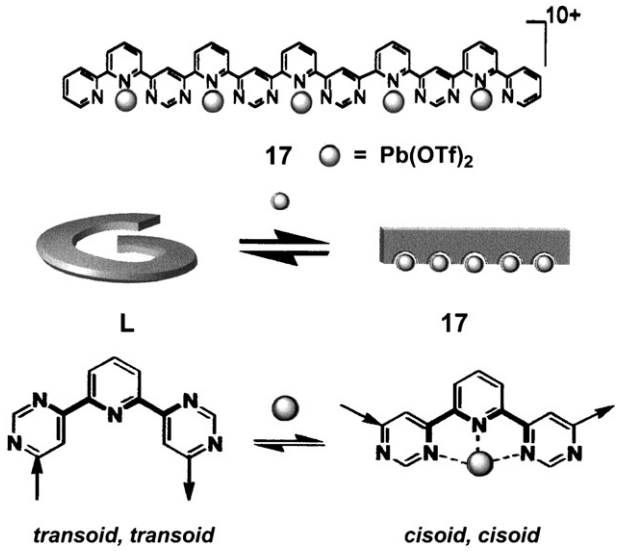

Scheme 7. Up: Structure of the extended rack-type complex **17**. Down: Schematic representation of the ion-triggered molecular dynamic device interconverting the helical free ligand and the extended linear multinuclear complex **17**. Reproduced from Ref. [74]. Copyright (2002) National Academy of Sciences, USA.

A very recent example of ^{1}H NMR monitoring of a chemical process has been recently reported by Lehn and co-workers [40], who followed the interconversion of the tetrameric grid $[Co_4L_4]^{8+}$ (**19**) into the pincer complex $[Co(CH_3CN)_2L]^{2+}$ (**20**), over a period of 11 days (Fig. 11). The ^{1}H resonances of these species are spread over a wide range of ppm (−40 to +70), due to their paramagnetic nature, but they are sharp and resolved, which is not often the case in paramagnetic compounds. In another application involving paramagnetic species, the formation of the dinuclear Co^{II} helicate **21** (Scheme 8) was followed by ^{1}H NMR titration [79]. Upon slow addition of $CoCl_2$, the diamagnetic peaks of the free ligand were steadily replaced by a single set of paramagnetically shifted peaks (from −30 to +35 ppm) of the helicate.

2.2. 2D NMR spectroscopy

The dispersion of the NMR spectrum into a second (and even a third and a fourth!) dimension has opened new perspectives for the use of NMR spectroscopy. Conventional 2D NMR experiments have become very popular since they efficiently map out interactions within, or sometimes between the molecules [80]. These interactions can be divided in through-bond (scalar) couplings, detected mainly by COSY, TOCSY, HMQC and HMBC experiments, or direct, through-space couplings, detected by NOESY and ROESY experiments. A third type of interaction, chemical exchange, will be discussed in the next section. A division between homonuclear and heteronuclear techniques can be made as well, depending on whether the interactions are detected between the same or different type of nuclides. In the next paragraphs we discuss some representative applications of the usual 2D NMR techniques to the investigation of metallosupramolecular assemblies.

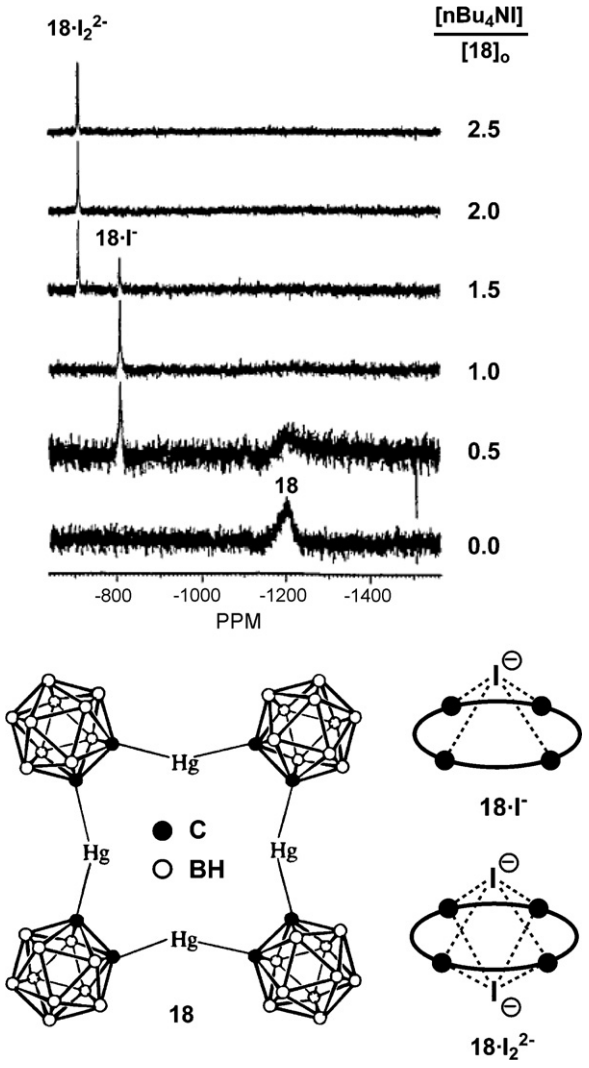

Fig. 10. Up: ^{199}Hg NMR (80.6 MHz, d^6-acetone) spectra illustrating the sequential reaction of [12]mercuracarborand-4 (**18**) with added ^{n}Bu$_4$NI. Down: Structure of **18**, **18**·I$^-$ and **18**·I$_2^{2-}$. Reprinted with permission from Refs. [77,78]. Copyright (1994, 1996) American Chemical Society.

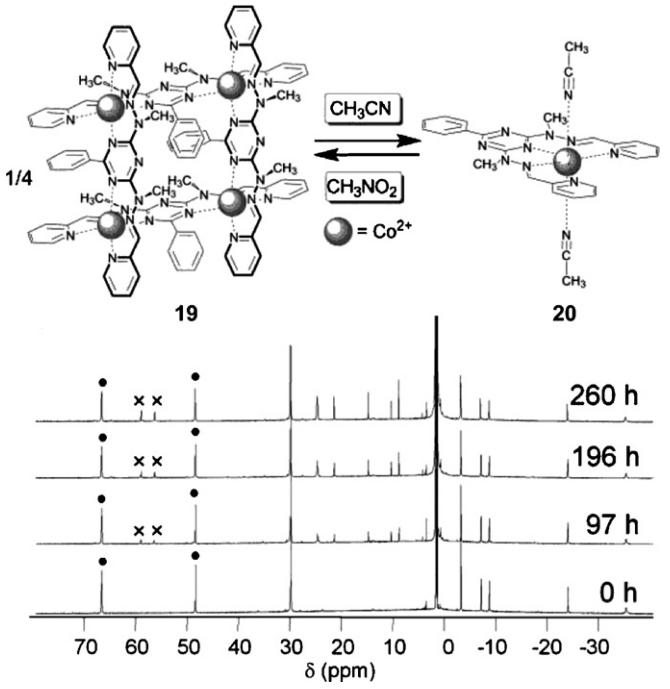

Fig. 11. Scheme and ^{1}H NMR spectra (400 MHz, CD_3CN, 55 °C) of the partial conversion of the grid $[Co_4\mathbf{L}_4]^{8+}$ (**19**, ●) into the pincer-like complex $[Co(CH_3CN)_2\mathbf{L}]^{2+}$ (**20**, ×). Reproduced from Ref. [40] with permission of The Royal Society of Chemistry.

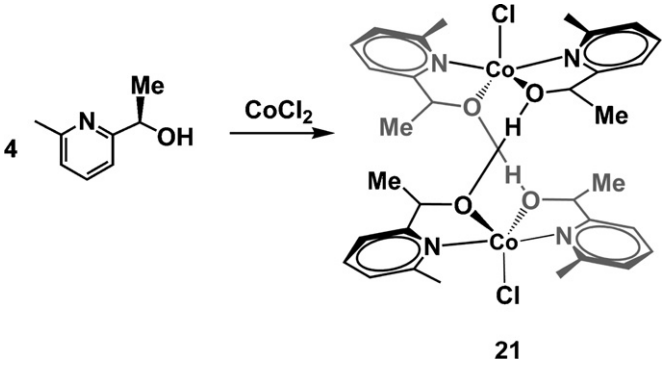

Scheme 8. Formation of the dinuclear Co^{II} helicate **21**.

2.2.1. COSY and TOCSY

Probably, the most used homonuclear 2D NMR experiment is the ^{1}H,^{1}H COSY (Correlation Spectroscopy) spectrum, which was also the first 2D pulse sequence proposed [81]. In all its different variants (absolute-value or phase-sensitive, with or without gradients, DQF, COSY-β, LR COSY, etc.) [82] this technique maps nuclei sharing a mutual scalar coupling within a molecule and thus it is a quick method to establish connectivities. Although it is most often used in ^{1}H spectroscopy, the methodology is equally applicable to any high-abundance nuclide, such as ^{31}P or ^{19}F.

There are many reports in the literature of the use of COSY experiments for the assignment of the ^{1}H resonances of metallosupramolecular species. For example, this methodology has been recently applied to characterization of the Ru^{II}/M^{II} heterometallomacrocyles **22a–c** (Scheme 9), for which the protons of the bpy and qtpy ligand could thus be distinguished [83]. Cohen and co-workers have used long-range (LR) ^{1}H COSY

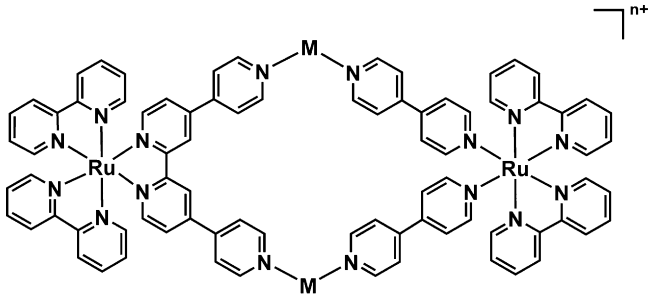

22a M = [Pd(en)]$^{2+}$; n = 8
22b M = [ReCl(CO)$_3$]$^+$; n = 4
22c M = [Pt(en)]$^{2+}$; n = 8

Scheme 9. Ru^{II}/M^{II} heterometallomacrocyles **22a–c**.

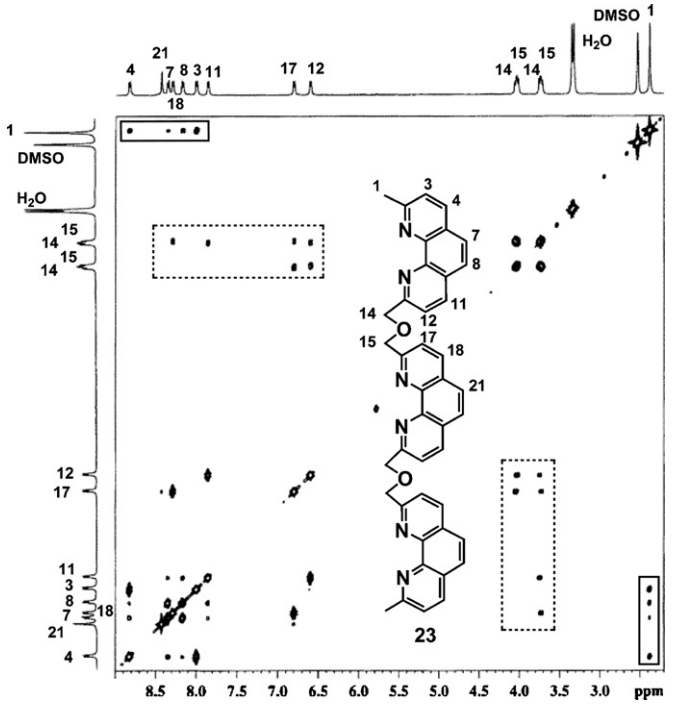

Fig. 12. LR ^{1}H COSY spectrum (500 MHz, d^{6}-DMSO) of the trinuclear double-stranded helicate $[(\mathbf{23})_2Cu_3]^{3+}$. Cross-peaks between the methyl protons H1 and the neighboring aromatic protons H3,H4 and even H7,H8 can be identified (rectangle), as well as between the methylene protons H14,H15 and the aromatic protons H11,H12,H17,H18 (dotted rectangle). Reprinted with permission from Ref. [86]. Copyright (1999) American Chemical Society.

experiments [84] for the characterization of trinuclear double-stranded helicates of general formula $[L_2M_3]^{3+}$ (M = Cu, Ag), where L is a phenanthroline-containing ligand [85,86]. Fig. 12 shows the LR ^{1}H COSY spectrum of the helicate $[(\mathbf{23})_2Cu_3]^{3+}$, for which couplings through up to eight bonds within the ligands can be clearly detected [86].

Another useful homonuclear 2D experiment is the Total Correlation Spectroscopy (TOCSY) [87], also called HOHAHA (Homonuclear Hartmann–Hahn). This technique is able to establish homonuclear correlations between *all* nuclei that sit within the same spin system, regardless of whether they are themselves coupled to one another. Such a feature is particularly advantageous for complex molecules with long sequences of coupled protons, which often result in ambiguities due to cross-peak overlap in the COSY spectra. Indeed, ^{1}H TOCSY experiments are frequently used in conjunction with COSY and graphical examples can be found in some of the references cited in this review [57,64,88–90]. In a recent application, Raymond and co-workers [27] have used a ^{1}H TOCSY experiment to confirm the encapsulation of [CpRu(*cis*-1,3,7-octatriene)]$^{+}$ ions inside the $[Ga_4L_6]^{12-}$ capsule **4**. Two independent cod spin systems could be distinguished in the spectrum of the inclusion complex due to the presence of two diastereomeric host–guest complexes. No such 16e^{-} Ru^{II} species had been previously isolated, and its stabilization in this case suggests that the supramolecular host structure **4** might be functioning as a large and non-coordinating counter ion [27].

2.2.2. HMQC, HSQC and HMBC

Correlations through the chemical bonds between different nuclides are established by means of the so-called heteronuclear shift correlations. Usually, these experiments are used to map connectivities between ^{1}H and ^{13}C, although ^{1}H,^{31}P and ^{1}H,^{15}N correlations are also common. Correlations to NMR-active metallic nuclides, such as ^{195}Pt or ^{107}Ag are possible as well. In their modern versions, all these ^{1}H,X experiments use ^{1}H detection (inverse techniques), with a considerable gain in sensitivity with respect to the older, heteroatom-detecting versions. Thus, the chemical shifts of the low-γ nuclides are determined indirectly in the second dimension of the spectra, avoiding the need for its direct, usually long-time requiring, observation [82]. The most common heteronuclear shift correlations are the HMQC [91] (Heteronuclear Multiple-Quantum Correlation) and HSQC [92] (Heteronuclear Single-Quantum Correlation) experiments, providing single-bond connectivities [93], and the HMBC [94] (Heteronuclear Multiple-Bond Correlation) correlation, providing long-range multiple-bond correlations, usually over 2 or 3 bonds. HMBC spectra are particularly useful, as they allow the assignment of quaternary carbon atoms through their correlations with the neighbouring protons. Connectivities across heteroatom linkages can also be frequently traced, piecing together otherwise uncorrelated molecular fragments.

The combination of one and long-range ^{1}H,^{13}C correlations usually allows the complete assignment of the molecular skeleton in organic molecules. Graphical examples of the application of these techniques to the characterization of metallosupramolecular assemblies can be found in many of the references cited in this review [27,30,85,86,88,95,96]. On the contrary, there are not so many applications of ^{1}H,X correlations where X is a metallic nuclide. Some nice examples have been reported by Lehn and co-workers, who have used ^{1}H,^{207}Pb HMQC experiments to characterize a series of linear coordination arrays such as **17** (drawn in Scheme 7) and related structures [74,75]. Fig. 13 shows the ^{1}H,^{207}Pb HMQC spectrum of the linear, rack-type complex **24**, formed by Pb^{II} complexation of an helical molecular strand [75]. Three resonances are indirectly observed in the ^{207}Pb dimension, confirming the presence of three types of Pb^{II} ions. The same research group [97] has very recently used a ^{1}H,^{107}Ag HMQC experiment to characterize the double-helical complex **25**, formed by Ag^{I} complexation of an hydrazone-based ligand which retains its helical shape (Fig. 14). **25** and related complexes form polymeric, wire-like highly ordered solid-state structures. In another report [72], a ^{1}H,^{107}Ag HMBC experiment was used to characterize the $[Ag_6L_5]^{6+}$ aggregate **26** (Scheme 10) closely related to the $[Ag_9L_6]^{9+}$ grid **16** drawn in Fig. 9. These grids form when a solution of Ag^{I} is added to a solution of the ligand in the adequate stoichiometry (9:6 for **16** and 6:5 for **26**).

2.2.3. NOESY and ROESY

While both the COSY and TOCSY experiments rely on *scalar couplings* between nuclei (indirect couplings through the electrons of the chemical bonds), the NOESY [98] (Nuclear Overhauser Spectroscopy) experiment relies on direct, through-space magnetic interactions (*dipolar couplings*), which give rise

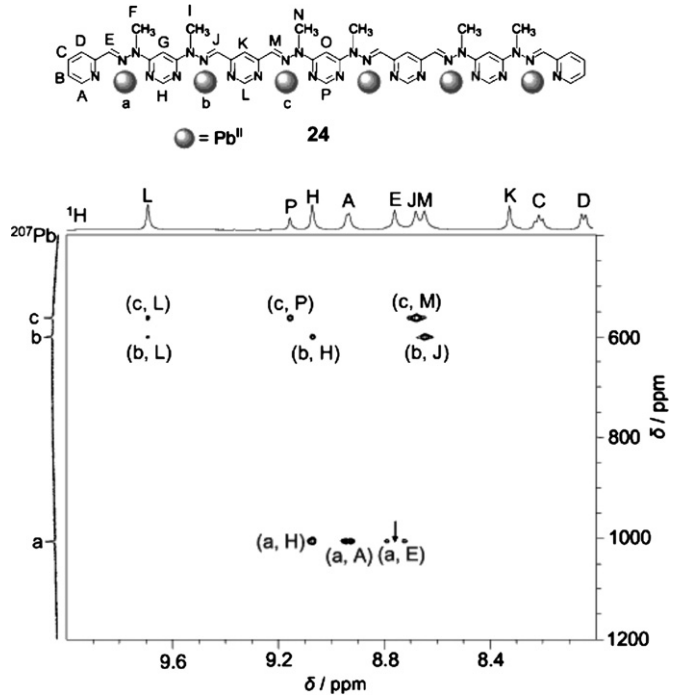

Fig. 13. ^{1}H,^{207}Pb HMQC spectrum (500 MHz, 1:1 CD_3CN/CD_3NO_2) of the rack-type complex **24**, formed by Pb^{II} complexation of an helical sequence of hydrazone–pyrimidine units. Reproduced with permission from Ref. [75]. Copyright Wiley-VCH Verlag GmbH & Co. KGaA.

to the nuclear Overhauser effect (NOE) [99]. The NOE decreases rapidly with the distance between the nuclei ($\propto d^{-6}$), and thus the ^{1}H NOESY spectrum only relates protons which are *spatially close to each other* (typically, closer than 5 Å), even if they are not connected by chemical bonds. The NOE is also closely related to the molecular motion in solution, being positive for small, rapidly tumbling molecules and negative for large molecules or at low temperatures. In an intermediate situation (mid-sized molecules with a mass of ca. 1000–2000 Da) the NOE can be very small or even zero [100]. In this situation the so-called Rotating Frame NOE (ROE) [101] may be used as an alternative, as this effect never becomes zero [102]. Thus, 2D ROESY experiments [103], although experimentally more challenging than NOESY, are frequently used in supramolecular chemistry, where large-sized species are the main object of investigation. The main feature of NOESY and ROESY experiments is their ability to provide in a single experiment all the spatial couplings within a molecule, being thus a very valuable tool for the elucidation of the 3D molecular geometry. In a recent example [90], a ^{1}H NOESY experiment has allowed the elucidation of a β-turn conformation for the peptide **27** when included inside the hydrophobic cavity of the hexanuclear prism-like porphyrin cage **28** (Fig. 15). As shown in the Fig., NOE cross-peaks were clearly detected between the N-terminal acetyl group *a* and the Ala 3 protons *g*,*j* of **27**, indicating the proximity of the N- and C-terminals due to the turn conformation [90]. It was concluded that this conformation, very unstable in short peptides, is stabilized due to an efficient host–guest interaction. The stabilization of the α-helical structure of a more complex peptide within a dimeric capsule formed by a $[Pt_6L_4]^{12+}$ bowl has been similarly proven [89].

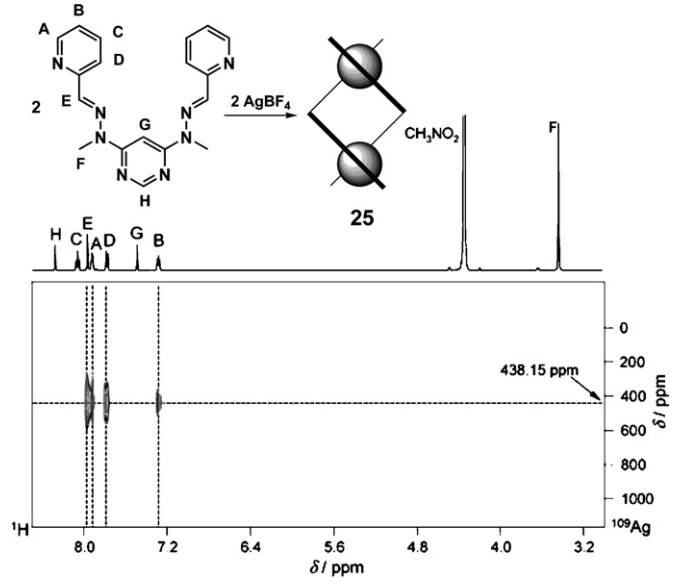

Fig. 14. ^{1}H,^{107}Ag HMQC spectrum (500 MHz, CD_3NO_2) of the dinuclear helical complex **25**, The coupling of the protons A, B, D and E with the Ag^{I} ion is detected. The ^{107}Ag chemical shift is read-out at 438 ppm (reference, $AgNO_3$). Reproduced with permission from Ref. [97]. Copyright Wiley-VCH Verlag GmbH & Co. KGaA.

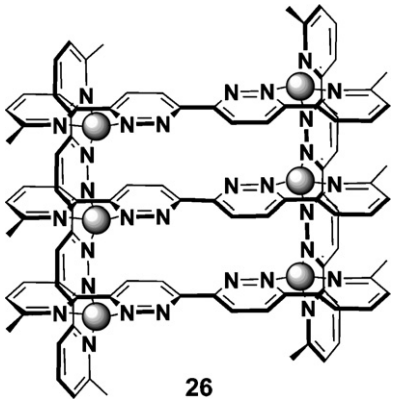

Scheme 10. Self-assembled [2 × 3] grid complex $[Ag_6L_5]^{6+}$ **26** (L = 6,6′-bis[2-(6-methylpyridyl)]-3,3′-bipyridazine). The spheres represent Ag^{+} ions.

A very interesting phenomenon in supramolecular chemistry is the self-recognition (or self-sorting), consisting in a preferential binding of like metal ions by like ligands in mixtures undergoing dynamic coordination equilibria. This phenomenon has been observed by Lehn and co-workers in the self-assembly of double and triple multinuclear helicates from mixtures of polypyridine ligands [104]. In a particular example [105], the selective parallel association of the ligand strands in the double helicate $[Cu_2Zn(\mathbf{29})_2]^{4+}$ (Scheme 11) was confirmed by a ^{1}H ROESY spectrum. Spatial contacts between the terminal methyl group of one strand and the methylene group from the same terminal in the second strand were detected. This parallel orientation is dictated by the preference of Cu^{I} and Zn^{II} cations for tetrahedral and octahedral geometries, respectively [105].

A ^{1}H ROESY spectrum has also confirmed the structure of the [3]catenate **30** (Scheme 12), formed by palladium-directed self-

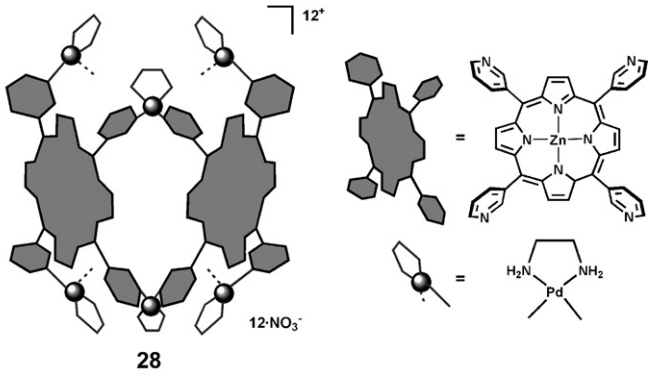

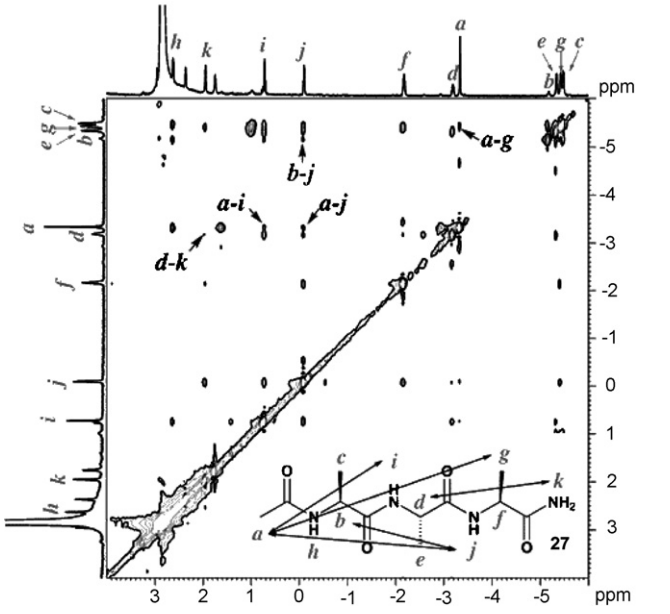

Fig. 15. ^{1}H NOESY spectrum (500 MHz, $H_2O/D_2O = 9.1$, 27 °C) of the host–guest complex **27** ⊂ **28**, allowing the elucidation of the β-turn conformation for the included peptide. Spectrum reprinted with permission from Ref. [90]. Copyright (2006) American Chemical Society.

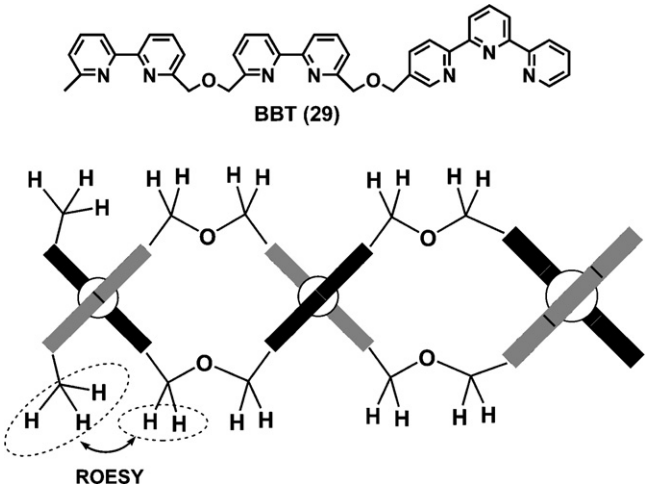

Scheme 11. Proximity of the protons of the terminal CH_3 group of one tritopic BBT (bipyridine, bipyridine, terpyridine) strand (**29**) to the methylene protons of the second strand in the parallel-stranded double helicate $[Cu_2Zn(\mathbf{29})_2]^{4+}$, as shown by the ^{1}H ROESY experiment.

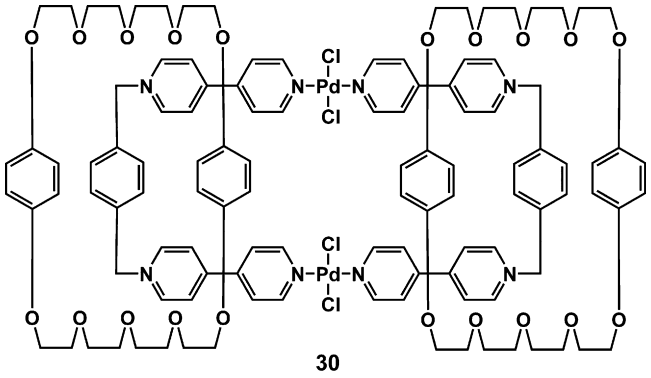

Scheme 12. Schematic drawing of the [3]catenate **30**, formed by palladium-directed self-assembly of a ligand based on 4,4′-bipyridinium, together with π donor/acceptor interactions with a dioxoaryl cyclophane.

assembly in conjunction with π donor/acceptor interactions. The location of the hydroquinol units inside the cavity of the metallomacrocycle was confirmed by ROE cross-peaks between the aromatic protons of the hydroquinol units and both the bipyrididium and phenylene protons of the nitrogenated ligand [95]. Fig. 16 shows the ^{1}H ROESY spectrum of the molecular rectangle **15** [69]. ROEs from the bipyridyl protons to both adjacent biphenyl and phosphine phenyl protons support the presence of *cis* biphenyl and bipyridyl units alternating in the ring.

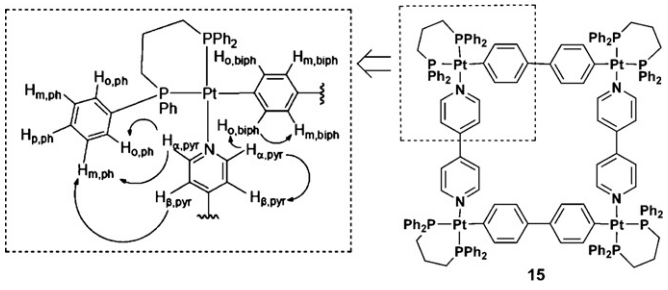

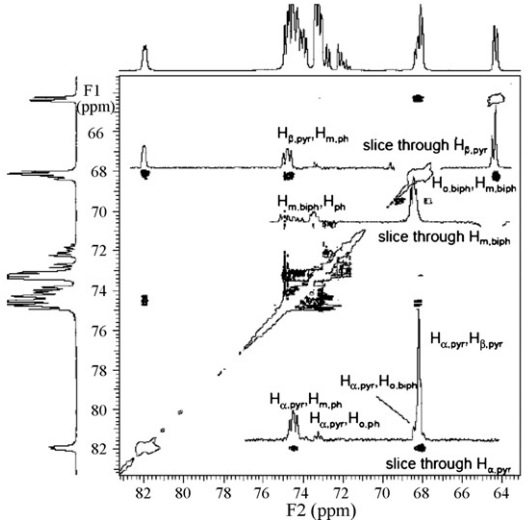

Fig. 16. ^{1}H ROESY spectrum of the molecular rectangle **15**. Key through-space contacts between $H_{\alpha,pyr}$ and $H_{\beta,pyr}$, $H_{o,biph}$, $H_{o,ph}$ and $H_{m,ph}$, as well as between $H_{\beta,pyr}$, and $H_{m,ph}$ are indicated by arrows and annotations in the amplified section of the drawn structure. Reprinted with permission from Ref. [69]. Copyright (2004) American Chemical Society.

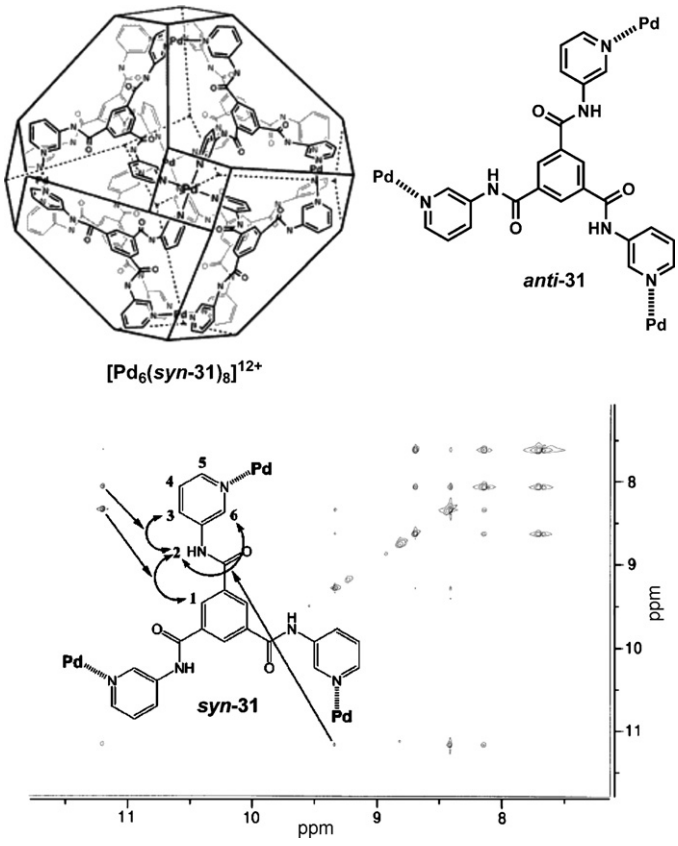

Fig. 17. ^{1}H ROESY spectrum (300 MHz, d^6-DMSO) of the truncated octahedral nanocage $[Pd_6(\mathbf{31})_8]^{12+}$. The observed cross-peaks indicate that the only species present in solution is the isomer with the ligand **31** in the *syn* conformation. While the coupling between H1 and H2 is present regardless of the ligand conformation, the strong coupling between H2 and H3 is expected only for the *syn* conformation. Reprinted with permission from Ref. [106]. Copyright (2006) American Chemical Society.

Sometimes selective NOE or ROE contacts allow the distinction between two isomeric structures. An example is shown in Fig. 17 for the truncated octahedral nanocage $[Pd_6(\mathbf{31})_8]^{12+}$ [106]. This species has been found by X-ray diffraction studies to exist in the solid-state as a 3:2 mixture of two conformational isomers, depending on the *syn* or *anti*-conformation of the tridentate ligand **31**. In solution, on the contrary, the ^{1}H spectrum reflects the presence of a single isomer. As shown in the figure, the ^{1}H ROESY spectrum has allowed the assignment of this isomer as the *syn* product, on the basis of the stronger coupling found between H2 and H3 (as expected for the *syn* conformation) than between H2 and H6 (as expected for the *anti*-conformation).

NOE/ROE contacts between an encapsulated guest and the inner protons of the host are especially useful to confirm the formation of a host–guest complex, as well as to elucidate the orientation of the guest within the cavity. Thus, for the self-assembled $[Ag_4L_2]^{4+}$ resorcinarene-based capsule **32** (Scheme 13) [107], NOE cross-peaks were found between the methylene and aromatic protons H_c, H_d and H_f of the capsule and the methyl protons of a 4,4′-diacetoxybiphenyl guest (not drawn), consistent with the situation of the methyl groups of the guest close to each end of the cavity. In another example, the enclathration of 1,3,5-triphenyl-2,4,6-triazine **33**

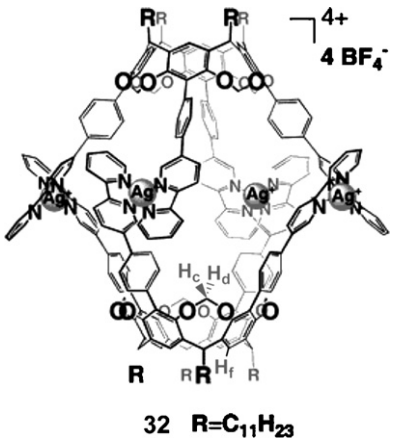

Scheme 13. Self-assembled $[Ag_4L_2]^{4+}$ resorcinarene-based capsule **32**. Reproduced from Ref. [107] with permission of The Royal Society of Chemistry.

inside the palladium-clipped aromatic sandwich **34** (Scheme 14) has been confirmed by the appearance of NOE cross-peaks between the protons H_j of the guest and H_f of the host [88]. Raymond and Tiedemann [57] have investigated inclusion complexes within the $[Ga_4L_6]^{12-}$ cluster **4** (drawn in Fig. 3). ^{1}H NOESY spectra were measured for complexes with guests such as Et_4N^+ [108] and $[CpRu(\eta^6\text{-}C_6H_6)]^+$ [109]. In particular, for the host–guest assembly $[\{CpRu\{\eta^6\text{-}C_6H_5(CH_2)_6SO_3\}\subset \mathbf{4}]$, NOEs were found between the phenyl and Cp protons of the guest and the host naphthalene protons, but *not* with the host catechol protons, indicating that the cationic "head" of the guest is buried deep within the host cavity, near the naphthyl ring walls [57]. Fujita and co-workers have also reported many applications of ^{1}H NOESY experiments to the investigation of host–guest assemblies. Thus, the AND/OR bimolecular recognition of sets of two different guests by the $[Pd_6L_4]^{12+}$ cage **1b** [110] (drawn in Fig. 1) was confirmed by the presence of NOE cross-peaks between the two encapsulated guests. The same group has very recently reported the hexanuclear Pd^{II} assembly **35**, where a porphine sandwhich is encapsulated inside an organic-pillared

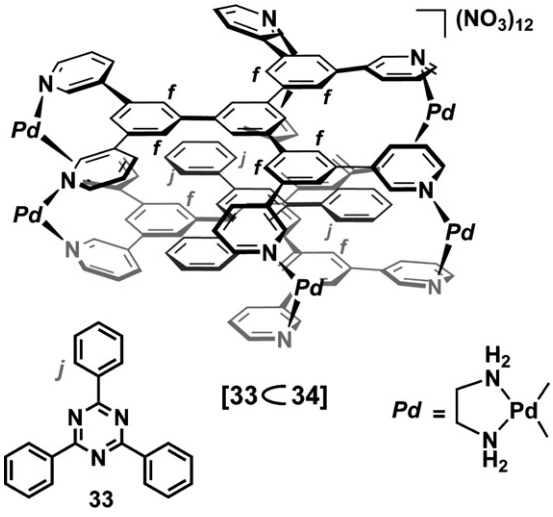

Scheme 14. Host–guest complex between the Pd-clipped aromatic sandwich **34** and 1,3,5-triphenyl-2,4,6-triazine **33**.

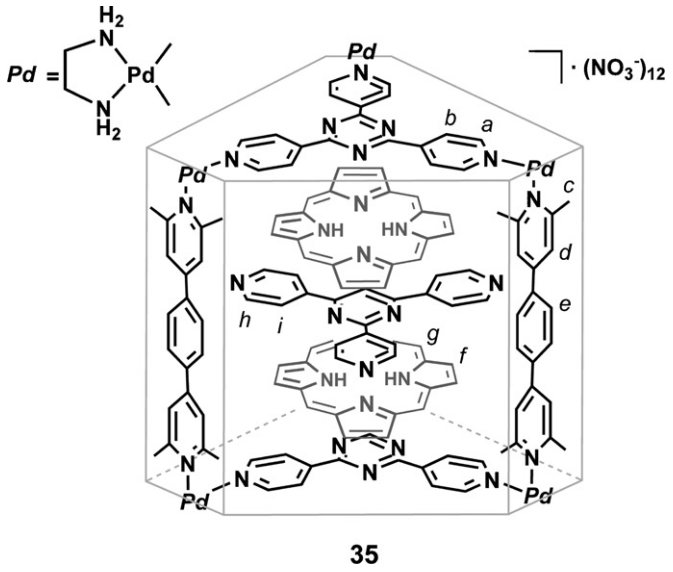

Scheme 15. Host–guest complex **35**, between a porphine sandwich and an organic-pillared hexanuclear coordination cage.

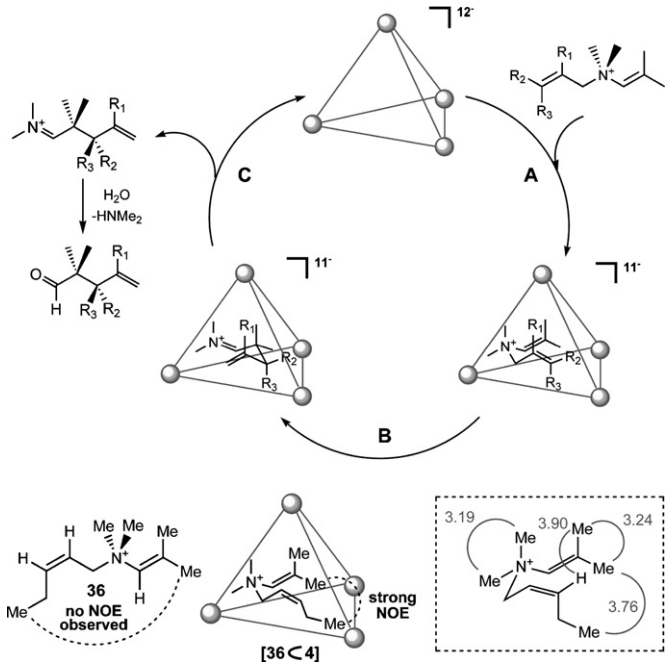

Scheme 16. Up: Proposed catalytic cycle for the cationic 3-aza Cope rearrangement catalyzed by the supramolecular tetrahedral structure $[Ga_4L_6]^{12-}$ **4**. Down: Conformations of the free and encapsulated substrate **36**. Dotted square: estimated distances (Å) between selected protons in the chairlike conformation of encapsulated **36**, as determined from NOE growth rates.

coordination cage (Scheme 15) [96]. A ^{1}H NOESY study supported the suggested situation of the guests inside the cage, as correlation signals were observed between the encapsulated tris-(4-pyridyl)triazine (H_h and H_i) and the middle portion of the pillars (H_d and H_e).

One of the most attractive applications of supramolecular nanocages is their utilization as "artificial enzymes" able to control chemical reactions by means of steric confinement and precisely positioned functional group interactions. In one interesting example Raymond and co-workers [33,34] have used their $[Ga_4L_6]^{12-}$ tetrahedral assembly **4** as a supramolecular catalyst for the aza-cope rearrangement of enammonium substrates. The proposed catalytic cycle is shown in Scheme 16. After encapsulation of the substrate (step A) a sigmatropic rearrangement leads to iminium cations (step B), which are subsequently hydrolyzed to the corresponding γ,δ-unsaturated aldehydes (step C). The inclusion of the substrate into the size- and shape-constrained cage results in a rate acceleration for the key enammonium–iminium arrangement step by up to three orders of magnitude, due to the selective binding of the substrate in the reactive chairlike conformation, bringing the two bond-forming carbon atoms into contact distances. This preorganization was nicely proven for the substrate **36** ($R^1 = R^2 = H$, $R^3 = Et$) by a ^{1}H NOESY spectrum of the host–guest complex [**36** ⊂ **4**] [34]. While the unbound substrate shows no NOEs between the pendant alkyl chains, the encapsulated enammonium cation displays strong dipolar couplings between the protons at the two distal ends of the molecules, as expected for a tight, chairlike conformation. NOE *growth rates* [111] were used to estimate the distances between selected protons in [**36** ⊂ **4**] [34]. The results, also shown in the scheme, confirm again the chairlike structure of the encapsulated substrate.

^{1}H NOESY spectroscopy is very useful for the characterization of ion pairs in solution, via the interionic NOE contacts [112,113]. In another chemical application of their polyvalent $[Ga_4L_6]^{12-}$ assembly **4**, Raymond and co-workers [32] have investigated the C–H activation reactions of aldehydes and ethers by encapsulated iridium complexes. A novel stepwise guest dissociation mechanism was found that proceeds via a strongly bound ion pair intermediate [114]. Thus, for the non-encapsulated $[Cp^*(PMe_3)Ir(Me)(PTA)]^+$ complex **37** (Fig. 18), NOE cross-peaks were found between the broad exterior Cp^* peaks of **37** and the three equivalent catecholate protons of **4** in the host–guest complex [NEt_4^+ ⊂ **4**], confirming the formation of the ion pair [NEt_4^+ ⊂ **4**]·(**37**) in D_2O. The Cp^* protons of **37** are shifted to 1.2 ppm from 1.87 ppm in the completely free complex, probably due to π-stacking interactions with the naphthalene ligand of **4**. NOE cross-peaks were also found between the encapsulated NEt_4^+ guest and the naphthalene protons of host **4** [32].

2.2.4. *Fluorinated compounds: ^{19}F NOESY and ^{1}H,^{19}F HOESY*

In spite of the high receptivity of ^{19}F nuclides, the extension of 2D NMR techniques to fluorinated compounds is complicated due to the dispersion of typical ^{19}F chemical shifts over 200 ppm, and the greater variation of the coupling constants [115]. These features pose technical problems such as the generation of pulses able to cover the entire chemical shift range, or the creation of the spin-lock necessary for a TOCSY experiment. Although through-space dipolar ^{19}F,^{19}F couplings are well known, very few publications (in all fields) describe the use ^{19}F NOESY experiments [115,116]. One example in supramolecular chemistry has been recently provided by Fujita and co-workers [117]. This research group has recently reported the synthesis

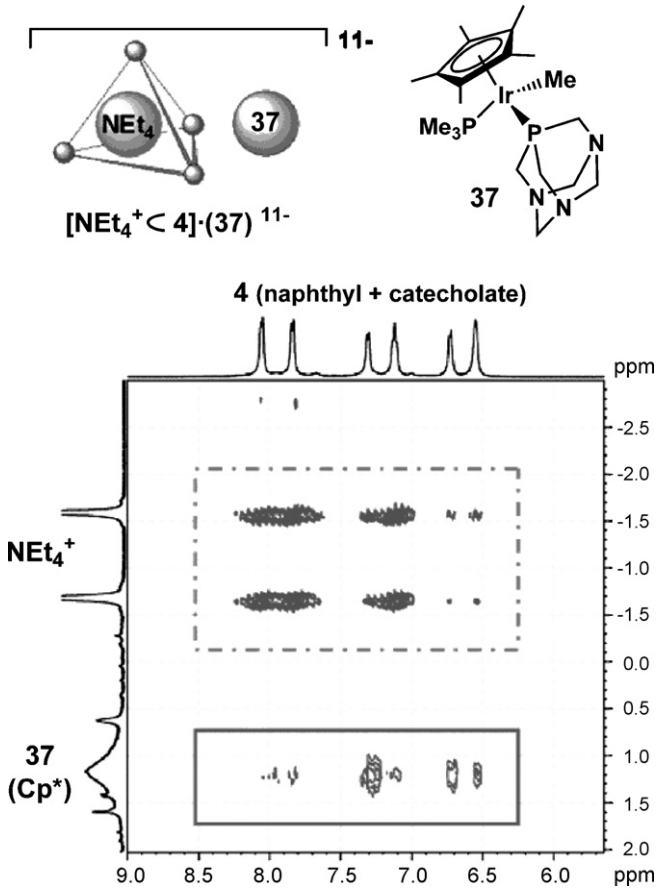

Fig. 18. Section of the ^{1}H NOESY (500 MHz, D_2O) spectrum of exterior **37** in ion pair with $[NEt_4^+ \subset \mathbf{4}]$ (**4** = $[Ga_4L_6]^{12-}$ in Fig. 3). The dashed box highlights correlations between the encapsulated NEt_4^+ with the three symmetry equivalent **4** host naphthyl protons. The solid box highlights correlations between the broad exterior Cp^* peaks of **37** and the three symmetry equivalent **4** host catecholate protons. Spectrum reprinted with permission from Ref. [32]. Copyright (2006) American Chemical Society.

of endofluorous "nanodroplets" **38a–d** (Fig. 19) consisting of self-assembled $Pd_{12}L_{24}$ nanocages where the bridging ligands contain perfluoroalkyl chains pointing inwards. The cuboctahedral symmetry of the cages was confirmed by the appearance of only one set of signals in the ^{1}H and ^{19}F NMR spectra. The ^{19}F resonances for the C_8F_{17} chains were assigned with the combined help of ^{19}F NOESY and ^{19}F COSY spectra (see figure). As it is usually the case in linear CF_2CF_2, four-bond ($^{4}J_{FF}$) couplings are stronger than the vicinal ($^{3}J_{FF}$) interactions [115].

Heteronuclear ^{1}H,^{19}F NOESY experiments (^{1}H,^{19}F HOESY, Heteronuclear Overhauser Effect Spectroscopy) are more common, especially in the field of transition metal complex ion pairs [113,118]. The HOESY [119] experiment detects heteronuclear through-space NOE interactions between non-bonded nuclei. Detection is carried out on the heteronucleus and thus, although HOESY spectra have been reported for several ^{1}H,X spin pairs (X = ^{13}C, ^{31}P, ^{19}F, ^{7}Li, ^{15}N) [102], the ^{1}H,^{19}F HOESY is the most favoured, due to the high receptivity of ^{19}F. Dalcanale and co-workers [46] have reported the use of quantitative ^{1}H,^{19}F HOESY experiments [120] to investigate the relative position of cation and anions in the coordination cage **3**. Fig. 20 shows how the encapsulated triflate anion displays NOE cross-peaks only with the OCH_2O protons (being the interaction stronger with the proton pointing *inwards*). Not surprisingly, it seems that the negatively charged sulfonate group of this inner $CF_3SO_3^-$ anion is pointed towards the positively charged Pd^{II} atoms, while the CF_3 group is oriented towards the OCH_2O moiety. The external triflate anions show the strongest contacts with the aryl protons of the dppp ligands and the methylene OCH_2O protons, suggesting that these anions are prevalently located on the "equatorial" plane containing the four Pd^{II} atoms. Weaker contacts are found between the external anions and the aliphatic and aromatic protons of the resorcinarene ligands, suggesting that at least two of the external triflates are located in the hydrocarbon pockets of these ligands. The same authors [121] have used ^{1}H,^{19}F HOESY experiments to investigate the relative cation–anion orientation in the self-assembled diplatinum or dipalladium cavitand frameworks [**39a**,**b**](OTf)$_8$ (Scheme 17). Interionic NOE contacts were selectively found in $CDCl_3$ between the OTf^- anions and *only* the protons of the tppb ligand and the pyridine groups (*not* with the protons of the cavitand cores), suggesting that the counterions are located close to the positively charged Pd^{II} centers. The interionic NOE contacts reveal the presence of strong ion pairs in chloroform, a common observation [122].

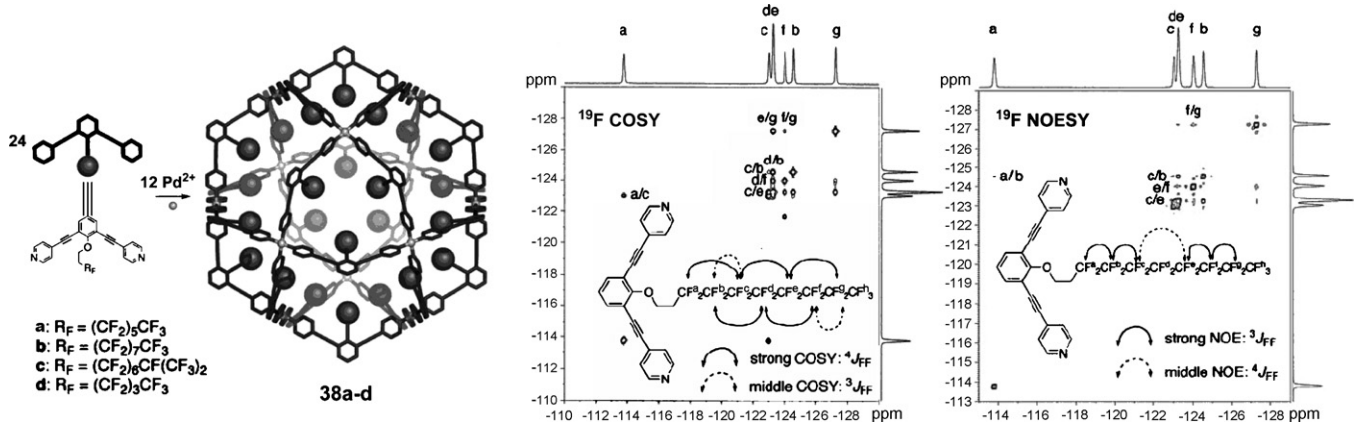

Fig. 19. Left: Self-assembly of endofluorous $Pd_{12}L_{24}$ molecular spheres **38a–d**. Right: ^{19}F NOESY and ^{19}F COSY spectra of ligand **b** (470 MHz, d^6-DMSO). From Ref. [117]. Reprinted with permission from AAAS.

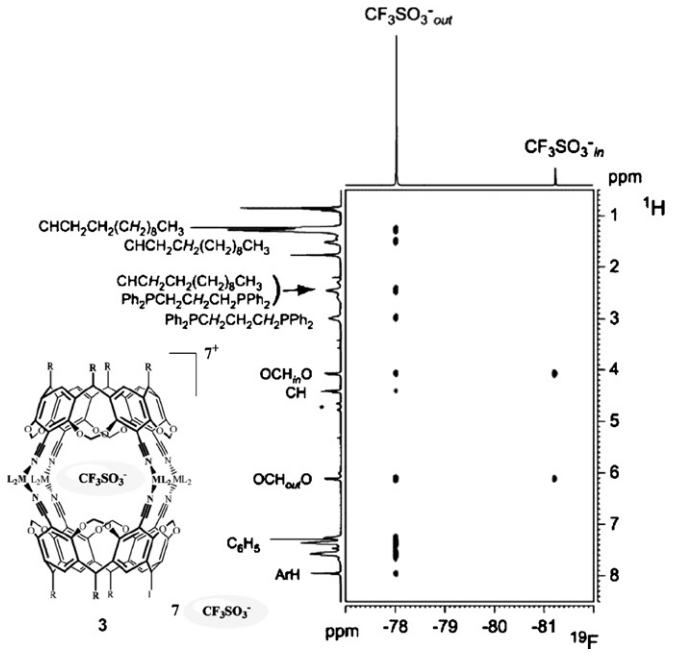

Fig. 20. $^{1}H,^{19}F$ HOESY spectrum (376.65 MHz, $CDCl_3$) of the coordination cage **3**, showing NOE cross-peaks between the external and encapsulated triflate anions and selected ^{1}H resonances of the host. Reprinted with permission from Ref. [46]. Copyright (2005) American Chemical Society.

2.3. Diffusion

We have chosen to dedicate a separate section to diffusion measurements, as this strategy is becoming increasingly popular in supramolecular chemistry. The self-diffusion coefficient (D) of a molecule is a measure of its mobility in solution and depends on the viscosity of the solvent and, most importantly, on the "effective" molecular size and shape. Thus, phenomena such as aggregation, encapsulation and other intermolecular and interionic interactions will be reflected on the measured D-value of a molecular species and can thus be investigated. Indeed, diffusion measurements are often used in conjunction with NOE to investigate intermolecular or interionic interactions, as shown in some recent reviews [112,118,122,123]. The following paragraphs aim to provide a short overview of the most common NMR techniques used for diffusion measurements, as well as some representative applications to coordination supramolecular chemistry.

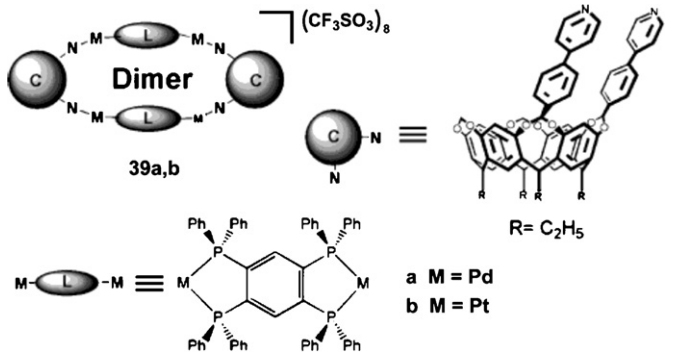

Scheme 17. Self-assembled nanoporous structures [**39a**,**b**](OTf)$_8$. Reprinted with permission from Ref. [121]. Copyright (2006) American Chemical Society.

2.3.1. PGSE measurements

The measurement of diffusion coefficients by NMR makes use of pulsed-field gradient spin-echo (PGSE) experiments [124]. Since the introduction of the basic PGSE sequence in 1965 [125], and especially with the generalization of gradient sets as standard equipment during the last decade, PGSE diffusion measurements have been applied in many different fields, such as the investigation of small organic, inorganic and organometallic molecules [112,118,126], dendrimers [127], polymers [128,129], zeolites [130], colloids and surfactants [131–133], liquid crystals [134,135], ionic liquids [136], medicine [137,138], biomolecules [139] and combinatorial and supramolecular chemistry [140–142]. Experimental and methodological aspects are described in many recent publications [122,123,143,144]. Some advantages of the PGSE methodology are the fast and non-invasive character of these measurements, as well as the requirement of only small samples. Moreover, several components of a mixture can be measured simultaneously, as long as they afford resolved NMR signals, making the technique especially valuable for the investigation of species in equilibrium. Although ^{1}H PGSE diffusion measurements are the most common, other nuclei such as ^{2}H [135], ^{3}He [138], ^{7}Li [129,145,146], ^{19}F [118,126,133], ^{31}P [132,146–148], ^{35}Cl [147,149] or ^{195}Pt [148] can be used as NMR probes in these experiments.

The size information is obtained from the diffusion coefficient via the Stokes–Einstein equation (Eq. (1)) [150], where k_B is the Boltzmann constant, T the absolute temperature, η the viscosity and r_H the hydrodynamic radius of the species under investigation. This r_H is the radius of a hypothetical sphere that diffuses with the same speed as the particle under examination and, thus, provides the information about the apparent size of the molecule, including any solvation, ion-pairing or other aggregation effects which may affect its mobility.

$$D = \frac{k_B T}{6\pi\eta r_H} \quad (1)$$

There are many examples in supramolecular chemistry of the use of PGSE diffusion measurements for the estimation of the size of supramolecular coordination complexes, including polymers [151] or oligomers [152]. In one of the first applications reported, Stang and co-workers [153] used PGSE measurements to assess the size of the nanoscopic metallocyclic dodecahedra **40a**,**b**, containing 60 Pt atoms (Scheme 18). The derived hydrodynamic diameters (5.2 and 7.5 nm, respectively) were comparable in size to those of small proteins and in good agreement with electrospray mass spectrometry (ESI-MS) and transmission electron microscopy (TEM) data.

A typical PGSE measurement is shown in Fig. 21 for the dimeric $[Ag_4L_2]^{4+}$ capsule **32** [107,154], already mentioned in Section 2.2.3. The results from the measurements on the capsule **32** (circles) and the resorcinarene ligand L (triangles) are displayed in the figure. The D-values are proportional to the slope of the regression lines [122,143,144].

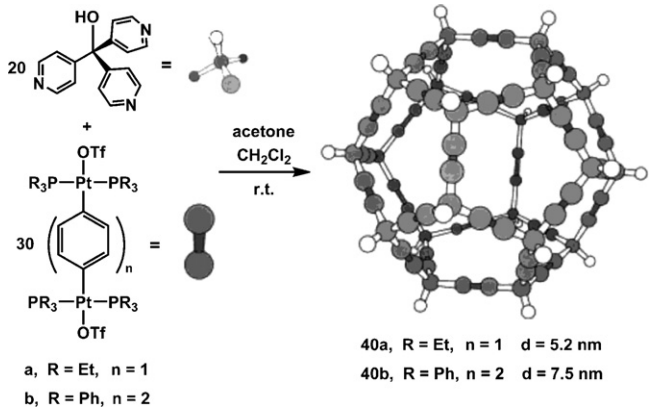

Scheme 18. Self-assembly of the nanoscopic dodecahedra **40a**,**b**. Reprinted with permission from Ref. [153]. Copyright (1999) American Chemical Society.

As expected, the value for the capsule (3.66×10^{-10} m^2 s^{-1}) is lower than for the ligand (4.79×10^{-10} m^2 s^{-1}) and the resulting ratio $D_{capsule}/D_{ligand} = 0.76$ is in reasonable agreement with the expected dimer/monomer ratio of ca. 0.72–0.75, based on theoretical calculations [107,154,155]. In a similar example, the dimeric structure of the cavitands [**39a**,**b**](OTf)$_8$ (drawn in Scheme 17) was also confirmed by ^{1}H PGSE measurements. The r_H determined for [**39a**](OTf)$_8$ in $CDCl_3$ (16.0 Å) is in good agreement with the average radius derived from Spartan calculations for a dimeric structure [121,156]. Cohen and co-workers [85,86] have also used ^{1}H PGSE diffusion measurements to confirm the double-stranded nature of the helicates [(**23**)$_2$Ag$_3$]$^{3+}$ and [(**23**)$_2$Zn$_3$]$^{6+}$ (see Fig. 12 for the structure of the ligand **23**). While the diffusion coefficients (in CD_3CN) of [(**23**)$_2$Ag$_3$]$^{3+}$ and [(**23**)$_2$Zn$_3$]$^{6+}$ were 0.72×10^{-5} cm^2 s^{-1} [86] and 0.81×10^{-5} cm^2 s^{-1} [85], respectively, the value for the free ligand was much higher (1.13×10^{-5} cm^2 s^{-1}).

A very interesting application of diffusion measurements is the investigation of interionic interactions in solution [126]. One can measure the diffusion coefficients separately for the cation and anion of an ionic species and thus determine whether or

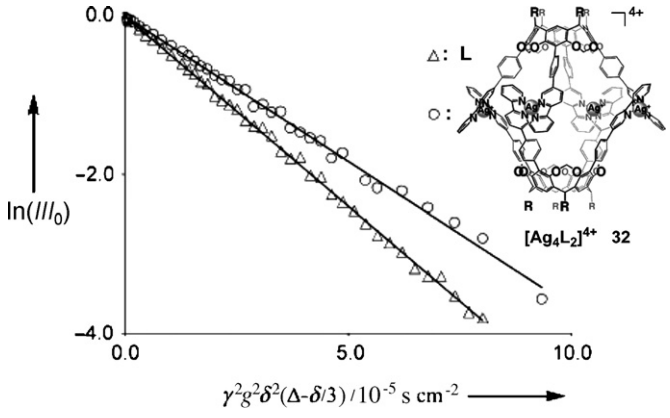

Fig. 21. Plot of the ^{1}H PGSE diffusion measurements ($CDCl_3$, 297 K) on the dimeric $[Ag_4L_2]^{4+}$ capsule **32** (circles) and the resorcinarene ligand L (triangles). Graph reproduced with permission from Ref. [154]. Copyright Wiley-VCH Verlag GmbH & Co. KGaA. Structure reproduced from Ref. [107] with permission of The Royal Society of Chemistry.

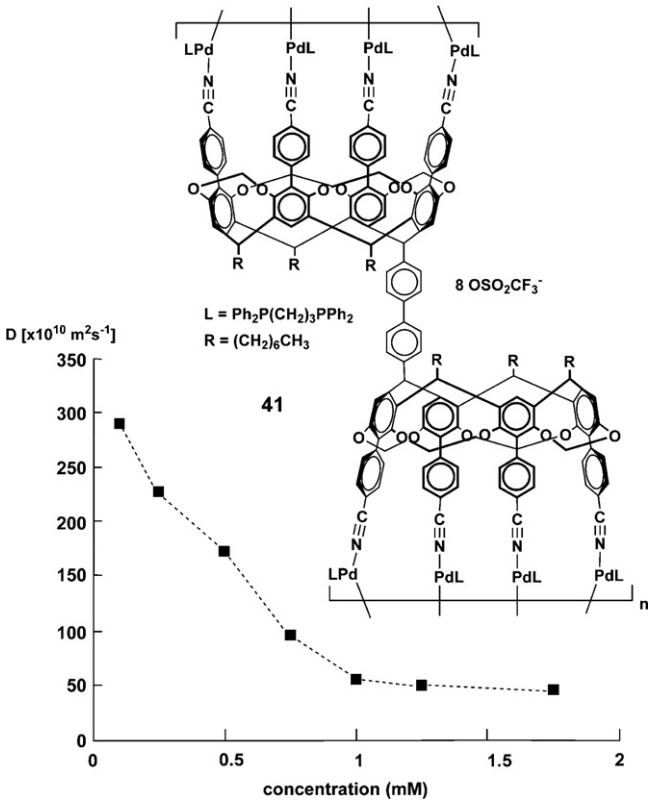

Fig. 22. Concentration dependence of the diffusion coefficients (in $CDCl_3$) of the coordination oligomer **41**, self-assembled from an octacyano-biscavitand and [Pd(dppp)(OTf)$_2$].

not, and to which extend, they interact. In this way, concentration and solvent effects, as well as the influence of the interionic interactions on the reactivity of the molecule can be investigated. For the cage **3** (Scheme 1) [46], it was found that in $CDCl_3$ the seven external anions are strongly associated to the cationic host–guest assembly. Thus, the ^{19}F resonance of the external anions afforded a D-value of 2.9×10^{-10} m^2 s^{-1}, very similar to that of the complex (2.7×10^{-10} m^2 s^{-1}). On the contrary, in the more polar 7:1 mixture of $CD_3NO_2/CDCl_3$ the D-value for the external anions was 8.7×10^{-10} m^2 s^{-1}, very different from the host–guest assembly (2.5×10^{-10} m^2 s^{-1}), suggesting weak or no ion-pairing. This is an example of solvent-dependent interionic interactions. Actually, strong ion-pairing in $CDCl_3$ is a very common observation, due to the low dielectric constant of this solvent [122,143]. Another example has been reported for the cavitand [**39a**](OTf)$_8$ (drawn in Scheme 17) [121], for which the D-values in $CDCl_3$ are 2.4×10^{-10} m^2 s^{-1} and 2.5×10^{-10} m^2 s^{-1} for cation and anion, respectively, indicating again strong ion-pairing in this solvent.

While the previous paragraph refers to solvent-dependent D-values, concentration-dependent D-values are also frequently found for ionic species. Fig. 22 shows an example for the oligomeric Pd capsule **41** [157]. The diffusion coefficient in $CDCl_3$ decreases markedly as the concentration increases from 0.1 to 1.0 mM, indicating a ca. 140-fold increase in the volume of the species present in solution, due to aggregation processes.

NMR diffusion measurements are also a powerful tool for detecting and probing encapsulation [140,142]. Since the encapsulated molecules form a kinetic unit with the capsule, host and guest will display the same *D*-value, even if they have very different sizes. Returning to cage **3**, the encapsulation of a triflate anion was confirmed by ^{19}F and ^{1}H PGSE diffusion measurements [46]. The encapsulated triflate anion and the cage show exactly the same *D*-value, both in $CDCl_3$ ($2.7 \times 10^{-10}\ m^2\ s^{-1}$) and in a 7:1 $CD_3NO_2/CDCl_3$ mixture ($2.5 \times 10^{-10}\ m^2\ s^{-1}$), confirming that in both solutions they translate together as a single molecular entity.

2.3.2. The DOSY technique

PGSE diffusion measurements can also be presented as a "2D spectrum", where the chemical shifts are displayed in one dimension and the diffusion coefficient in the second one. Such an experiment is called DOSY [158,159] (Diffusion Ordered Spectroscopy) and has also been referred to as "NMR chromatography", for its ability to "separate" the components of a complex mixture according to their diffusion coefficients. Thus, the different molecular species can be identified on the basis of their molecular sizes. This methodology has also been widely used in several areas of chemistry [159], such as polymers [160], resins [161], biochemistry [162], organic [163] and inorganic/organometallic [164] chemistry, including supramolecular assemblies [140,165].

In a recent application, Lehn and co-workers [166] have used ^{1}H DOSY NMR spectroscopy to investigate a series of double-stranded helicates of increasing length, ranging from mononuclear to pentanuclear, $[Cu^{I}_{n}(\mathbf{42a–e})_2]$ ($n = 1$–5), formed by self-assembly from oligotopic strands **42a–e** (Fig. 23). As shown in the figure, the 2D DOSY spectrum decomposes the 1D pattern into a vertical stacking of spectra, each level representing a different species in solution, distinguishable by its diffusion coefficient. The signals in the spectral region of the methylene protons are particularly well separated, as shown in the expansion. These results nicely illustrate the ability of the DOSY analysis to resolve a mixture of metallosupramolecular entities into its components, acting as a "spectral chromatography".

The DOSY technique is being increasingly used for the determination of diffusion coefficients even of single components, as an alternative to the "traditional" linear PGSE plots. Schmittel and co-workers [167] have applied ^{1}H DOSY experiments to investigate the formation of the bis-porphyrinic heterometallic rectangles **43a**,**b** by coordinative pyridine–zinc dimerization of the dinuclear complexes **44a**,**b** (Scheme 19). A single diffusion coefficient was found for each of these systems ($7.0 \times 10^{-10}\ m^2\ s^{-1}$ for the system **43a/44a** and $6.1 \times 10^{-10}\ m^2\ s^{-1}$ for **43b/44b**, in CD_2Cl_2). As these observed *D*-values are much lower than the diffusion coefficient of a reference compound, **45** (also drawn in the scheme), the results suggest that **44a**,**b** exist in solution *only* as their supramolecular dimers, **43a**,**b**.

The same authors [168] have also used ^{1}H DOSY spectra to investigate the formation of the multiporphyrin arrangements **46a–c**, formed by orthogonal coordination of the supramolecular porphyrin tweezer **47** with different linear spacers **48a–c**

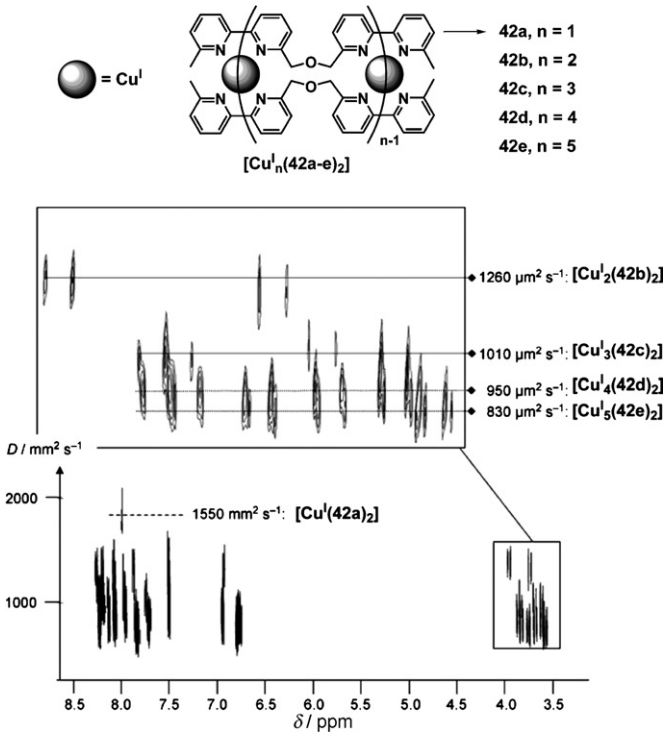

Fig. 23. ^{1}H DOSY spectrum (500 MHz, CD_3CN) of an equimolar mixture of the helicates $[Cu^{I}_{n}(\mathbf{42a}–e)_2]$ ($n = 1$–5), formed by self-assembly of oligotopic strands **42a–e** of increasing length. The expansion shows the methylene region group ($\delta = 3.5$–4 ppm). Spectrum reproduced with permission from Ref. [166]. Copyright Wiley-VCH Verlag GmbH & Co. KGaA.

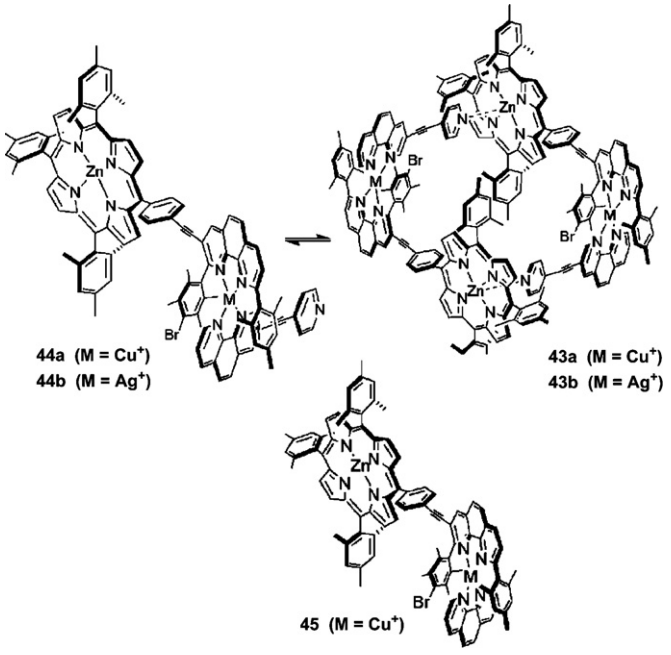

Scheme 19. Up: self-assembly of the bis-porphyrinic supramolecular assemblies **43a**,**b** from the dinuclear complexes **44a**,**b**. Down: reference compound **45**. Reproduced from Ref. [167] with permission of The Royal Society of Chemistry.

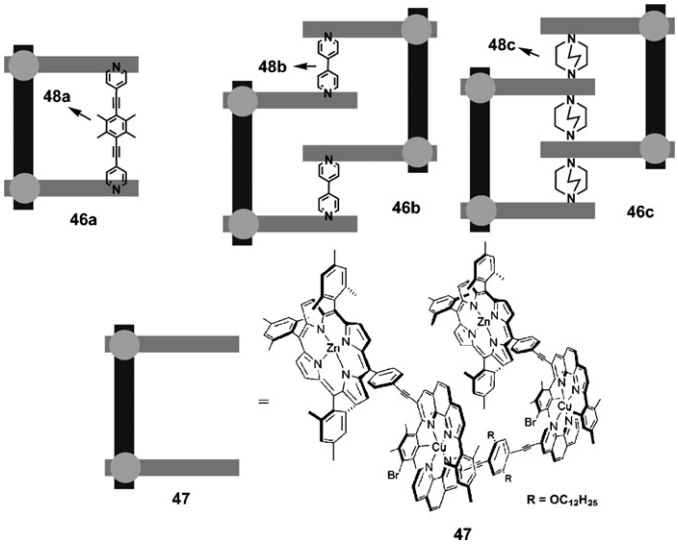

Scheme 20. Multiporphyrin arrangements **46a–c** self-assembled through orthogonal coordination of the porphyrin tweezer **47** and the linear spacers **48a–c**. The resulting structure is controlled by the length of the linear ligand. Structure reproduced from Ref. [167] with permission of The Royal Society of Chemistry.

(Scheme 20). The stoichiometries **47**·**48a** for **46a**, $(\mathbf{47})_2\cdot(\mathbf{48b})_2$ for **46b** and $(\mathbf{47})_2\cdot(\mathbf{48c})_3$ for **46c** could be established by fitting the obtained *D*-values to a calibration curve correlating molecular weights and experimentally determined diffusion coefficients of related known compounds. Use was made of the general assumption that the ratio of the diffusion coefficients for two different molecular species (D_i/D_j) is inversely proportional to the square or cubic root of the ratio of their molecular weights (M_i/M_j), for rod-like and spherical molecules, respectively (Eq. (2)) [169].

$$\sqrt[3]{\frac{M_j}{M_i}} \leq \frac{D_i}{D_j} \leq \sqrt{\frac{M_j}{M_i}} \quad (2)$$

Fujita and co-workers have reported many applications of DOSY spectroscopy in coordination supramolecular chemistry. Thus, ^{1}H and ^{19}F DOSY measurements have confirmed the estimated diameter of 4.3 nm for the endofluorous "nanodroplets" **38a–d**, drawn in Fig. 19 [117]. Very similar nanoparticles with other internal pendant groups [170], as well as other spherical coordination networks [171], have also been investigated using this methodology. Fig. 24 shows a very nice work from the same research group [172], in which the self-assembly of a Pd^{II} "figure-of-eight"-shaped molecule (**49**) into a dimeric double loop $(\mathbf{49})_2$ and a circular tris[2]catenane $(\mathbf{49})_3$ was reported. The mixture of the three species was nicely "separated" by a DOSY spectrum, as shown in the figure. Another catenane-related application illustrated with nice DOSY figures had been previously reported by the same authors [173]. Still the same group [174] has very recently prepared the self-assembled saccharide-coated $[Pd_{12}L_{24}]^{24+}$ molecular spheres **50a–f** (Scheme 21). ^{1}H DOSY spectroscopy confirmed the selective formation of a single species in each case, being the *D*-values in agreement with the estimated sizes of 5.2, 6.1 and 7.0 nm for the mono-, di-

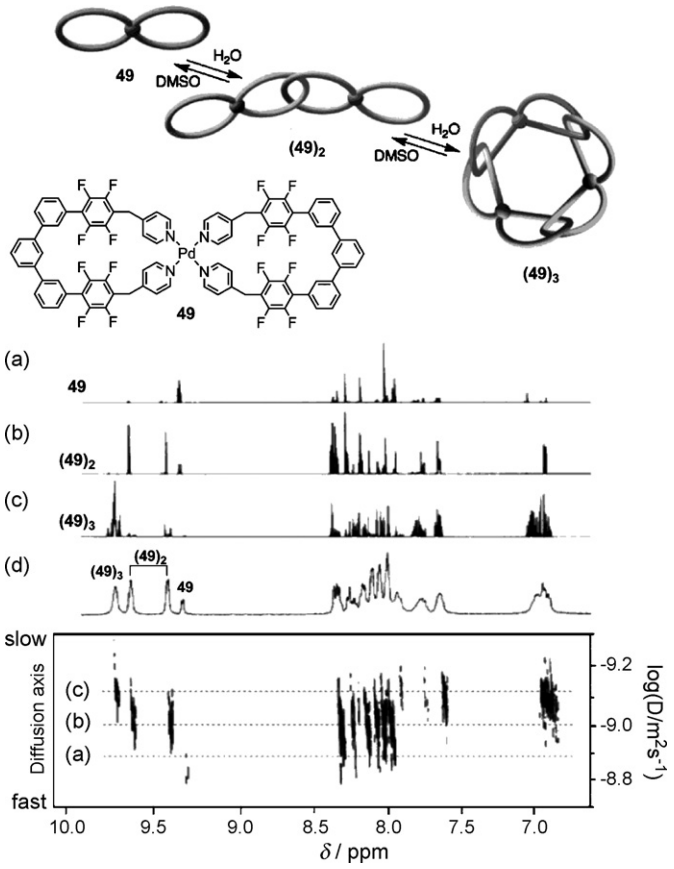

Fig. 24. ^{1}H DOSY (1.5:1 D_2O/d^6-DMSO, 500 MHz, 60 °C) spectrum of a mixture of the self-assembled components (**49**), $(\mathbf{49})_2$ and $(\mathbf{49})_3$, showing the slices of the 2D DOSY spectrum at the *D*-values for (a) (**49**), (b) dimer $(\mathbf{49})_2$ and (c) trimer $(\mathbf{49})_3$; (d) shows the complete ^{1}H NMR spectrum of the mixture. Reproduced from Ref. [172] with permission of The Royal Society of Chemistry.

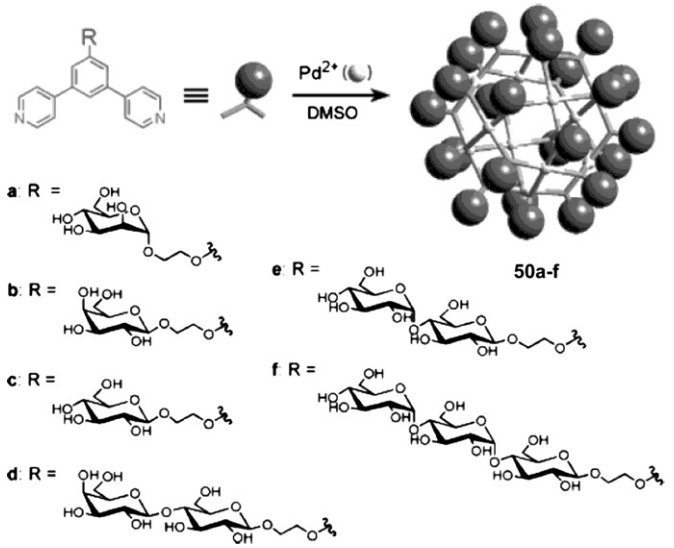

Scheme 21. Self-assembly of $[Pd_{12}L_{24}]^{24+}$ complexes **50a–f**, with 24 saccharide moieties at the periphery. Reprinted with permission from Ref. [174]. Copyright (2007) American Chemical Society.

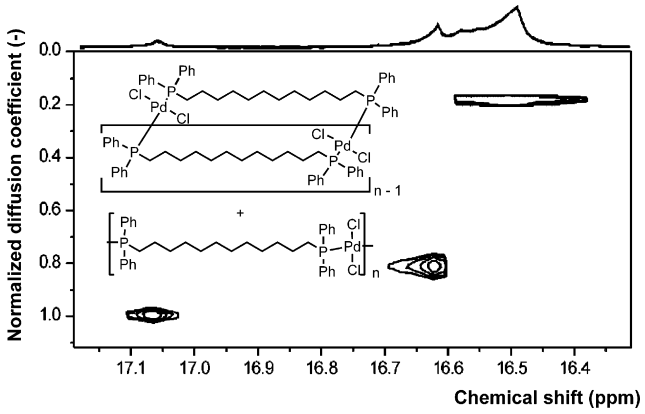

Fig. 25. ^{31}P DOSY ($CDCl_3$, 202.4 MHz) spectrum of a 0.2 M solution of [$PdCl_2$(dppdd)], containing a mixture of momeric, dimeric and oligomeric species. Reprinted from Ref. [176] with permission of The Royal Society of Chemistry.

and trisaccharide-appended spheres, respectively. These spheres form interesting colloidal aggregates with proteins, which might lead to biomedical applications [174].

^{1}H DOSY spectra have also been used in the characterization of other molecules already mentioned in the previous sections of this review, such as the molecular rectangle **15** (Scheme 6), for which a comparison with the *D*-value of the precursor 4,4′-bis[*cis*-Pt(dppp)(NO_3)]biphenyl complex was used [69]. For the [3]catenate **30** (Scheme 12) [95], the resonances from the two organic components of the assembly (the nitrogenated ligand and the macrocycle) where found to display the same diffusion coefficients in CD_3CN, confirming that these components diffuse as a whole due to their intercatenation. A ^{1}H DOSY experiment has also been performed on the dimer/monomer mixture of the Ti^{IV} catecholate complexes **11** and **12** (drawn in Fig. 8) [39]. In d^6-acetone diffusion coefficients of $D = 8.94 \times 10^{-10}$ m^2 s^{-1} for the monomer and 7.89×10^{-10} m^2 s^{-1} for the dimer were obtained. In this case the ratio $D_{dimer}/D_{monomer}$ is larger than expected (0.88) probably due to the effect of acetone solvation and the different charges of the compounds. Other applications of the DOSY methodology to confirm the size or investigate the nature of coordination supramolecular assemblies [175], as well as to characterize supramolecular coordination polymers [176,177] have been reported in recent years.

Similarly to the "traditional" PGSE experiments, DOSY measurements can also be performed using nuclides other than ^{1}H. Fig. 25 shows a ^{31}P NMR DOSY spectrum of an equilibrium mixture of *trans*-[$PdCl_2$(dppdd)]$_n$ containing momomeric, dimeric and oligomeric species [176]. The *D*-value of the cyclic monomer has been taken as reference for normalization ($D_{Nmonomer} = 1$). The D_N of the dimer turns out to be slightly lower (0.78) while the mixture of oligomers affords a much lower D_N (0.19).

3. Thermodynamic and dynamic properties

The thermodynamic properties and the dynamic behaviour of supramolecular complexes play an essential role in the development of their practical applications. Thus, a fast kinetic is desirable for an efficient catalytic activity, while a regulated release of the guest is essential in drug delivery strategies. On the other hand, a strong and selective binding in host–guest complexes may be of interest for analytical or environmental purposes. In this context, NMR spectroscopy has again revealed itself as a powerful tool to gain insight into these key aspects of supramolecular chemistry.

3.1. Thermodynamic properties

The calculation of association constants in solution (K_a) is of central significance not only for the description of a supramolecular system but, most importantly, for the development of relationships between structure and activity which can guide future developments. Moreover, when the equilibrium constants over a significant temperature range are known, a van't Hoff analysis of $K_a(T)$ can lead to the thermodynamic parameters of the system, which in turn can provide insight into the nature of the binding interaction. Thus, according to Eq. (3), a plot of ln K_a vs. T^{-1} yields the enthalpy (ΔH) from the slope of the regression line and the entropy (ΔS) from the *y*-intercept. This method is based on the assumption that both magnitudes are invariant over the temperature range of the experiments, which is usually a valid approximation. Significantly, a compensation between enthalpic and entropic effects has been repeatedly observed for a great number of systems [178].

$$\ln K_a = \frac{-\Delta H}{RT} + \frac{\Delta S}{R} \quad (3)$$

where K_a = equilibrium/association constant, T = temperature (K) and $R = 8.31$ J K^{-1} mol^{-1}.

The determination of association constants by NMR has become a common strategy [179,180]. Compared with UV and fluorescence techniques, the results based on NMR have the advantage that they are more reliable in the presence of minor impurities [140]. Another great advantage of NMR spectroscopy is the possibility to evaluate the equilibria on the basis of several independent signals for the same species [179]. In the following sections we will discuss the three most common NMR techniques used for the calculation of association constants: complexation-induced shifts (CIS), diffusion measurements and relaxation.

3.1.1. Evaluation of association constants by complexation-induced shifts (CIS)

3.1.1.1. Slow exchange: integration. The formation of supramolecular complexes usually results in significant changes in the chemical shifts of the individual components, as outlined in Section 2.1 of this review. Under *slow exchange* conditions, separate NMR resonances will be observed for the different species involved in the equilibrium (for example, the free and the encapsulated guest), and thus, a simple signal integration allows the determination of the molar fractions of reactants and product and, consequently, the calculation of the association constant [179]. ^{1}H NMR spectra are commonly used, no only due to the high sensitivity of this nuclide, but also because protons are positioned at the periphery of the molecules

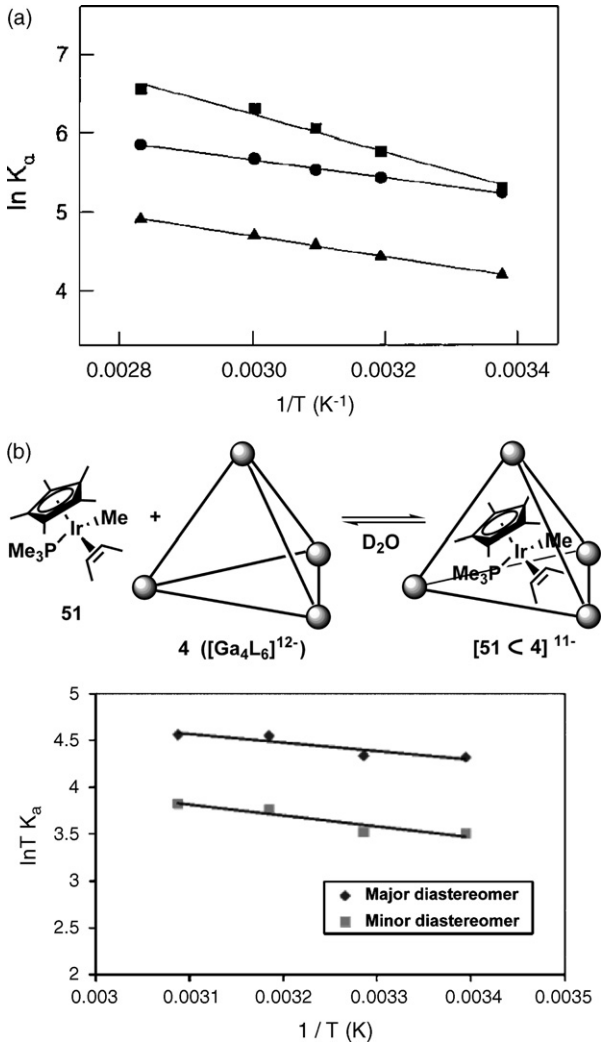

Fig. 26. (a) van't Hoff plots for the encapsulation of aqueous alkylammonium cations into the cavity of $[Ga_4L_6]^{12-}$ (**4**). ●: Pr_4N^+, ■ $Me_2Pr_2N^+$, ▲: single protonated *N*,*N*,*N*′,*N*′-tetramethyl-1,3-propanediamine. Reproduced from Ref. [181]. (b) van't Hoff plots for the inclusion of **51** inside Na_{12}**4** in D_2O. Reprinted with permission from Ref. [32]. Copyright (2006) American Chemical Society.

and are therefore more exposed to intermolecular shielding effects and thus more prone to suffer complexation-induced shifts [179,180].

Raymond and co-workers [181] have investigated the principles of recognition between the tetrahedral container $[Ga_4L_6]^{12-}$ (**4** in Fig. 3) and various alkylammonium cations in water, as well as the driving force for the encapsulation. The thermodynamic parameters were determined by following the temperature dependence of the association constants between 295 and 353 K. Fig. 26a shows the van't Hoff plots for the exchange of the occluded water by each of the three guests. All three plots show that the encapsulation of the cationic guests is an endothermic process, with ΔH ranging from 9.2 to 19.7 kJ mol^{-1}. This observation is explained as a consequence of the very large solvation enthalpies of the ions. The values of ΔS range from 71.1 to 108.7 J K^{-1} mol^{-1}, showing that the spontaneous encapsulation is an entropy-driven process, due to the release of bound water from the solvation shell of the guest, as well as from the cavity of the "empty" host into the bulk solvent [181]. A similar result was obtained for the two diastereomeric inclusion complexes of **4** with the chiral $[Cp^*(PMe_3)Ir(Me)(cis\text{-butene})]^+$ complex **51** (see Fig. 26b) [32]. The van't Hoff analysis reveals that the formation of these complexes is enthalpically disfavoured ($\Delta H_{major} = 7.5$ kJ mol^{-1} and $\Delta H_{minor} = 9.6$ kJ mol^{-1}; the two diastereomers are formed in a dr of 70:30), and entropically favoured ($\Delta S_{major} = \Delta S_{minor} = 62.7$ J K^{-1} mol^{-1}). We have already mentioned (see end of Section 2.2.3) that iridium complexes such as **51** are able to selectively activate C–H bonds of aldehyde and ether substrates.

A van't Hoff plot has also been obtained for the encapsulation of a 4,4′-diacetoxybiphenyl guest inside the dimeric $[Ag_4L_2]^{4+}$ capsule **32** (drawn in Scheme 13) [154]. Well-separated resonances were observed for the bound and free guest, indicating a sizable kinetic barrier for the exchange process, and allowing the determination of five values of K_a between 268 and 323 K. A plot of ln K_a vs. T^{-1} afforded values of $\Delta H = -23.5$ kJ mol^{-1} and $\Delta S = 17.6$ J K^{-1} mol^{-1}, indicating that the encapsulation process is both enthalpically and entropy-driven. The positive enthalpy is attributed to a variety of favorable noncovalent interactions (van der Waals, electrostatic, etc.) between host and guest. The positive entropy is explained as due to the desolvation of the cavity [154]. A compensation between these two magnitudes was observed, showing that a stronger attractive interaction between host and guest results in a more reduced freedom of the guest movement in the supramolecular complex (an entropic loss).

Stang and co-workers [182] have described the dynamic equilibrium between a supramolecular dimeric rhomboid and a trimeric hexagon, prepared by metal-directed self-assembly. As expected, the van't Hoff analysis showed that the dimeric species is favored by the entropic factor, whereas the trimer is the enthalpic product.

3.1.1.2. Fast exchange: NMR titration. The previous section was concerned with slow exchange, resulting in separate resonances in the NMR spectra. However, the most common situation in host–guest assemblies is a *fast exchange* between the free and bound components. In this situation, the observed chemical shifts for host (δ_{obsH}) and guest (δ_{obsG}) are the mole fraction weighed average of the values in the free (δ_H and δ_G) and bound situation (δ_{HG}). Association constants can then be obtained from a series of NMR spectra measured at different initial concentrations of host and guest, a method known as NMR titration. There are two possibilities for data treatment: (a) graphical (or linearization) methods, designed to produce a (non-real) linear relationship between δ_{obs} and K_a, so that the NMR data can be treated graphically, and (b) non-linear curve fitting procedures, based on the calculation of a titration curve (also called binding isotherm) which is iteratively compared with the experimental data [180]. The graphical methods were developed before powerful computers became easily available but they are still frequently used due to their simplicity, although sometimes they may lead to incorrect values [179]. On the contrary, the modern computerized curve fitting procedures are the most reliable and

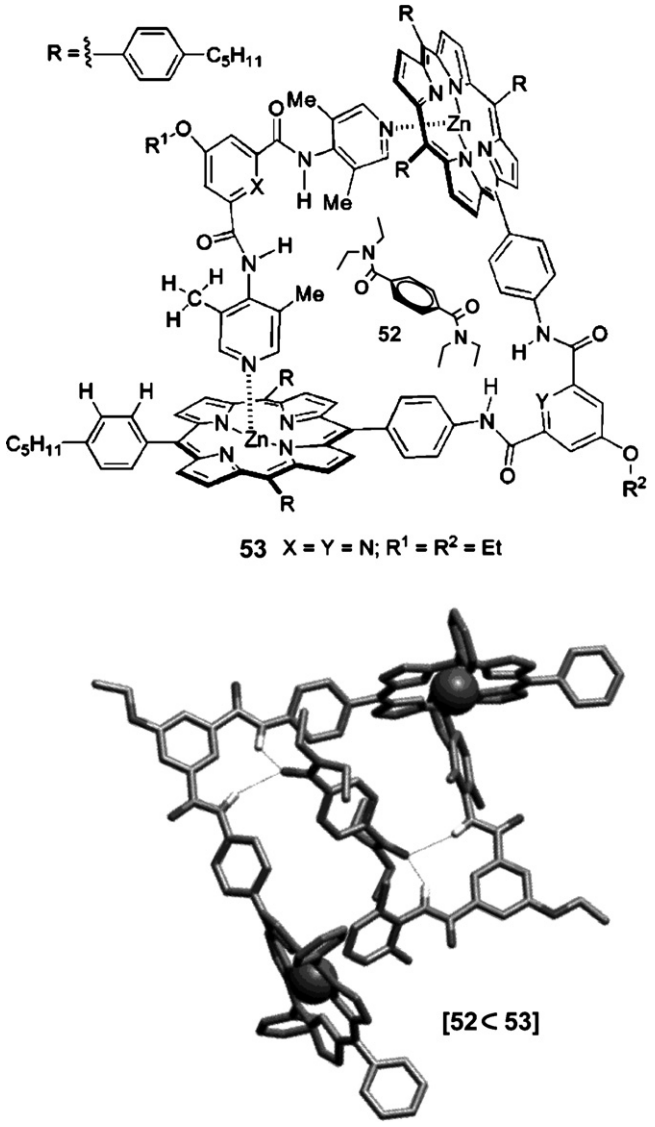

Fig. 27. Up: Structure of the heterodimeric tetralactam macrocycle **53** and the *N*,*N*,*N*′,*N*′-tetraethyltereftalamide guest **52**. Down: Minimized structure (MMFF94 force field) of the inclusion complex **52** ⊂ **53**, showing the hydrogen bonds between host and guest. Reprinted with permission from Ref. [183]. Copyright (2005) American Chemical Society.

accurate and, although they require more effort to establish a working procedure, it is possible to choose among the proliferation of programs available to do the job [180]. A clear advantage of the curve fitting methods is that the experimental conditions are less constrained and more complex binding models can be investigated. In general, NMR titration methods are most useful for equilibrium constants in the range 10–10^4 M^{-1}.

In one application of this methodology, the binding of *N*,*N*,*N*′,*N*′-tetraethylterephthalamide (**52**) inside the cavity of the heterodimeric tetralactam macrocycle **53** was investigated (Fig. 27) [183]. **53** is quantitatively assembled from a bispyridyl ligand and a zinc bisporphyrin through two kinetically labile zinc–pyridine interactions. Upon addition of the guest **52**, the NH resonances of the macrocycle **53** shift to higher frequencies (by 0.16 and 0.44 ppm), due to the formation of up to

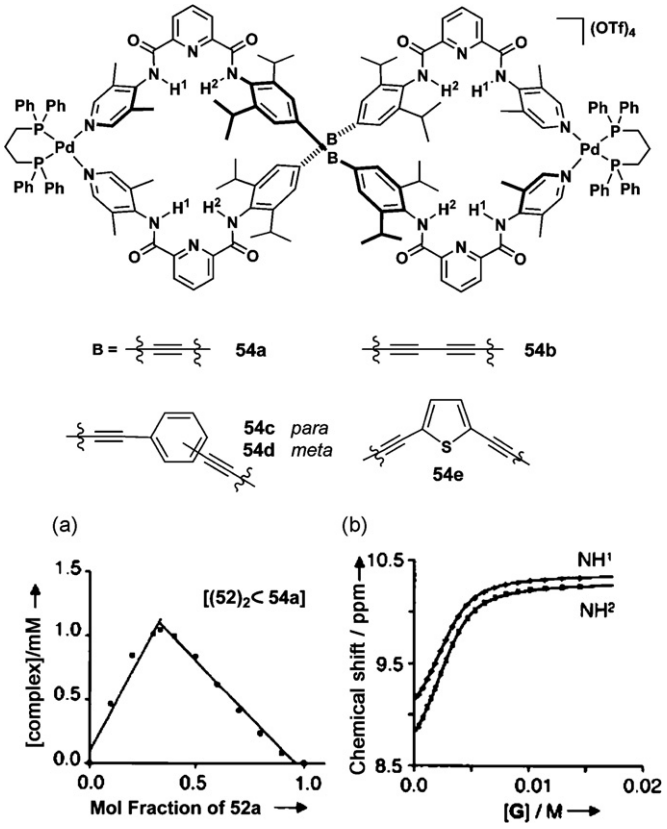

Fig. 28. Up: Structure of the metallocycles **54a–e**. Down: (a) Job plot and (b) NMR titration curves for the inclusion of two molecules of guest **52** inside the cavities of **54a**. Graphs reproduced with permission from Ref. [184]. Copyright Wiley-VCH Verlag GmbH & Co. KGaA.

four hydrogen bonds with the carbonyl oxygen atoms of the terephthalamide (Fig. 27b). The titration data obtained for these resonances were fitted to a 1:1 binding model, affording a value of $K_a = 160\ M^{-1}$.

A similar investigation has been performed for the encapsulation of the same guest **52** inside the metallocycles **54a–e** (Fig. 28), self-assembled from S-shaped bispyridyl ligands and [Pd(dppp)$(OTf)_2$] [184]. These structures fold to create two symmetrical binding cavities possessing hydrogen-bonding sites. The variation of the chemical shifts of the NH protons of the host **54a** upon encapsulation and hydrogen-bonding with the guest was followed by NMR titration using a non-linear least-squares fitting. Both the titration curves and the Job plot [179], also shown in the figure, supported a 1:2 binding mode. The binding constants were found to be $K_1 = 1600\ M^{-1}$ (for the 1:1 complex) and $K_2 = 1400\ M^{-1}$ (for the 1:2 complex), values which reflect a positively cooperative binding of two molecules of the guest [184].

Reek and co-workers have developed a new class of potential supramolecular transition metal catalysts formed by the assembly of a tetraanionic calix[4]arene, **55**, with a palladium complex **56**, containing a tetracationic diphosphine ligand (Scheme 22) [185]. In this capsule the metal is not involved in the assembly process and is therefore available for catalytic processes. A ^{1}H NMR titration was carried out at 298 K, providing a stability constant of $K_{\mathbf{55}\cdot\mathbf{56}} = 6 \times 10^3\ M^{-1}$. As expected, both the titration

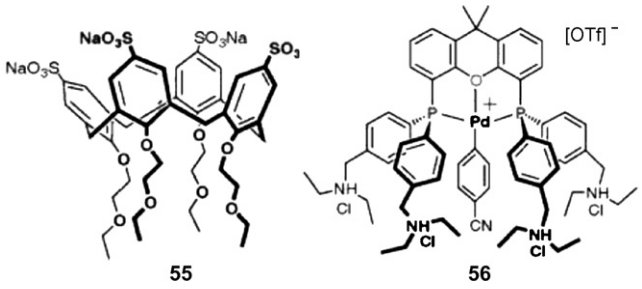

Scheme 22. Structure of the tetraionic calix[4]arene **55** and the palladium complex **56**, containing a tetracationic diphosphine ligand. Reproduced from Ref. [185] with permission of The Royal Society of Chemistry.

curve and the Job plot fitted to a 1:1 binding model [185].

3.1.2. Evaluation of association constants by diffusion spectroscopy

Diffusion coefficients measured by NMR can also be used to determine the association constants of supramolecular assemblies and host–guest complexes, in a situation of fast exchange between the free and bound components. Under these conditions the observed diffusion coefficient of a component will be given (as the chemical shift) by the mole fraction weighted average of the diffusion coefficients in the free and bound situation [140,186]. Thus, for the simple case of a 1:1 host–guest complex (HG) formed between a host (H) and a guest (G) (Eq. (4)), the observed D-value for the guest will be given by Eq. (5), which can be rewritten as Eq. (6) taking into account that $X_G = 1 - X_{HG}$:

$$H + G \rightleftharpoons HG \tag{4}$$

$$D_G^{obs} = X_G D_G + X_{HG} D_{HG} \tag{5}$$

$$X_{HG} = \frac{D_G - D_{obs}}{D_G - D_{HG}} \tag{6}$$

D_G and D_H can be obtained from diffusion measurements in separate solutions of host and guest. D_{HG}, however, is unknown, as the host–guest assembly is in fast equilibrium with its components. In principle, an NMR titration could be used, as described in the previous section for the chemical shift method. However, one advantage of this methodology is that usually the encapsulation of a small guest inside a large host is not expected to significantly change the size of the host, so that it can be assumed that $D_{HG} = D_H$ and with this approximation the need for a complete titration can be eliminated. X_{HG} can then be easily obtained from Eq. (6) and the association constant can be calculated from Eq. (7) [187], where $[H]_o$ and $[G]_o$ are the known total concentrations of host and guest, respectively.

$$K_a = \frac{[H \cdot G]}{[H][G]} = \frac{X_{HG}}{(1 - X_{HG})([G_o] - X_{HG}[H]_o)} \tag{7}$$

The determination of association constants from diffusion NMR measurements is especially useful when changes in chemical shift due to complexation are small. On the contrary, this methodology is less sensitive or even impractical when the diffusion coefficients of the unbound host and guest are not significantly different [188]. Several applications of this methodology to organic host–guest assemblies, as well as a more detailed explanation can be found in the recent review by Cohen et al. [140].

3.1.3. Evaluation of association constants by relaxation time (T_1) measurements

The longitudinal or spin-lattice relaxation rate ($1/T_1$) is another NMR parameter that can be used to measure association constants. As for the other parameters discussed in previous sections (chemical shifts and D-values), the observed relaxation rate for host and guest under fast exchange conditions will be the weighted average of the rates corresponding to the bound and free molecules. Nevertheless, there has been little use of the relaxation time method for the calculation of association constants in the field of host–guest chemistry, probably because the measurement of this parameter is more time-consuming than the previously discussed methods [180].

3.2. Dynamic properties of supramolecular complexes: dynamic NMR

The dynamic behaviour of supramolecular assemblies often determines their specific properties and potential applications. NMR is a very important technique for the investigation of the kinetics of the chemical reactions, most notably of exchange processes under equilibrium conditions, a common characteristic in supramolecular chemistry. In this section we describe the most commonly used NMR methodologies used for the qualitative and quantitative investigation of dynamic supramolecular equilibria. Reaction rates over a range of more than ten orders of magnitude (typically, 10^{-2} to 10^{8} s^{-1}) can be measured by different NMR methods. Additionally, the temperature dependence of the rate constants can be used to build Arrhenius [189] or Eyring plots [190], which provide the activation parameters (E_A, $\Delta H^{\neq}$ and $\Delta S^{\neq}$) for the process under investigation [179].

3.2.1. 1D dynamic NMR

3.2.1.1. Lineshape analysis. Processes with a rate constant (k) in the range of ca. 10–10^5 s^{-1} cause a significant and analyzable line broadening in the NMR spectra, from which kinetic parameters can be obtained via the so-called lineshape or bandshape analysis [191]. For an equally populated two-site system, approximate values of rate constants can be easily obtained at the coalescence temperature ("the coalescence method"), and from this value the activation energy ($\Delta G^{\neq}$) for the process can be derived using the Eyring equation (Eq. (8)) [191]. This method can also be applied to unequally populated sites [192].

$$k = \frac{k_B T}{h} e^{-\Delta G^{\neq}/RT} \tag{8}$$

k_B = Boltzmann constant, h = Planck constant, T = temperature (K), $\Delta G^{\neq}$ = activation energy (J mol^{-1}) and $R = 8.31$ J K^{-1} mol^{-1}.

At temperatures below and above the coalescence, the rate constants can also be derived from the lineshapes using several mathematical equations [191]. However, the most accurate results are obtained with the use of simulation programs [193], which iteratively compare the experimental lineshapes with

those calculated from different sets of kinetic and spectroscopic parameters. This methodology is especially useful for the analysis of multi-site-exchange problems, since it provides not only the rate constants but also the confirmation of the exchange mechanism [191].

If the rate constants are determined over a significant temperature range, the kinetic parameters E_A and $\Delta H^{\neq}$, $\Delta S^{\neq}$ can be determined from the Arrhenius (Eq. (9)) and Eyring (Eq. (10)) equations, respectively. Thus, according to Eq. (9), a plot of $\ln k$ vs. T^{-1} yields the empirical activation energy, E_A, from the slope of the regression line, while, according to Eq. (10) a plot of $\ln(k/T)$ vs. T^{-1} yields the activation enthalpy, $\Delta H^{\neq}$, and entropy, $\Delta S^{\neq}$, from the slope of the regression line and the *y*-intercept, respectively.

$$\ln k = \ln A - \frac{E_A}{RT} \tag{9}$$

A, frequency factor, E_A, empirical activation energy ($J\,mol^{-1}$), $R = 8.31\,J\,K^{-1}\,mol^{-1}$ and T = temperature (K).

$$\ln\left(\frac{k}{T}\right) = -\frac{\Delta H^{\neq}}{RT} + \frac{\Delta S^{\neq}}{R} + \ln\left(\frac{k_B}{h}\right) \tag{10}$$

T = temperature (K), $\Delta H^{\neq}$ = activation enthalpy ($J\,mol^{-1}$), $R = 8.31\,J\,K^{-1}\,mol^{-1}$, $\Delta S^{\neq}$ = activation entropy ($J\,K^{-1}\,mol^{-1}$) and $\ln(k_B/h) = 23.760$.

Cohen and co-workers [85] have used the coalescence method to investigate the dynamic behaviour of the silver double-stranded helicate $[(\mathbf{23})_2Ag_3]^{3+}$ in DMSO-d_6 (Fig. 29). The protons of the CH_2OCH_2 bridges of ligand **23** in the complex are diastereotopic at room temperature due to the chiral nature of the helicate. At 335 K the two AB systems collapse into two broad singlets with relatively small changes in their chemical shifts, indicating partial unfolding with reorganization around the metal centers. The free activation energy for this enantiomerization process at the coalescence temperature was calculated as $\Delta G^{\neq}_{335} = 69.4\,kJ\,mol^{-1}$. At higher temperatures, the two broad singlets sharpen and shift to higher frequencies until at 431 K they resemble the spectrum of the free ligand, pointing to the dissociation of the helicate.

In another application, Fujita and co-workers have reported the synthesis of the dodecanuclear palladium nanotube **57**, which forms only in the presence of suitable templates such as the strand guest molecules **58a**,**b** (Fig. 30) [194]. The desymmetrization of the tubular framework by the encapsulation of **58a** is evident in the ^1H spectrum measured at room temperature. Separate resonances are observed for the protons Hd,Hd′ and Hi,Hi′, corresponding to the two halves of the organic ligand in **57**. At 327 K these pairs of peaks coalesce, due to a dynamic guest-encapsulation/dissociation process. From the coalescence temperature the activation energy for this process was estimated to be $66.6\,kJ\,mol^{-1}$. Notably, the activation energy for the guest **58b** turned out to be significantly larger ($71.1\,kJ\,mol^{-1}$), pointing to a stronger binding [194].

Stang and co-workers [195] have investigated the restricted rotation around the metal–nitrogen heteroaryl bond in the com-

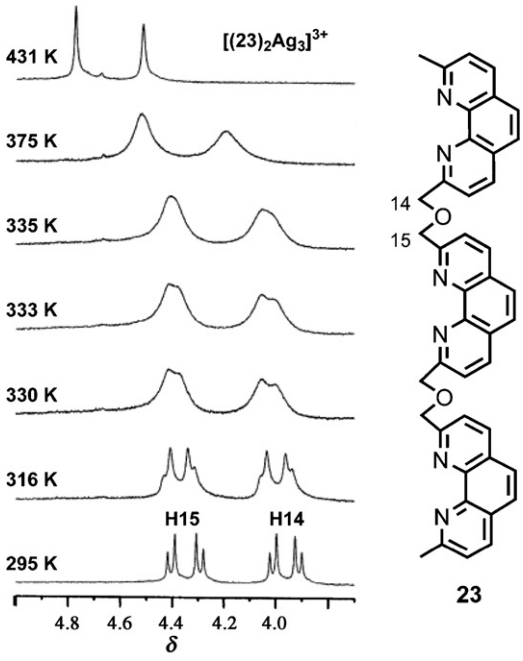

Fig. 29. ^1H VT NMR spectra (500 MHz, d^6-DMSO) of the protons of the CH_2OCH_2 bridges of $[(\mathbf{23})_2Ag_3]^{3+}$. Reproduced from Ref. [85] with permission of The Royal Society of Chemistry.

plexes [M(*R*-(+)-BINAP)(3-picoline)$_2$][OTf]$_2$ (M = Pd, Pt) by VT ^1H NMR spectroscopy. The rotation barriers were determined by lineshape analysis of the methyl signals affording interesting mechanistic information.

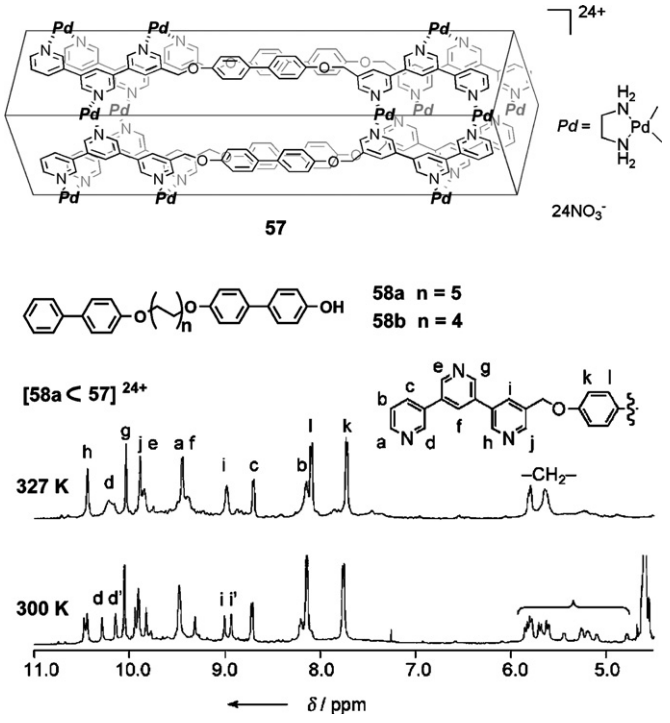

Fig. 30. Up: Dodecanuclear palladium nanotube **57** and strand guest molecules **58a**,**b**. Down: VT ^1H NMR spectra (300 MHz, 1:1 D_2O/CD_3CN) of **58a** ⊂ **57** recorded at 327 K and 300 K. Spectra reproduced with permission from Ref. [194]. Copyright Wiley-VCH Verlag GmbH & Co. KGaA.

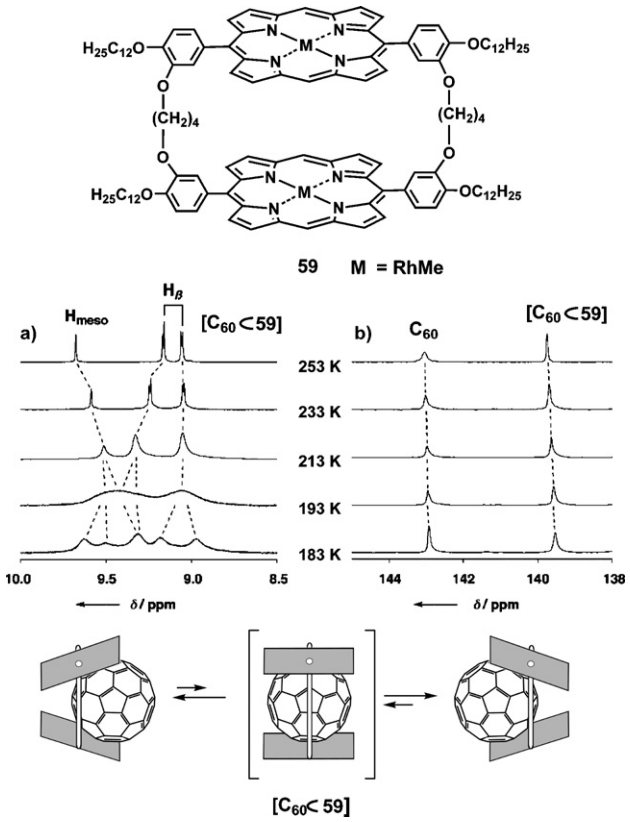

Fig. 31. Up: Molecular structure of the cyclic host **59**. Center: (a) Section of the VT ^{1}H NMR spectra (500 MHz, toluene-d_8) of the inclusion complex $C_{60} \subset$ **59**. (b) VT ^{13}C NMR spectra (125.7 MHz, toluene-d_8) of a 1:2 mixture of **59** and ^{13}C-enriched (10–15%) C_{60}. Down: Schematic representation of the dynamic slip-through motion of the guest C_{60} inside **59**. Spectra reproduced with permission from Ref. [49]. Copyright Wiley-VCH Verlag GmbH & Co. KGaA.

^{1}H and ^{13}C lineshape analysis performed with the simulation program DNMR5 has been used to investigate the dynamic behaviour of the inclusion complex $C_{60} \subset$ **59**, where **59** is a cyclic methylrhodium porphyrin dimer (Fig. 31) [49,50]. The ^{1}H NMR spectrum at 183 K (Fig. 31a) shows split pairs of meso and pyrrole β proton signals, indicating that the two metalloporphyrin units adopt a nonparallel, tilted geometry. These pairs of signals coalesce at around 193 K and become simplified upon further heating, when a single resonance for the four equivalent meso protons and two resonances for the two groups of eight equivalent pyrrole protons are observed. This coalescence phenomenon could be due to (a) a rapid guest-exchange of $C_{60} \subset$ **59** (disassembly/reassembly dynamics) or (b) a rapid slip-through motion of guest C_{60} in $C_{60} \subset$ **59**. The first possibility was separately evaluated by VT ^{13}C NMR spectroscopy of a mixture of $C_{60} \subset$ **59**, and free C_{60} (Fig. 31b). At 183 K, two ^{13}C resonances are observed for free (142.9 ppm) and complexed (139.5 ppm) C_{60}, respectively. These two signals do not coalesce over a wide temperature range up to 253 K, indicating a rather slow guest-exchange dynamics. Lineshape analysis using the DNMR5 program afforded a rate constant $k_{\text{site-exchange}} = 340\ \text{s}^{-1}$ at 193 K for the pyrrole protons, while from the ^{13}C spectrum the guest-exchange at the same temperature was found to occur with $k_{\text{guest-exchange}} = 5\ \text{s}^{-1}$. Based on the difference of two orders of magnitude in the calculated rate constants the authors conclude that the dynamic behaviour observed in the VT ^{1}H NMR spectra is mainly due to a slip-through motion of the guest, schematically depicted in the figure. This conclusion is further supported by the fact that for the larger guest C_{70} the coalescence temperature for the site-exchange in the ^{1}H spectra is higher (233 K), reflecting the higher steric hindrance for the motion of the guest, while for the guest C_{76} no coalescence is observed even at 273 K [49].

3.2.1.2. Selective inversion recovery (SIR) experiments. The last example of the previous section shows how in the case of simultaneous dynamic processes they all contribute to the lineshapes in the NMR spectra and their influences may be difficult or impossible to distinguish. Selective inversion recovery experiments, on the contrary, offer the possibility of discriminating among different dynamic processes. This methodology consists in the selective inversion of one resonance and the observation of the changes in the intensity of both the inverted and the exchange-related resonances, as a function of a magnetization transfer delay [196]. The z magnetization of each of the NMR lines will regain its equilibrium value under the influence of both relaxation and exchange, and this evolution is governed by a set of coupled differential equations [197]. Consequently, with a table of observed intensities as a function of the magnetization transfer delay, and a proposed mechanism, it is possible to use a computer program to find the set of parameters (rates, relaxation times, initial and equilibrium intensities) that best fits the experimental data. One such program is CIFIT, developed by Alex Bain [198]. The need for separated NMR resonances for the two sites undergoing chemical exchanges implies that this technique can only be applied to systems undergoing slow chemical exchange. Both the mechanism and the rate constant of the dynamic process can be determined with this methodology which, additionally, is relatively fast and requires little space for data storage.

Raymond and co-workers [199] have used selective inversion recovery experiments to investigate the guest self-exchange in their tetrahedral host $[Ga_4L_6]^{12-}$ **4** (drawn in Fig. 3). Several cationic guests were investigated in D_2O. An example is shown in Fig. 32 for the guest NPr_4^+. The exchange between the inverted CH_3 resonance (at 0.7 ppm) of the exterior NPr_4^+ and the corresponding resonance of the encapsulated NPr_4^+ population is evidenced by the dip in the intensity of the second at intermediate delay times. The rate constants were evaluated using the CIFIT program. The experiment was repeated at several temperatures and an Eyring analysis on $k(T)$ provided the activation parameters for the process. The results are shown in the table within Fig. 32, together with the rate and binding constants at 298 K. Except for $NMe_2Pr_2^+$, the Table shows a good correlation between the guest self-exchange rates and the guest binding affinities (strongly bound guests are more stabilized relative to the transition state than weakly bound guests). The $\Delta H^{\neq}$ values follow the same trend, without exception, and their low values indicate that the metal–catecholate bonds of the host are not broken in the exchange reaction. The negative $\Delta S^{\neq}$ values do not indicate bond rupture either, and instead appear

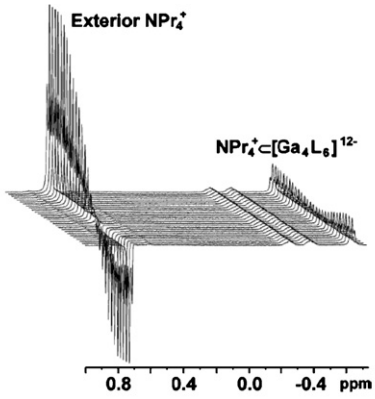

Guest Self-Exchange in $[Ga_4L_6]^{12-}$

guest	log $K_{binding}$ (298 K)	$\Delta H^{\ddagger}$ (kJ mol^{-1})	$\Delta S^{\ddagger}$ (J mol^{-1} K^{-1})	$\Delta G^{\ddagger}_{298}$ (kJ mol^{-1})	k_{298} (s^{-1})
PEt_4^+	5.0(2)	74(3)	−46(6)	78(4)	0.003
NEt_4^+	4.55(6)	69(2)	−52(5)	76(3)	0.009
$NMe_2Pr_2^+$	3.5(2)	52(2)	−56(7)	60(3)	4.4
NPr_4^+	2.0(2)	42(1)	−102(4)	63(3)	1.4

Fig. 32. Up: ^{1}H NMR SIR experiment (500 MHz, D_2O) for the exchange between free NPr_4^+ and $NPr_4^+ \subset$ **4**. The magnetisation transfer delay between the selective inversion pulse and spectrum acquisition increases from the bottom to the top. Down: Guest self-exchange data for several cations within **4**. Reprinted with permission from Ref. [199]. Copyright (2006) American Chemical Society.

to reflect the entropy cost in correctly orientating each guest for passage through the tight host aperture. The high rate constant for the self-exchange of guest $NMe_2Pr_2^+$ at 298 K would be due to a more facile passage through the host aperture, due to its streamlined conformation. Selective inversion recovery experiments were also performed at different pressures to determine the $\Delta V^{\neq}$. The calculated values were +13 and +31 cm^3 mol^{-1} for the exchange of $NMe_2Pr_2^+$ and NPr_4^+, respectively. These positive values have been interpreted in terms of the expansion suffered by the host in the transition state and support a non-dissociative mechanism.

In another paper by the same group [200], guest self-exchange rates have also been calculated for two protonated diamines (*N*,*N*,*N*′,*N*′-tetramethyl-1,4-diaminobutane, **60**, and *N*,*N*,*N*′,*N*′-tetraethyl-1,2-diaminoethane, **61**) encapsulated within the cavity of **4**. The rate determinations were done using the CIFIT program at five different temperatures (from 300 to 340 K) in order to extract the activation parameters. The Eyring plots are reproduced in Fig. 33. The values obtained were $\Delta H^{\neq} = 45.1$, 69.8 kJ mol^{-1} and $\Delta S^{\neq} = -117.0$, -45.6 J K^{-1} mol^{-1} for the encapsulation of **60** and **61**, respectively. These results are consistent with those found for other tetraalkylammonium cations (Fig. 32) [199], pointing to a similar mechanism. The stabilization of protonated substrates by encapsulation inside **4** has been applied to the catalysis of the acidic orthoformate hydrolysis in basic solution [200].

A comparison between the activation parameters obtained from lineshape analysis and SIR experiments has been carried out by Stang and co-workers [201] for the hindered Pt-N(bipyridyl) rotation in the self-assembled rectangle **62** and triangle **63** (Scheme 23). Selective inversion recovery experiments provided more accurate data since they were measured at lower temperatures, where intermolecular bipyridyl exchange processes are suppressed. $\Delta H^{\neq}$ was found to be 52.2 and 59.1 kJ mol^{-1} for **62** and **63**, respectively, while $\Delta S^{\neq}$ was equal to −58.1 and −71.8 J K^{-1} mol^{-1}. These large negative entropy values were interpreted in terms of the solvent reorganization involved in the rotation process.

3.2.2. EXSY

As shown in the previous section, chemical exchange between two spins results in a transfer of longitudinal magnetisation between their positions. The same effect is caused by the dipolar coupling that gives rise to the NOE and, thus, NOE and chemical exchange can be detected by the same NMR experiments, even if the mechanisms of both phenomena are quite unrelated [202]. According to this, a NOESY experiment not only provides cross-peaks due to NOE but also cross-peaks between mutually exchanging positions and, when used for this purpose, this experiment is frequently termed EXSY (Exchange Spectroscopy) [203]. The NOESY/EXSY pulse sequence is a phase-sensitive experiment and the cross-peaks due to exchange can be distinguished because they appear with the same sign as

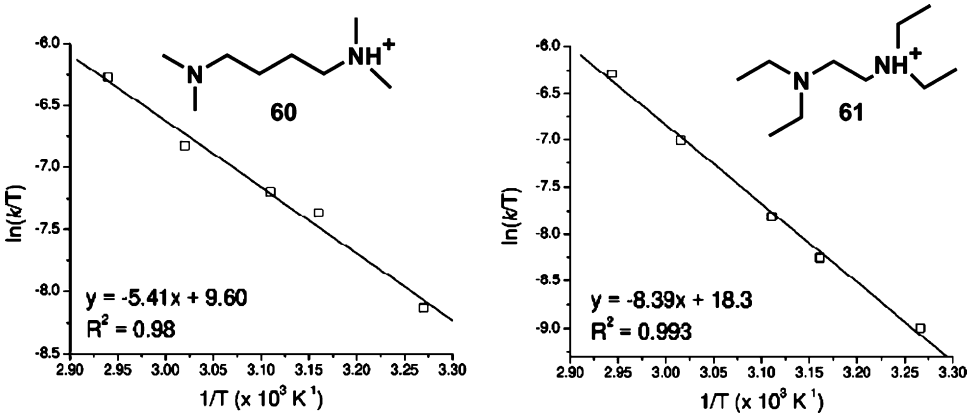

Fig. 33. Eyring plots for the self-exchange of guests **60** (left) and **61** (right) inside the host $[Ga_4L_6]^{12-}$ (**4**) in D_2O. From Ref. [201]. Reprinted with permission from AAAS.

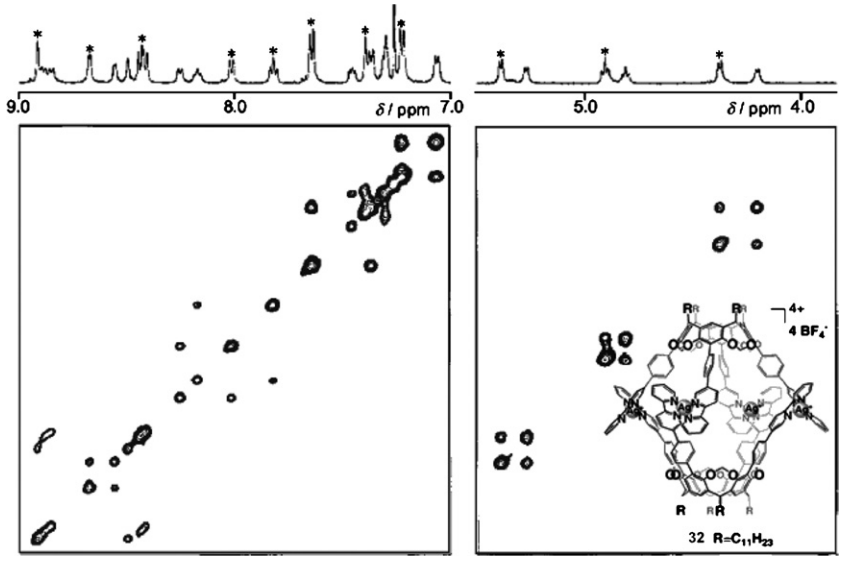

Fig. 34. Two sections of the ^{1}H EXSY (600 MHz, $CDCl_3$) spectrum of a mixture of the $[Ag_4L_2]^{4+}$ capsule **32** (0.40 mM) and the free resorcinarene ligand L (1.00 mM). The resonances of the free ligand are marked with an asterisk and only the phase of the spectrum corresponding to the exchange cross-peaks is shown. Spectra reproduced with permission from Ref. [154]. Copyright Wiley-VCH Verlag GmbH & Co. KGaA. Structure reproduced from Ref. [107] with permission of The Royal Society of Chemistry.

the diagonal peaks, while the NOE cross-peaks have the opposite sign.

Exchange processes which can be investigated with EXSY must be slow on the NMR timescale (i.e., the exchanging resonances must be resolved), but not too slow, as otherwise relaxation processes occurring during the mixing time of the experiment will remove all memory of the exchange process [202]. In practice, exchange processes with rates $k \approx 10^2$ to 10^{-2} s^{-1} can be investigated. Most usually, the EXSY experiment is used to elucidate qualitative aspects of exchange and its major advantage over 1D methods is the possibility to map complex exchange networks and elucidate exchange mechanisms [192]. However, EXSY spectra can also be used quantitatively for determination of the rate constants, based on the diagonal- and cross-peak intensities, although this approach requires either collecting EXSY spectra over a range of mixing time values (a time-consuming procedure) or using computational analysis on a single experiment (in this case the adequate selection of the mixing time is critical for success) [202,204]. The second procedure was used to evaluate the rate constants for guest uptake (3.9×10^3 M^{-1} s^{-1}) and release (32.9 s^{-1}) in the host–guest complex formed between a camphor molecule and the trinuclear Zn^{II} complex $[Zn_3(tib)_2(OAc)_6]$ (tib = 1,3,5-tris(imidazol-1-ylmethyl)benzene) [53].

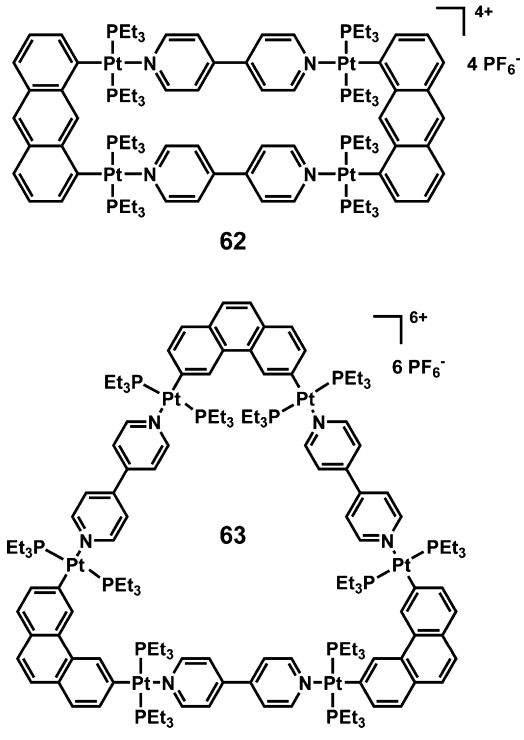

Scheme 23. Structure of the self-assembled rectangle **62** and triangle **63**.

Two sections of a typical ^{1}H EXSY spectrum are shown in Fig. 34 for a mixture of the $[Ag_4L_2]^{4+}$ capsule **32** and the free resorcinarene ligand L [154]. The signals of the ligand are marked with an asterisk. Only the phase of the spectrum corresponding to the exchange cross-peaks is shown, and the slow exchange between free and complexed ligand can be clearly appreciated.

Jeong and Park [205] have investigated the dynamic behaviour of the rotaxanes **64a–c**, self-assembled by hydrogen-bonding between the metallocycles **65a–c** and the dumbbell systems **66a–c**, two of them containing dendritic branches (Fig. 35). The activation energies for the formation of the rotaxanes were determined to be 66.5–70.2 kJ mol^{-1}, based on the diagonal and cross-peaks intensities of the separate NH signals of the complex and the free metallocycle in ^{1}H EXSY experiments (see Fig. 35 for an example). The activation energy

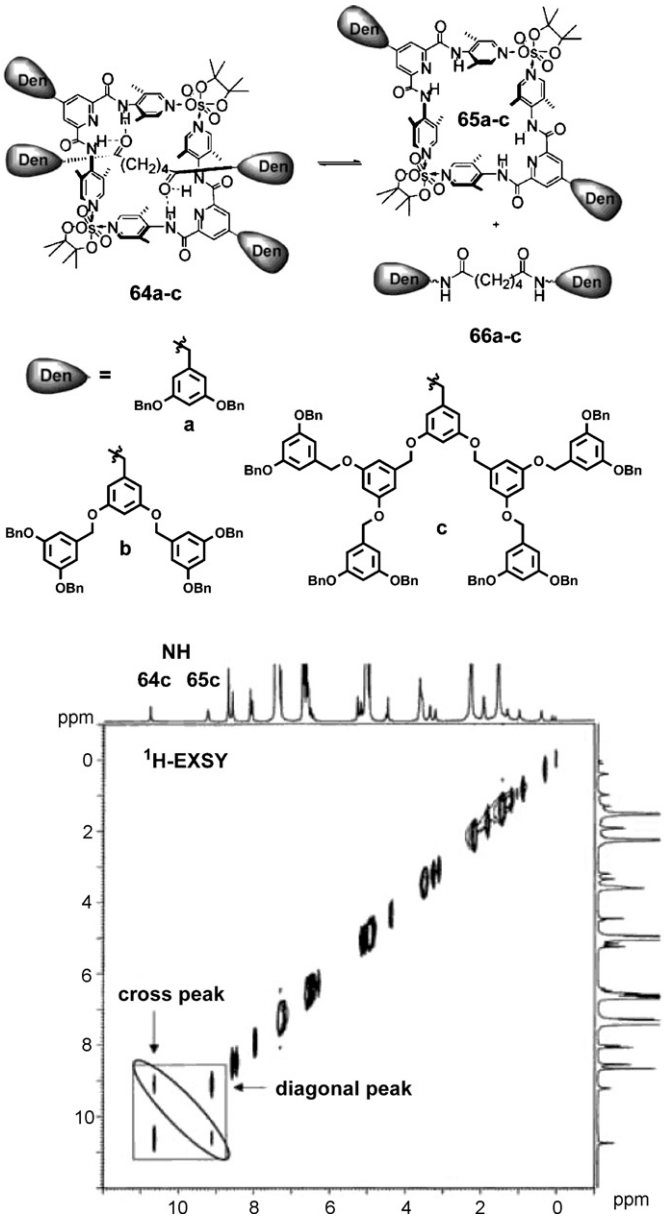

Fig. 35. Up: Rotaxanes **64a–c** are in slow exchange with their components, the metallocycles **65a–c** and the dumbbell molecules **66a–c**. Down: ^{1}H EXSY spectrum (500 MHz, $CDCl_3$) of a mixture of **65c** and **66c** (1–5 mM of each component) at 298 K. The cross-peaks relating the NH resonances of **65c** and **64c** (the second shifted to higher frequency due to the formation of a H-bond in the rotaxane) have been marked. Reprinted with permission from Ref. [206]. Copyright (2004) American Chemical Society.

increases with the size of the dendritic dumbbell, probably due to steric reasons. In another example by the same group [206], the dynamic behaviour of the rotaxanes **67a–d**, self-assembled from the metallomacrocycles **68a–d** and the dumbbell adipamide **69** (Scheme 24), was similarly investigated. The kinetic stabilities at room temperature follow the order **67a** (64.8 kJ mol^{-1}) < **67b** (66.9 kJ mol^{-1}) < **67c** (68.6 kJ mol^{-1}) < **67d** (which does not disassemble into its components at room temperature). In this example, the kinetic stabilities are directly related to the strength of the coordination bond in the metallomacrocycle [206].

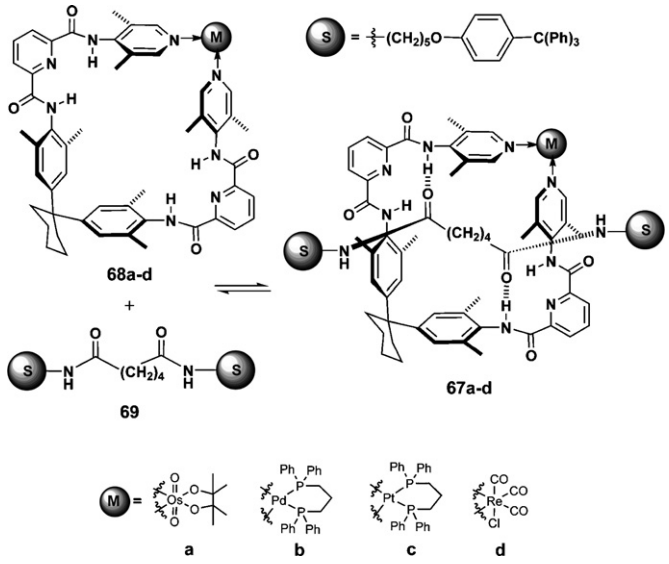

Scheme 24. The rotaxanes **67a–d** are formed by self-assembly of the metallomacrocycles **68a–d** and the dumbbell adipamide **69**.

In another application related to rotaxanes, the dynamic behaviour of the rectangular macrocycle **53** (formed by self-assembly of complementary bispyridine (**70**) and Zn–bisporphyrin (**71**) units) and of its rotaxane complex with the dumbbell diamide **72** (**53·72**) has been investigated (Scheme 25) [183]. The exchange between free **53** and the rotaxane **53·72**, as well as between the free bisporphyrin **71** and **71** bound within the macrocycle **53** could be simultaneously investigated using a ^{1}H EXSY spectrum at 253 K, as both processes are slow on the NMR time scale at that temperature. The rate constants were found to be $k_{rotaxane} = 13\ s^{-1}$ for the first process and $k_{macrocycle} = 2.2\ s^{-1}$ for the second. No cross-peaks were observed between the resonances of the rotaxane **53·72** and the free bisporphyrin **71**. Consequently, at this temperature, the interconversion between the rotaxane **53·72** and its components macrocycle **53** and diamide **72** is faster than any of the possible exchanges involving the free bisporphyrin **71**.

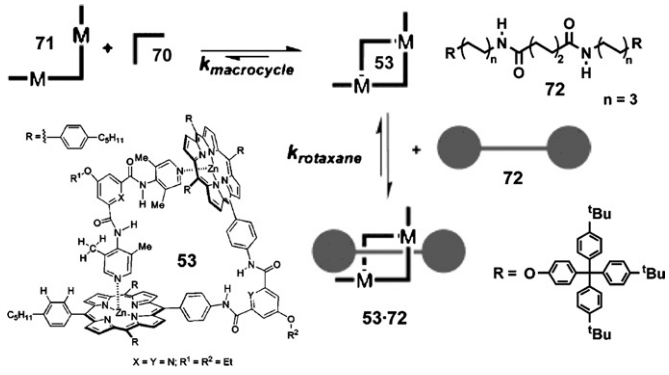

Scheme 25. Schematic representation of the dynamic processes involving the self-assembly of the macrocycle **53** (drawn in larger scale in Fig. 27) from the bispyridine **70** and the Zn–bisporphyrin **71**, and the formation of a rotaxane complex between **53** and the diamide **72**. Reprinted with permission from Ref. [183]. Copyright (2005) American Chemical Society.

4. Summary and outlook

Through the use of many, and mostly recent, examples we have tried to reflect how NMR is profusely and successfully used in the investigation of the structure and even the thermodynamic and kinetic properties of supramolecular complexes. We have described the most commonly used techniques, without elaborating on technical and theoretical issues which can be found in many of the cited references. Classic 1D ^{1}H, ^{13}C, ^{19}F and ^{31}P spectra reflect characteristic chemical shift changes due to metal–ligand interactions or encapsulation, a useful tool to monitor the formation of supramolecular complexes and host–guest assemblies. NMR-active metal nuclides turn out to be an alternative or complementary probe for the characterization of the coordination assemblies. 2D correlation experiments are ubiquitous in the literature, providing through-bond connectivities (COSY, TOCSY, HMQC, HMBC) and spatial interactions (NOESY, ROESY and HOESY), while PGSE diffusion measurements provide information about molecular size, intermolecular interactions and even association constants. We have also described other frequently used methodologies for the evaluation of association constants (simple signal integration and NMR titration) and how the thermodynamic parameters ΔH and ΔS of a supramolecular system can be derived from a van't Hoff analysis of $K_a(T)$. Finally, we have summarized the application of dynamic NMR methodologies (lineshape analysis, selective inversion recovery and 2D EXSY) to the calculation of the rate constants of dynamic supramolecular equilibria, as well as the use of Arrhenius and Eyring plots for the evaluation of the activation parameters (E_A, $\Delta H^{\neq}$ and $\Delta S^{\neq}$) of such processes.

The possibilities and applications of NMR seem to be in an endless expansion. Technical improvements in the standard equipment (stronger fields, widespread field gradients and temperature-control units, more versatile probes and powerful computers) as well as in the software (acquisition, processing, simulation, graphics) are accompanied by the development of new and more complicated pulse sequences and continuous improvements in those already existing. With an increasing efficiency, these advances are being rapidly incorporated into the toolkit of the supramolecular chemists, who are faced in their research with ever more challenging structural and functional questions. Due to its intrinsic complexity, we are convinced that supramolecular chemistry will continue to provide in the future one of the best showcases for exciting and impressive NMR applications.

Acknowledgements

A. Pastor thanks Prof. M. Alajarin for introducing her to Supramolecular Chemistry. A. Pastor is also grateful to the "Ministerio de Educación y Ciencia" (MEC) of Spain and FEDER funds (Project CTQ2005-02323/BQU) as well to the "Fundación Séneca-CARM" (Project 00458/PI/04) for funding. E. Martínez-Viviente thanks the MEC and the University of Murcia for her R&C research contract, as well as the MEC and FEDER for funding (projects CTQ2004-05396 and CTQ2007-60808/BQU), and Prof. J. Vicente and the "Organometallic Chemistry Research Group" for support in writing this review. Both authors are grateful to Prof. Pregosin for his invitation to participate in this special issue and his helpful comments.

References

[1] J.-M. Lehn, Angew. Chem. Int. Ed. Engl. 27 (1988) 90.
[2] J.F. Stoddart (Ed.), Monographs in Supramolecular Chemistry, Royal Society of Chemistry, Cambridge, 1989–2007;
V. Balzani, L. DeCola (Eds.), Supramolecular Chemistry, Kluwer Academic Publishers, 1992;
F. Vögtle, Supramolecular Chemistry—An Introduction, Wiley, New York, 1993;
J.-M. Lehn (Ed.), Perspectives in Supramolecular Chemistry, John Wiley & Sons, 1994–2004;
J.-M. Lehn, Supramolecular Chemistry: Concepts and Perspectives, VCH, Weinheim, 1995;
J.L. Atwood, J.E.D. Davies, D.D. MacNicol, F. Vögtle (Eds.), Comprehensive Supramolecular Chemistry, Pergamon, Oxford, 1996;
P.D. Beer, P.A. Gale, D.K. Smith, Supramolecular Chemistry, Oxford University Press, 1999;
J.W. Steed, J.L. Atwood, Supramolecular Chemistry, Wiley, Chichester, 2000;
J. Halpern (Ed.), Special-issue, Proc. Natl. Acad. Sci. U.S.A. 99 (2002) 4762;
P.A. Gale (Ed.), Special-issue, Chem. Soc. Rev. 36 (2007) 141.
[3] D.N. Reinhoudt, M. Crego-Calama, Science 295 (2002) 2403.
[4] V. Balzani, A. Credi, F.M. Raymo, J.F. Stoddart, Angew. Chem. Int. Ed. 39 (2000) 3348;
J. Halpern, Proc. Natl. Acad. Sci. U.S.A. 99 (2002) 4762;
G.M. Whitesides, M. Boncheva, Proc. Natl. Acad. Sci. U.S.A. 99 (2002) 4769;
H. Dodziuk, Introduction to Supramolecular Chemistry, Springer, 2002.
[5] D.N. Reinhoudt (Ed.), Perspectives in Supramolecular Chemistry, vol. 4, John Wiley & Sons, 1999.
[6] F.M. Menger, Proc. Natl. Acad. Sci. U.S.A. 99 (2002) 4818.
[7] J.-M. Lehn, Pure Appl. Chem. 66 (1994) 1961;
D.S. Lawrence, T. Jiang, M. Levett, Chem. Rev. 95 (1995) 2229;
I.M. Atkinson, L.F. Lindoy, Self-assembly in Supramolecular Systems (Monographs in Supramolecular Chemistry), RSC Publishing, 2000.
[8] D. Philp, J.F. Stoddart, Angew. Chem. Int. Ed. Engl. 35 (1996) 1155.
[9] P.J. Stang, B. Olenyuk, Acc. Chem. Res. 30 (1997) 502.
[10] S. Leininger, B. Olenyuk, P.J. Stang, Chem. Rev. 100 (2000) 853.
[11] A. Lützen, Angew. Chem. Int. Ed. 44 (2005) 1000.
[12] J.E. Varner (Ed.), Self-assembling Architecture, Alan R. Liss, New York, 1988;
F. Cramer, Chaos and Order. The Complex Structure of Living Systems, VCH, Weinheim, 1993;
L.M. Greig, D. Philp, Chem. Soc. Rev. 30 (2001) 287;
T.D. Hamilton, L.R. MacGillivray, in: J.L. Atwood, J.W. Steed (Eds.), Encyclopedia of Supramolecular Chemistry, Dekker, New York, 2004, p. 1257.
[13] J. Rebek Jr., Acc. Chem. Res. 32 (1999) 278;
L.J. Prins, D.N. Reinhoudt, P. Timmerman, Angew. Chem. Int. Ed. 40 (2001) 2382;
M. Alajarín, A. López-Lázaro, A. Pastor, P.D. Prince, J.W. Steed, R. Arakawa, Chem. Commun. (2001) 169;
M. Alajarín, A. Pastor, R.A. Orenes, J.W. Steed, J. Org. Chem. 67 (2002) 7091;
M. Alajarín, A. Pastor, R.A. Orenes, J.W. Steed, R. Arakawa, Chem. Eur. J. 67 (2004) 1383.
[14] M. Fujita, K. Ogura, Coord. Chem. Rev. 148 (1996) 249;
M.M. Conn, J. Rebek Jr., Chem. Rev. 97 (1997) 1647;
R.W. Saalfrank, B. Demleitner, in: J.P. Sauvage (Ed.), Perspectives in Supramolecular Chemistry: Transition Metals in Supramolecular Chemistry, John Wiley & Sons, 1999, p. 1.

[15] B. Linton, A.D. Hamilton, Chem. Rev. 97 (1997) 1669.
[16] M. Fujita, Chem. Soc. Rev. 27 (1998) 417;
D.L. Caulder, K.N. Raymond, J. Chem. Soc. Dalton Trans. (1999) 1185;
S.R. Seidel, P.J. Stang, Acc. Chem. Res. 35 (2002) 972.
[17] C.J. Jones, Chem. Soc. Rev. 27 (1998) 289;
C.H.M. Amijs, G.P.M. van Klink, G. van Koten, Dalton Trans. (2006) 308.
[18] J.-P. Sauvage, Acc. Chem. Res. 31 (1998) 611;
B.J. Holliday, C.A. Mirkin, Angew. Chem. Int. Ed. 40 (2001) 2022;
M. Ruben, J. Rojo, F.J. Romero-Salguero, L.H. Uppadine, J.-M. Lehn, Angew. Chem. Int. Ed. 43 (2004) 3644.
[19] G.F. Swiegers, T.J. Malefetse, Chem. Rev. 100 (2000) 3483;
M. Fujita, M.K. Umemoto, M. Yoshizawa, N. Fujita, T. Kusukawa, K. Biradha, Chem. Commun. (2001) 509;
G.F. Swiegers, T.J. Malefetse, Coord. Chem. Rev. 225 (2002) 91;
M. Fujita, M. Tominaga, A.B Hori, B. Therrien, Acc. Chem. Res. 38 (2005) 369.
[20] J.-P. Sauvage (Ed.), Perspectives in Supramolecular Chemistry, vol. 5, John Wiley & Sons, 1999;
R.M. Yeh, A.V. Davis, K.N. Raymond, in: J.A. McCleverty, T.J. Meyer (Eds.), Comprehensive Coordination Chemistry II, Elsevier, Oxford, 2004, p. 327.
[21] F. Wurthner, C.C. You, C.R. Saha-Moller, Chem. Soc. Rev. 33 (2004) 133.
[22] G.A. Morris, S.T. Nguyen, J.T. Hupp, J. Mol. Catal. A: Chem. 174 (2001) 15;
S.J. Lee, A.G. Hu, W.B. Lin, J. Am. Chem. Soc. 124 (2002) 12948;
N.C. Gianneschi, M.S. Masar, C.A. Mirkin, Acc. Chem. Res. 38 (2005) 825;
M.J. Wilkinson, P.W.N.M. van Leeuwen, J.N.H. Reek, Org. Biomol. Chem. 3 (2005) 2371;
A.W. Kleij, J.N.H. Reek, Chem. Eur. J. 12 (2006) 4218.
[23] D. Fiedler, D.H. Leung, R.G. Bergman, K.N. Raymond, Acc. Chem. Res. 38 (2005) 351.
[24] E.R. Kay, D.A. Leigh, F. Zerbetto, Angew. Chem. Int. Ed. 46 (2007) 72.
[25] D.R. Turner, A. Pastor, M. Alajarin, J.W. Steed, Struct. Bonding 108 (2004) 97.
[26] M. Yoshizawa, T. Kusukawa, M. Fujita, S. Sakamoto, K. Yamaguchi, J. Am. Chem. Soc. 123 (2001) 10454;
M. Yoshizawa, T. Kusukawa, M. Fujita, K. Yamaguchi, J. Am. Chem. Soc. 122 (2000) 6311;
J.L. Brumaghim, M. Michels, D. Pagliero, K.N. Raymond, Eur. J. Org. Chem. (2004) 5115.
[27] D. Fiedler, R.G. Bergman, K.N. Raymond, Angew. Chem. Int. Ed. 45 (2006) 745.
[28] M.D. Pluth, K.N. Raymond, Chem. Soc. Rev. 36 (2007) 161.
[29] M. Yoshizawa, Y. Takeyama, T. Kusukawa, M. Fujita, Angew. Chem. Int. Ed. 41 (2002) 1347;
M. Yoshizawa, Y. Takeyama, T. Okano, M. Fujita, J. Am. Chem. Soc. 125 (2003) 3243.
[30] T. Furusawa, M. Kawano, M. Fujita, Angew. Chem. Int. Ed. 46 (2007) 5717.
[31] D.H. Leung, D. Fiedler, R.G. Bergman, K.N. Raymond, Angew. Chem. Int. Ed. 43 (2004) 963.
[32] D.H. Leung, R.G. Bergman, K.N. Raymond, J. Am. Chem. Soc. 128 (2006) 9781.
[33] D. Fiedler, R.G. Bergman, K.N. Raymond, Angew. Chem. Int. Ed. 43 (2004) 6748.
[34] D. Fiedler, H. van Halbeek, R.G. Bergman, K.N. Raymond, J. Am. Chem. Soc. 128 (2006) 10240.
[35] M. Yoshizawa, M. Tamura, M. Fujita, Science 312 (2006) 251;
D.H. Leung, R.G. Bergman, K.N. Raymond, J. Am. Chem. Soc. 129 (2007) 2746.
[36] C.A. Schalley (Ed.), Analytical Methods in Supramolecular Chemistry, Wiley, 2007.
[37] B. Hasenknopf, J.-M. Lehn, N. Boumediene, A. Dupont-Gervais, A. Van Dorsselaer, B. Kneisel, D. Fenske, J. Am. Chem. Soc. 119 (1997) 10956;
J.S. Fleming, K.L.V. Mann, C.-A. Carraz, E. Psillakis, J.C. Jeffery, J.A. McCleverty, M.D. Ward, Angew. Chem. Int. Ed. 37 (1998) 1279;
M. Scherer, D.L. Caulder, D.W. Johnson, K.N. Raymond, Angew. Chem. Int. Ed. 38 (1999) 1588;
K. Umemoto, K. Yamaguchi, M. Fujita, J. Am. Chem. Soc. 122 (2000) 7150.
[38] K. Kobayashi, Y. Yamada, M. Yamanaka, Y. Sei, K. Yamaguchi, J. Am. Chem. Soc. 126 (2004) 13896.
[39] M. Albrecht, S. Mirtschin, M. de Groot, I. Janser, J. Runsink, G. Raabe, M. Kogej, C.A. Schalley, R. Fröhlich, J. Am. Chem. Soc. 127 (2005) 10371.
[40] J. Ramírez, A.-M. Stadler, N. Kyritsakas, J.-M. Lehn, Chem. Commun. (2007) 237.
[41] M. Fujita, O. Sasaki, T. Mitsuhashi, T. Fujita, J. Yazaki, K. Yamaguchi, K. Ogura, Chem. Commun. (1996) 1535;
S.B. Lee, S. Hwang, D.S. Chung, H. Yun, J.-I. Hong, Tetrahedron Lett. 39 (1998) 873.
[42] T. Kusukawa, M. Yoshizawa, M. Fujita, Angew. Chem. Int. Ed. 40 (2001) 1879.
[43] A.V. Davis, R.M. Yeh, K.N. Raymond, Proc. Natl. Acad. Sci. U.S.A. 99 (2002) 4793.
[44] R.M. Silverstein, F.X. Webster, D. Kiemle, Spectrometric Identification of Organic Compounds, Wiley, 2005.
[45] J.-P. Bourgeois, M. Fujita, M. Kawano, S. Sakamoto, K. Yamaguchi, J. Am. Chem. Soc. 125 (2003) 9260.
[46] D. Zuccaccia, L. Pirondini, R. Pinalli, E. Dalcanale, A. Macchioni, J. Am. Chem. Soc. 127 (2005) 7025.
[47] T.N. Parac, M. Scherer, K.N. Raymond, Angew. Chem. Int. Ed. 39 (2000) 1239.
[48] A. Ikeda, M. Yoshimura, H. Udzu, C. Fukuhara, S. Shinkai, J. Am. Chem. Soc. 121 (1999) 4296.
[49] A. Ouchi, K. Tashiro, K. Yamaguchi, T. Tsuchiya, T. Akasaka, T. Aida, Angew. Chem. Int. Ed. 45 (2006) 3542.
[50] K. Tashiro, T. Aida, Chem. Soc. Rev. 36 (2007) 189.
[51] S. Tashiro, M. Tominaga, T. Kusukawa, M. Kawano, S. Sakamoto, K. Yamaguchi, M. Fujita, Angew. Chem. Int. Ed. 42 (2003) 3267.
[52] T. Kusukawa, M. Fujita, Angew. Chem. Int. Ed. 37 (1998) 3142.
[53] H.-K. Liu, W.-Y. Sun, D.-J. Ma, K.-B. Yu, W.-X. Tang, Chem. Commun. (2000) 591.
[54] G. Schürmann, F. Diederich, Tetrahedron Lett. 27 (1986) 4249.
[55] C.W. Lim, J.-I. Hong, Tetrahedron Lett. 41 (2000) 3113.
[56] C.-Y. Su, Y.-P. Cai, C.-L. Chen, F. Lissner, B.-S. Kang, W. Kaim, Angew. Chem. Int. Ed. 41 (2002) 3371;
Y.-P. Cai, C.-Y. Su, C.-L. Chen, Y.-M. Li, B.-S. Kang, A.S.C. Chan, W. Kaim, Inorg. Chem. 42 (2003) 163.
[57] B.E.F. Tiedemann, K.N. Raymond, Angew. Chem. Int. Ed. 45 (2006) 83.
[58] P.J. Stang, B. Olenyuk, Angew. Chem. Int. Ed. Engl. 35 (1996) 732.
[59] P.J. Stang, B. Olenyuk, D.C. Muddiman, R.D. Smith, Organometallics 16 (1997) 3094.
[60] J.M. Rivera, T. Martin, J. Rebek Jr., Science 279 (1998) 1021;
C. Nuckolls, F. Hof, T. Martín, J. Rebek Jr., J. Am. Chem. Soc. 121 (1999) 10281;
J.M. Rivera, T. Martín, J. Rebek Jr., J. Am. Chem. Soc. 123 (2001) 5213.
[61] A. Scarso, J. Rebek Jr., Supramolecular Chirality (in Topics in Current Chemistry), Springer, Berlin, 2006, p. 1.
[62] G. Seeber, B.E.F. Tiedemann, K.N. Raymond, Supramolecular Chirality (in Topics in Current Chemistry), Springer, Berlin, 2006, p. 147.
[63] S. Hiraoka, M. Fujita, J. Am. Chem. Soc. 121 (1999) 10239.
[64] J.L. Brumaghim, M. Michels, K.N. Raymond, Eur. J. Org. Chem. (2004) 4552.
[65] D. Fiedler, D.H. Leung, R.G. Bergman, K.N. Raymond, J. Am. Chem. Soc. 126 (2004) 3674.
[66] A. Ikeda, H. Udzu, Z. Zhong, S. Shinkai, S. Sakamoto, K. Yamaguchi, J. Am. Chem. Soc. 123 (2001) 3872.
[67] E. Lindner, M. Khanfar, J. Organomet. Chem. 630 (2001) 244.
[68] E. Lindner, M. Khanfar, M. Steimann, Eur. J. Inorg. Chem. (2001) 2411.
[69] D.C. Caskey, R.K. Shoemaker, J. Michl, Org. Lett. 6 (2004) 2093.
[70] P.N.W. Baxter, J.-M. Lehn, J. Fischer, M.-T. Youinou, Angew. Chem. Int. Ed. Engl. 33 (1994) 2284.

[71] P.N.W. Baxter, J.-M. Lehn, B.O. Kneisel, D. Fenske, Angew. Chem. Int. Ed. Engl. 36 (1997) 1978.
[72] A. Marquis, J.-P. Kintzinger, R. Graff, P.N.W. Baxter, J.-M. Lehn, Angew. Chem. Int. Ed. 41 (2002) 2760.
[73] O. Mamula, F.J. Monlien, A. Porquet, G. Hopfgartner, A.E. Merbach, A. von Zelewsky, Chem. Eur. J. 7 (2001) 533.
[74] M. Barboiu, J.-M. Lehn, Proc. Nat. Acad. Sci. U.S.A. 99 (2002) 5201.
[75] A.-M. Stadler, N. Kyritsakas, R. Graff, J.-M. Lehn, Chem. Eur. J. 12 (2006) 4503.
[76] M.F. Hawthorne, X. Yang, Z. Zheng, Pure Appl. Chem. 66 (1994) 245; Z.P. Zheng, C.B. Knobler, M.D. Mortimer, G.G. Kong, M.F. Hawthorne, Inorg. Chem. 35 (1996) 1235.
[77] X.G. Yang, C.B. Knobler, Z.P. Zheng, M.F. Hawthorne, J. Am. Chem. Soc. 116 (1994) 7142.
[78] A.A. Zinn, Z.P. Zheng, C.B. Knobler, M.F. Hawthorne, J. Am. Chem. Soc. 118 (1996) 70.
[79] S.G. Telfer, R. Kuroda, Chem. Eur. J. 11 (2005) 57.
[80] T.D.W. Claridge, High Resolution NMR Techniques in Organic Chemistry, Pergamon, Oxford, 1999.
[81] J. Jeener, Ampère International Summer School Basko Polje, Yugoslavia (1971); A. Bax, R. Freeman, J. Magn. Reson. 44 (1981) 542.
[82] Ref. [80] (Chapter 5).
[83] P. de Wolf, P. Waywell, M. Hanson, S.L. Heath, A.J.H.M. Meijer, S.J. Teat, J.A. Thomas, Chem. Eur. J. 12 (2006) 2188.
[84] The LR COSY experiment is a slight modification of the basic COSY sequence and allows the detection of weak long-range ^{1}H,^{1}H couplings. See A. Bax, R. Freeman, J. Magn. Reson. 44 (1981) 542.
[85] M. Greenwald, D. Wessely, I. Goldberg, Y. Cohen, New J. Chem. (1999) 337.
[86] M. Shaul, Y. Cohen, J. Org. Chem. 64 (1999) 9358.
[87] L. Braunschweiler, R.R. Ernst, J. Magn. Reson. 53 (1983) 521.
[88] K. Kumazawa, Y. Yamanoi, M. Yoshizawa, T. Kusukawa, M. Fujita, Angew. Chem. Int. Ed. 43 (2004) 5936.
[89] S. Tashiro, M. Tominaga, Y. Yamaguchi, K. Kato, M. Fujita, Chem. Eur. J. 12 (2006) 3211.
[90] S. Tashiro, M. Kobayashi, M. Fujita, J. Am. Chem. Soc. 128 (2006) 9280.
[91] A. Bax, S. Subramanian, J. Magn. Reson. 67 (1986) 565.
[92] G. Bodenhausen, D.J. Ruben, Chem. Phys. Lett. 69 (1980) 185.
[93] Compared with the HMQC, the HSQC experiment results in higher resolution in the second dimension and is more flexible with regard to modifications in the pulse sequence. However, the long HSQC pulse sequence is more sensitive to field inhomogeneity and pulse miscalibration. This problem has a greater significance for ^{13}C than for ^{15}N, owing to the greater frequency spread of the former. Consequently, the HMQC experiment has been traditionally favoured by experimental chemists for ^{1}H,^{13}C correlations, while the HSQC experiment has been widely used in biochemistry for ^{1}H,^{15}N correlations.
[94] A. Bax, M.F. Summers, J. Am. Chem. Soc. 108 (1986) 2093.
[95] M. Chas, V. Blanco, C. Peinador, J.M. Quintela, Org. Lett. 9 (2007) 675.
[96] K. Ono, M. Yoshizawa, T. Kato, K. Watanabe, M. Fujita, Angew. Chem. Int. Ed. 46 (2007) 1803.
[97] A.-M. Stadler, N. Kyritsakas, G. Vaughan, J.-M. Lehn, Chem. Eur. J. 13 (2007) 59.
[98] S. Macura, Y. Huang, D. Suter, R.R. Ernst, J. Magn. Reson. 43 (1981) 259.
[99] The Nuclear Overhauser Effect (NOE) is the change in intensity of a resonance when the spin transitions of another are somehow perturbed from their equilibrium populations. See ref. [80] (Chapter 8).
[100] The sign and size of the NOE depends on the product $\omega_o \cdot \tau_c$, where ω_o is the spectrometer observation frequency and τ_c is the correlation time, a parameter inversely proportional to the speed of the tumbling motion of the molecule. Thus, changes in the spectrometer, the temperature and the solvent can strongly influence the NOE.
[101] ROEs develop while the magnetisation is held static in the transverse plane, rather than along the longitudinal axis, as NOEs.
[102] Ref. [80] (Chapter 8).
[103] A.A. Borthner-By, R.L. Stephens, J. Lee, J. Am. Chem. Soc. 106 (1984) 811; A. Bax, D.G. Davis, J. Magn. Reson. 63 (1985) 207; The ROESY experiment is also termed CAMELSPIN (Cross-relaxation Appropiate for Minimolecules Emulated by Locked SPINs), as the cross-relaxation takes place in the rotating frame with spin-locked magnetization.
[104] R. Krämer, J.-M. Lehn, A. Marquis-Rigault, Proc. Natl. Acad. Sci. U.S.A. 90 (1993) 5394.
[105] A. Marquis, V. Smith, J. Harrowfield, J.-M. Lehn, H. Herschbach, R. Sanvito, E. Leize-Wagner, A. Van Dorsselaer, Chem. Eur. J. 12 (2006) 5632.
[106] D. Moon, S. Kang, J. Park, K. Lee, R.P. John, H. Won, G.H. Seong, Y.S. Kim, G.H. Kim, H. Rhee, M.S. Lah, J. Am. Chem. Soc. 128 (2006) 3530.
[107] T. Haino, M. Kobayashi, M. Chikaraishi, Y. Fukazawa, Chem. Commun. (2005) 2321.
[108] D.L. Caulder, C. Bruckner, R.E. Powers, S. Konig, T.N. Parac, J.A. Leary, K.N. Raymond, J. Am. Chem. Soc. 123 (2001) 8923.
[109] D. Fiedler, D. Pagliero, J.L. Brumaghim, R.G. Bergman, K.N. Raymond, Inorg. Chem. 43 (2004) 846.
[110] M. Yoshizawa, M. Tamura, M. Fujita, J. Am. Chem. Soc. 126 (2004) 6846.
[111] Assuming a linear NOE growth, the magnitude of the enhancement between two spins A and B after a time τ will be proportional to the cross-relaxation rate, which in turn depends on the distance $r_{AB}^{1/6}$. Using a known internal distance as a reference, r_{XY}, and determining the NOE growth rates σ for that reference and the unknown distance, the latter can be calculated, according to $r_{AB} = r_{XY}(\sigma_{XY}/\sigma_{AB})^{1/6}$. See D. Neuhaus, M.P. Williamson, The Nuclear Overhauser Effect in Structural and Conformational Analysis, VCH Publishers, New York, 2001. Due to the $r^{1/6}$ dependence, the calculated r_{AB} is relatively insensitive to the experimental accuracy (a factor of 2 error in the growth rate leads to only ca. 10% error in the distance).
[112] B. Binotti, A. Macchioni, C. Zuccaccia, D. Zuccaccia, Comments Inorg. Chem. 23 (2002) 417.
[113] A. Macchioni, Eur. J. Inorg. Chem. (2003) 195.
[114] This guest dissociation is slower than the rate of C–H bond activation, indicating that the reactions with the encapsulated guest occur within the cavity of the host.
[115] J.L. Battiste, N. Jing, R.A. Newmark, J. Fluorine Chem. 125 (2004) 1331.
[116] M.F. Mahon, M.K. Whittlesey, P.T. Wood, Organometallics 18 (1999) 4068; H. Li, C. Frieden, Biochemistry 45 (2006) 6272; C. Lu, D.D. DesMarteau, J. Fluorine Chem. 128 (2007) 832.
[117] S. Sato, J. Iida, K. Suzuki, M. Kawano, T. Ozeki, M. Fujita, Science 313 (2006) 1273.
[118] P. Pregosin, P.G.A. Kumar, I. Fernandez, Chem. Rev. 105 (2005) 2977.
[119] P.L. Rinaldi, J. Am. Chem. Soc. 105 (1983) 5167.
[120] A quantitative comparison between NOE's requires a mixing time within the initial linear buildup of the NOE, as well as a recycle delay higher than 5 times T_1, to avoid saturation effects.
[121] E. Menozzi, M. Busi, C. Massera, F. Ugozzoli, D. Zuccaccia, A. Macchioni, E. Dalcanale, J. Org. Chem. 71 (2006) 2617.
[122] P.S. Pregosin, E. Martínez-Viviente, P.G.A. Kumar, Dalton Trans. (2003) 4007.
[123] T. Brand, E.J. Cabrita, S. Berger, Prog. Nucl. Magn. Reson. Spectrosc. 46 (2005) 159.
[124] P. Stilbs, Progr. Nucl. Magn. Reson. Spectrosc. 19 (1987) 1; W.S. Price, Annu. Rep. NMR Spectrosc. 32 (1996) 51; W.S. Price, Concepts Magn. Reson. 9 (1997) 299; W.S. Price, Concepts Magn. Reson. 10 (1998) 197.
[125] E.O. Stejskal, J.E. Tanner, J. Chem. Phys. 42 (1965) 288.
[126] P.S. Pregosin, Prog. Nucl. Magn. Reson. Spectrosc. 49 (2006) 261.
[127] R. Van de Coevering, A.P. Alfers, J.D. Meeldijk, E. Martínez-Viviente, P.S. Pregosin, R.J.M. Klein Gebbink, G. van Koten, J. Am. Chem. Soc. 128 (2006) 12700; D. Zuccaccia, L. Busetto, M.C. Cassani, A. Macchioni, R. Mazzoni, Organometallics 25 (2006) 2201;

D. Sobransingh, A.E. Kaifer, Chem. Commun. (2005) 5071.
[128] T. Nose, Annu. Rep. NMR Spectrosc. 27 (1993) 218;
E. Bukhaltsev, L. Frish, Y. Cohen, A. Vigalok, Org. Lett. 7 (2005) 5123.
[129] K. Hayamizu, E. Akiba, T. Bando, Y. Aihara, W.S. Price, Macromolecules 36 (2003) 2785.
[130] J. Kärger, D.M. Ruthven (Eds.), Diffusion in Zeolites and Other Microporous Solids, Wiley, New York, 1992.
[131] O. Söderman, P. Stilbs, Prog. Nucl. Magn. Reson. Spectrosc. 26 (1994) 445.
[132] J. Plass, D. Emeis, B. Blumich, J. Surfactants Deterg. 4 (2001) 379.
[133] E. Johannessen, H. Walderhaug, B. Balinov, Langmuir 20 (2004) 336.
[134] G. Lindblom, G. Oradd, Prog. Nucl. Magn. Reson. Spectrosc. 26 (1994) 483;
M. Cifelli, P.J. McDonald, C.A. Veracini, Phys. Chem. Chem. Phys. 6 (2004) 4701.
[135] S.V. Dvinskikh, I. Furo, D. Sandstrom, A. Maliniak, H. Zimmermann, J. Magn. Reson. 153 (2001) 83.
[136] D. Nama, P.G. Anil Kumar, P.S. Pregosin, T. Geldbach, P.J. Dyson, Inorg. Chim. Acta 359 (2006) 1907.
[137] M.J. Hubley, T.S. Moerland, NMR Biomed. (1995) 113;
A. Accardo, E. Tesauro, P. Roscigno, E. Gianolio, L. Paduano, G. D'Errico, C. Pedone, G. Morelli, J. Am. Chem. Soc. 126 (2004) 3097.
[138] S. Fichele, M.N.J. Paley, N. Woodhouse, P.D. Griffiths, E.J.R. van Beek, J.M. Wild, J. Magn. Reson. 167 (2004) 1.
[139] S.G. Yao, G.J. Howlett, R.S. Norton, J. Biomol. NMR 16 (2000) 109;
M.S. Kaucher, Y.-F. Lam, S. Pieraccini, G.A. Gottarelli, J.T. Davis, Chem. Eur. J. 11 (2005) 164.
[140] Y. Cohen, L. Avram, L. Frish, Angew. Chem. Int. Ed. 44 (2005) 520.
[141] M. Alajarín, A. Pastor, R.A. Orenes, E. Martínez-Viviente, P.S. Pregosin, Chem. Eur. J. 12 (2006) 877.
[142] M. Alajarín, A. Pastor, R.-A. Orenes, E. Martínez-Viviente, H. Rüegger, P.S. Pregosin, Chem. Eur. J. 13 (2007) 1559.
[143] M. Valentini, H. Ruegger, P.S. Pregosin, Helv. Chim. Acta 84 (2001) 2833.
[144] E. Martínez-Viviente, P. Pregosin, Helv. Chim. Acta 86 (2003) 2364.
[145] F. Hallwass, M. Engelsberg, A.M. Simas, J. Phys. Chem. A 106 (2002) 589.
[146] I. Fernández, E. Martínez-Viviente, F. Breher, P.S. Pregosin, Chem. Eur. J. 11 (2005) 1495.
[147] E. Martínez-Viviente, H. Rüegger, P.S. Pregosin, J. Lopez-Serrano, Organometallics 21 (2002) 5841.
[148] D. Nama, P.G. Anil Kumar, P.S. Pregosin, Magn. Reson. Chem. 43 (2005) 246.
[149] S.R. Heil, M. Holz, T.M. Kastner, H. Weingärtner, J. Chem. Soc. Faraday Trans. 91 (1995) 1877.
[150] It is accepted that the factor 6 in the Stokes–Einstein Equation is not valid for small species which are comparable in size to the solvent molecules. The limits for this condition are not clear, but in general when $r_{solute}/r_{solvent}$ = ca. 2 the substitution of 6 by 4, or its multiplication by an empirical factor f ($f < 1$) have been proposed. See for instance;
A. Spernol, K. Wirtz, Z. Naturforsch. A 8 (1953) 522;
A. Gierer, K. Wirtz, Z. Naturforsch. A 8 (1953) 532;
H.C. Chen, S.H. Chen, J. Phys. Chem. 88 (1984) 5118;
J.T. Edward, J. Chem. Ed. 47 (1970) 261;
M.J. Ue, Electrochem. Soc. 141 (1994) 3336.
[151] U. Michelsen, C.A. Hunter, Angew. Chem. Int. Ed. 39 (2000) 764.
[152] X. Ribas, J.C. Dias, J. Morgado, K. Wurst, M. Almeida, T. Parella, J. Veciana, C. Rovira, Angew. Chem. Int. Ed. 43 (2004) 4049.
[153] B. Olenyuk, M.D. Levin, J.A. Whiteford, J.E. Shield, P.J. Stang, J. Am. Chem. Soc. 121 (1999) 10434.
[154] T. Haino, M. Kobayashi, Y. Fukazawa, Chem. Eur. J. 12 (2006) 3310.
[155] These theoretical calculations have been made for large-sized molecules, such as proteins. For lower sized molecules the expected ratio $D_{dimer}/D_{monomer}$ would be ca. 0.79, supposing molecular spheres and $V_{dimer} = 2V_{monomer}$ ($r_{dimer} = 1.25\ r_{monomer}$);
V.V. Krishnan, J. Magn. Reson. 124 (1997) 468.
[156] The three semi-axes of the dimeric structure deriving from Spartan calculations are 18.3, 11.8 and 11.7 (average: 13.9) for the monomer and 22.8, 18.3 and 11.7 (average: 17.6) for the dimer. Although the r_H of 16.0 seems to be closer to a dimer, it has to be considered that this r_H-value includes the four OTf counterions, which in $CDCl_3$ diffuse together with the cation, as confirmed by NOE and PGSE measurements.
[157] C. Ihm, Y.J. Ko, J.H. Shin, K. Paek, Tetrahedron Lett. 47 (2006) 8847.
[158] K.F. Morris, C.S.J. Johnson, J. Am. Chem. Soc. 114 (1992) 3139.
[159] C.S.J. Johnson, Prog. Nucl. Magn. Reson. Spectrosc. 34 (1999) 203.
[160] G. Ligthart, H. Ohkawa, R.P. Sijbesma, E.W. Meijer, J. Am. Chem. Soc. 127 (2005) 810;
J. Barberá, L. Puig, P. Romero, J.L. Serrano, T. Sierra, J. Am. Chem. Soc. 127 (2005) 458;
T. Zhao, H.W. Beckham, H.W. Gibson, Macromolecules 36 (2003) 4833.
[161] C. Gambs, T.J. Dickerson, S. Mahajan, L.B. Pasternack, K.D. Janda, J. Org. Chem. 68 (2003) 3673.
[162] A. Ambrus, D. Yang, Anal. Biochem. 367 (2007) 56;
S. Viel, D. Capitani, L. Mannina, A. Segre, Biomacromolecules 4 (2003) 1843.
[163] E.J. Cabrita, S. Berger, Magn. Reson. Chem. 39 (2001) S142;
S. Viel, L. Mannina, A. Segre, Tetrahedron Lett. 43 (2002) 2515.
[164] A. Hijazi, J.P. Djukic, L. Allouche, A. De Cian, M. Pfeffer, X.-F. Le Goff, L. Ricard, Organometallics 26 (2007) 4180;
I. Keresztes, P.G. Williard, J. Am. Chem. Soc. 122 (2000) 10228.
[165] S.J. Dalgarno, J. Fischer, C.L. Raston, Chem. Eur. J. 12 (2006) 2772;
J. Barberá, L. Puig, P. Romero, J.L. Serrano, T. Sierra, J. Am. Chem. Soc. 128 (2006) 4487;
S.A. Fernandes, L.F. Cabeca, A.J. Marsaioli, E. Paula, J. Incl. Phenom. Macrocycl. Chem. 57 (2007) 395;
H. Kato, C. Boettcher, A. Hirsch, Eur. J. Org. Chem. (2007) 2659.
[166] L. Allouche, A. Marquis, J.-M. Lehn, Chem. Eur. J. 12 (2006) 7520.
[167] R.S.K. Kishore, V. Kalsani, M. Schmittel, Chem. Commun. (2006) 3690.
[168] R.S.K. Kishore, T. Paululat, M. Schmittel, Chem. Eur. J. 12 (2006) 8136.
[169] P. Timmerman, J.L. Weidmann, K.A. Jolliffe, L.J. Prins, D.N. Reinhoudt, S. Shinkai, L. Frish, Y. Cohen, J. Chem. Soc. Perkin Trans. (2000) 2077.
[170] T. Murase, S. Sato, M. Fujita, Angew. Chem. Int. Ed. 46 (2007) 1083.
[171] M. Tominaga, K. Suzuki, M. Kawano, T. Kusukawa, T. Ozeki, S. Sakamoto, K. Yamaguchi, M. Fujita, Angew. Chem. Int. Ed. 43 (2004) 5621.
[172] A. Hori, K. Yamashita, T. Kusukawa, A. Akasaka, K. Biradha, M. Fujita, Chem. Commun. (2004) 1798.
[173] A. Hori, K. Kumazawa, T. Kusukawa, D.K. Chand, M. Fujita, S. Sakamoto, K. Yamaguchi, Chem. Eur. J. 7 (2001) 4142.
[174] N. Kamiya, M. Tominaga, S. Sato, M. Fujita, J. Am. Chem. Soc. 129 (2007) 3816.
[175] T. Megyes, H. Jude, T. Grosz, I. Bako, T. Radnai, G. Tarkanyi, G. Palinkas, P.J. Stang, J. Am. Chem. Soc. 127 (2005) 10731;
K.D. Johnstone, K. Yamaguchi, M.J. Gunter, Org. Biomol. Chem. 3 (2005) 3008;
Y. Chang-Cheng, C. Hippius, M. Grüne, F. Würthner, Chem. Eur. J. 12 (2006) 7510;
V. Marin, E. Holder, R. Hoogenboom, E. Tekin, U.S. Schubert, Dalton Trans. (2006) 1636.
[176] J.M.J. Paulusse, R.P. Sijbesma, Chem. Commun. (2003) 1494.
[177] R. Dobrawa, M. Lysetska, P. Ballester, M. Grüne, F. Würthner, Macromolecules 38 (2005) 1315;
T. Vermonden, J. van der Gucht, P. de Waard, A.T.M. Marcelis, N.A.M. Besseling, E.J.R. Sudhölter, G.J. Fleer, M.A.C. Stuart, Macromolecules 36 (2003) 7035;
M. Ikeda, Y. Tanaka, T. Hasegawa, Y. Furusho, E. Yashima, J. Am. Chem. Soc. 128 (2006) 6806.
[178] K.N. Houk, A.G. Leach, S.P. Kim, X. Zhang, Angew. Chem. Int. Ed. 42 (2003) 4872.
[179] H.-J. Schneider, A. Yatsimirsky, Principles and Methods in Supramolecular Chemistry, Wiley & Sons, Ltd., Chichester, 2000.
[180] L. Fielding, Tetrahedron 56 (2000) 6151.
[181] T.N. Parac, D.L. Caulder, K.N. Raymond, J. Am. Chem. Soc. 120 (1998) 8003.
[182] T. Yamamoto, A.M. Arif, P.J. Stang, J. Am. Chem. Soc. 125 (2003) 12309.

[183] P. Ballester, A. Costa, P.M. Deyà, A. Frontera, R.M. Gomila, A.I. Oliva, J.K.M. Sanders, C.A. Hunter, J. Org. Chem. 70 (2005) 6616.
[184] S.Y. Chang, H.Y. Jang, K.S. Jeong, Chem. Eur. J. 10 (2004) 4358.
[185] T.S. Koblenz, H.L. Dekker, C.G. de Koster, P.W.N.M. van Leeuwen, J.N.H. Reek, Chem. Commun. (2006) 1700.
[186] K.S. Cameron, L. Fielding, J. Org. Chem. 66 (2001) 6891.
[187] The following equations apply for Eq. (7), according to the mass balance in the reaction: $[HG] = X_{HG}[H]_o$, $[H] = (1 - X_{HG})[H]_o$ and $[G] = [G]_o - X_{HG}[H]_o$.
[188] O. Mayzel, Y. Cohen, J. Chem. Soc., Chem. Commun. (1994) 1901.
[189] S. Arrhenius, Z. Phys. Chem. 4 (1889) 226.
[190] H. Eyring, Chem. Rev. 17 (1935) 65.
[191] J. Sandström, Dynamic NMR Spectroscopy, Academic Press, London, 1982.
[192] M. Pons, O. Millet, Prog. Nucl. Magn. Reson. Spectrosc. 38 (2001) 267.
[193] Some of the most frequently used programs are DNMR (D.S. Stephenson, G. Binsch, J. Magn. Reson. 32 (1978) 145); gNMR (http://home.cc.umanitoba.ca/~budzelaa/gNMR/gNMR.html); MEX/MEXICO (http://www.chemistry.mcmaster.ca/bain/exchange.html and A.D. Bain, G.J. Duns, Can. J. Chem. 74 (1996) 819), and WIN-DYNAMICS (by Bruker).
[194] K. Yamaguchi, S. Tashiro, M. Tominaga, M. Kawano, T. Ozeki, M. Fujita, Chem. Asian J. 2 (2007) 468.
[195] M. Fuss, H.-U. Siehl, B. Olenyuk, P.J. Stang, Organometallics 18 (1999) 758.
[196] R.A. Hoffman, S. Forsén, Prog. Nucl. Magn. Reson. Spectrosc. 1 (1966) 15.
[197] A.D. Bain, J.A. Cramer, J. Magn. Reson. A 103 (1993) 217.
[198] http://www.chemistry.mcmaster.ca/bain/cifman.pdf.
[199] A.V. Davis, D. Fiedler, G. Seeber, A. Zahl, R. van Eldik, K.N. Raymond, J. Am. Chem. Soc. 128 (2006) 1324.
[200] M.D. Pluth, R.G. Bergman, K.N. Raymond, Science 316 (2007) 85.
[201] G. Tárkányi, H. Jude, G. Pálinkás, P.J. Stang, Org. Lett. 7 (2005) 4971.
[202] Ref. [80] (Section 8.7.4).
[203] J. Jeener, B.H. Meier, P. Bachmann, R.R. Ernst, J. Chem. Phys. 72 (1979) 4546.
[204] C.L. Perrin, T.J. Dwyer, Chem. Rev. 90 (1990) 935.
[205] K.-S. Jeong, E.-J. Park, J. Org. Chem. 69 (2004) 2618.
[206] S.-Y. Chang, J.-Y. Jang, K.-S. Jeong, Chem. Eur. J. 9 (2003) 1535.